Equilibrium Configurations of a Symmetric Body Immersed in a Stationary Navier–Stokes Flow in a Planar Channel

SIAM J. MATH. ANAL.
Vol. 56, No. 3, pp. 3759–3801

EQUILIBRIUM CONFIGURATIONS OF A SYMMETRIC BODY IMMERSED IN A STATIONARY NAVIER–STOKES FLOW IN A PLANAR CHANNEL*

ELVISE BERCHIO†, DENIS BONHEURE‡, GIOVANNI P. GALDI§, FILIPPO GAZZOLA¶, AND SIMONA PEROTTO¶

Abstract. We study the equilibrium configurations for several fluid-structure interaction problems. The fluid is confined in a 2D unbounded channel that contains a body, free to move inside the channel with rigid motions (transversal translations and rotations). The motion of the fluid is generated by a Poiseuille inflow/outflow at infinity and governed by the stationary Navier–Stokes equations. For a model where the fluid is the air and the body represents the cross-section of a suspension bridge, therefore also subject to restoring elastic forces, we prove that for small inflows there exists a unique equilibrium position, while for large inflows we numerically show the appearance of additional equilibria. A similar uniqueness result is also obtained for a discretized 3D bridge, consisting in a finite number of cross-sections interacting with the adjacent ones. The very same model, but without restoring forces, is used to describe the mechanism of the Leonardo da Vinci ferry, which is able to cross a river without engines. We numerically determine the optimal orientation of the ferry that allows it to cross the river in minimal time.

Key words. equilibrium configurations, fluid-structure interaction problems, Navier–Stokes equations

MSC codes. 35Q35, 76D05, 74F10

DOI. 10.1137/23M1568752

1. Introduction.

We study some fluid-structure interaction problems in an unbounded 2D channel containing a body and a fluid whose motion is governed by the Navier–Stokes equations and is generated by a Poiseuille inflow/outflow at infinity. The models considered in this paper are inspired from previous works by the authors and their collaborators [2, 4, 5, 7, 8, 9, 16, 18, 21], frequently used also by the International Association for Wind Engineering [28].

The first model views the cross-section of the deck of a suspension bridge as a rigid rectangular body B immersed in an unbounded 2D channel

$$\mathcal{C}_L = \mathbb{R} \times (-L, L) \tag{1.1}$$

*Received by the editors April 26, 2023; accepted for publication February 20, 2024; published electronically June 3, 2024.

https://doi.org/10.1137/23M1568752

Funding: This work was supported by the MUR grant Dipartimento di Eccellenza 2023-2027 (Italy) and Thelam Fund (Belgium) grant FRB 2020-J1150080. The work of the second author was also supported by the Fondation Francqui as a Francqui Research Professor and the ARC Avance 2020 at ULB. The work of the third author was also partially supported by NSF grant DMS2307811. The work of the first and fourth authors was also partially supported by the PRIN project Direct and Inverse Problems for Partial Differential Equations: Theoretical Aspects and Applications and the Gruppo Nazionale per l'Analisi Matematica, la Probabilita e le loro Applicazioni (GNAMPA) of the Istituto Nazionale di Alta Matematica (INdAM).

†Department of Mathematical Sciences, Politecnico di Torino, Turin, Italy (elvise.berchio@polito.it).

‡Department of Mathematics, Université Libre de Bruxelles, Brussels, Belgium (denis.bonheure@ulb.ac.be).

§Department of Mechanical Engineering, University of Pittsburgh, Pittsburgh, PA 15261 USA (galdi@pitt.edu).

¶Department of Mathematics, Politecnico di Milano, Milan 20133, Italy (filippo.gazzola@polimi.it, simona.perotto@polimi.it).

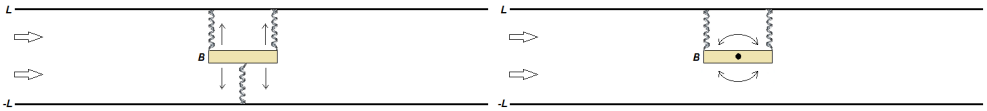

FIG. 1. *The channel $\mathcal{C}_L$ with the vertically moving body B on the left and the rotating body B on the right.*

for some $L > 0$. The cross-section is free to move vertically and to rotate around its barycenter under the action of the fluid flow and two restoring forces. A preliminary analysis of the equilibrium configurations for this model was performed in [5] (see also [6] for a revised version) by decoupling the vertical and the rotational displacements. More precisely, in the model considered in [5], B was allowed to move either vertically or to rotate (as in Figure 1). The full analysis is performed in the present paper by coupling the vertical and rotational motions (see section 2.1); as we shall see, two degrees of freedom make the analysis much more challenging. In particular, the behavior of the fluid forces was only announced (with no proofs) in [5], while a rigorous approach involves several delicate arguments covering a number of pages; see section 3. Moreover, Theorem 3.5 and the numerical results in section 6.5 suggest that the coupled system is more unstable than with just one degree of freedom.

The vertical displacements in Figure 1 (left) are generated by three kinds of forces. There is an upwards restoring force due to the elastic action of both the hangers and the sustaining cables of the bridge: the hangers behave as nonlinear springs which may slacken [1, Chapter 9-VI] so that they have no downwards action. There is the weight of the deck acting constantly downwards: this is why there will be no odd requirement on the vertical restoring force considered in the model. Finally, there is an elastic resistance to both bending and stretching of the whole deck for which B merely represents a cross-section: this force is superlinear and prevents the deck from wandering too far from its symmetric equilibrium configuration.

The detailed physical description of the model is reported in section 2, where we also derive the system of coupled PDEs/ODEs, in dimensionless form, governing the fluid-structure interaction problem. The equilibrium configurations are found by solving the associated steady-state problem; see (2.11)–(2.12). Since it is written in dimensionless form, only the Reynolds number $\mathcal{R}$ and the stiffness of the restoring forces remain as overall parameters, but, while the latter are fixed, we discuss the behavior of the solutions as $\mathcal{R}$ varies. Our strategy is to solve first the fluid equations (2.11) for any admissible position of B within $\mathcal{C}_L$ and then to determine the *equilibrium configurations* of B for which also (2.12) is satisfied. The first step is quite standard and is performed in section 2.3, where the only difficult part is to determine a solenoidal extension of the boundary data in order to reduce the original inhomogeneous Dirichlet problem to a related nonslip problem; it turns out that the relevant a priori bounds are *independent* of the position of B.

Before tackling (2.12) we need to define rigorously the fluid forces—the *lift* and *torque*. This is done in section 3, where we also analyze the main properties and recall several equivalent ways of computing both the lift and the torque. Since these forces depend on the (variable) position of B and on the (variable) Reynolds number $\mathcal{R}$, we need to compute their derivatives with respect to these variables. This is done in section 3.2, where, to perform these computations, we follow the strategy of [10], which relies on the classical argument of [3] reformulated in the setting of weak solutions to avoid estimates on the pressure. In fact, the alternative strategy of

[3] uses the boundedness of the fluid domain, which is not the case for $\mathcal{C}_L \setminus B$. For this reason, the crucial point here and in [10] is to use a volume-preserving change of variables and a solenoidal velocity after the change of variable, as in [36]. With these derivatives in hand, we prove the main result of section 3, which is Theorem 3.5, allowing us to compare the stabilities of models with one/two degrees of freedom.

These results and tools allow us to tackle (2.12). In section 4 (Theorem 4.3) we prove existence, uniqueness, and stability of the equilibrium configuration for small $\mathcal{R}$. This result raises the natural question of whether uniqueness is lost for large $\mathcal{R}$. Although we do not have a theoretical answer, in section 6 we bring numerical evidence that the answer might be positive: for large $\mathcal{R}$ it seems that the equilibrium configurations are at least three.

In section 5 we use the same model to describe a discrete 3D bridge with multiple cross-sections interacting with the adjacent sections; their mutual action is the above-mentioned elastic resistance of the deck. The main result (Theorem 5.1) is similar to Theorem 4.3 and states existence, uniqueness, and stability of the equilibrium configuration for small $\mathcal{R}$.

In section 7 we show that our 2D model can also be adapted to describe the functioning of the Leonardo da Vinci ferry in Imbersago (Italy); in this case, the body is the ferry, whereas the fluid is the water within the river flow. Besides this, the only differences between the two models are physical in nature. While for the bridge there are (elastic) restoring forces, for the ferry there are none. Whereas for the stability of the bridge one aims to *minimize the lift* in order to reduce the oscillations, for the Leonardo ferry one aims to *maximize the lift* in order to increase the velocity of the ferry and to minimize the crossing time. By exploiting the numerics in section 6, we explain how to reach this target in section 7.2.

Overall, we emphasize that we do not aim to give quantitative results, but we believe that our qualitative analysis already explains some of the important phenomena in the considered fluid-structure interaction models.

2. The cross-section of the deck of a bridge in a wind flow. The (3D) deck of a suspension bridge is usually hit by a transversal (horizontal) wind and is then subject to both vertical and rotational displacements that are visible in each cross-section of the deck. We focus here on a single cross-section, while in section 5 we consider multiple cross-sections.

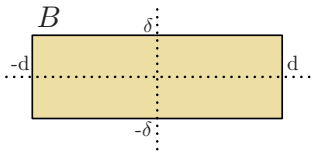

2.1. The 2D model. In the figure above, we show the (2D) cross-section of the deck of a bridge as a rigid rectangular body $B = [-d, d] \times [-\delta, \delta] \subset \mathbb{R}^2$ $(d > \delta > 0)$ immersed in a channel flow occupying the unbounded strip $\mathcal{C}_L$ in (1.1), which represents an atmosphere layer where B is free to move, both vertically and rotationally around its barycenter, under the action of a horizontal Poiseuille fluid flow and two restoring forces. The position of B is identified by two parameters, h and θ, representing, respectively, a vertical translation and a rotation around its barycenter; see (2.3) and (2.4) below. The body is subject to two restoring forces. The first force $\partial_h F$ tends to keep the body in the middle of the channel $(h = 0)$, while the second force $\partial_\theta F$ tends to maintain the body horizontally $(\theta = 0)$. These elastic forces represent, respectively, the action of the whole (3D) deck of the suspension bridge on the cross-section B and

the action of the sustaining cables. They are the partial derivatives of a potential $F = F(h,\theta)$ which satisfies several (physical) assumptions that will be introduced and discussed in their dimensionless form; see (2.6)–(2.7)–(2.8)–(2.9) below.

The channel $\mathcal{C}_L$ is crossed by a horizontal fluid flow (the wind hitting the cross-section), and we denote by $\wp > 0$ its pressure drop and by $\mu > 0$ its shear viscosity coefficient. Then the corresponding Poiseuille velocity field $\boldsymbol{v}_P := v_P(x_2)\boldsymbol{e}_1$ is such that

$$\frac{d^2 v_P}{dx_2^2} = -\frac{\wp}{\mu}, \quad v_P(-L) = v_P(L) = 0 \qquad \Longrightarrow \qquad v_P(x_2) = \frac{\wp L^2}{2\mu}\left(1 - \frac{x_2^2}{L^2}\right).$$

Incidentally, we recall that $\boldsymbol{v}_P$ is a stationary solution of both the Stokes and Navier–Stokes equations in $\mathcal{C}_L$ with the boundary condition $\boldsymbol{v}_P|_{\partial\mathcal{C}_L} = 0$.

We may now set up the fluid-structure interaction evolution problem where the motion of B is driven by the fluid flow and by the restoring forces $\partial_h F, \partial_\theta F$ on some interval of time, possibly $\mathbb{R}_+$. Let $\boldsymbol{u}$ and p be the velocity and pressure of the fluid in the plane containing the cross-section $B_{h,\theta}$. Since both h and θ depend on time, also the fluid domain $\Omega_{h,\theta} := \mathcal{C}_L \setminus B_{h,\theta}$ depends on time, and the space-time fluid domain *is not* a standard cylinder but, instead,

$$\Omega_+ := \bigcup_{t>0} \Omega_{h(t),\theta(t)} \times \{t\}.$$

The governing equations of the fluid-structure interaction problem are then given by the following combined system of PDEs/ODEs:

$$\begin{aligned}
&\rho(\boldsymbol{u}_t + \boldsymbol{u}\cdot\nabla\boldsymbol{u}) - \mu\Delta u + \nabla p = 0,\ \mathrm{div}\boldsymbol{u} = 0 \quad \text{in } \Omega_+,\\
&\boldsymbol{u}|_{S_{h,\theta}} = \dot\theta\,(\boldsymbol{x}-\boldsymbol{h})^\perp + \dot{\boldsymbol{h}},\ \boldsymbol{u}|_{\partial\mathcal{C}_L} = 0,\ \lim_{|x_1|\to+\infty} \boldsymbol{u}(t,x_1,x_2) = v_P(x_2)\boldsymbol{e}_1,\\
&m\ddot h + \partial_h F(h,\theta) = -\boldsymbol{e}_2 \cdot \int_{S_{h,\theta}} \Big(\mu(\nabla\boldsymbol{u} + \nabla\boldsymbol{u}^\top) - p\boldsymbol{I}\Big)\cdot\boldsymbol{n}, \quad t>0,\\
&I\ddot\theta + \partial_\theta F(h,\theta) = -\int_{S_{h,\theta}} (\boldsymbol{x}-\boldsymbol{h})^\perp \cdot \Big(\mu(\nabla\boldsymbol{u} + \nabla\boldsymbol{u}^\top) - p\boldsymbol{I}\Big)\cdot\boldsymbol{n}, \quad t>0,
\end{aligned} \tag{2.1}$$

where $\rho > 0$ denotes the planar density of the fluid, I is the component of the inertia tensor of B with respect to its barycenter and $m > 0$ its mass, $\boldsymbol{I}$ is the 2×2 identity matrix, $S_{h,\theta} = \partial B_{h,\theta}$, $\boldsymbol{n}$ is the outward normal to $\Omega_{h,\theta}$ (pointing inward into $B_{h,\theta}$), and

$$\boldsymbol{h} = \boldsymbol{h}(t) = \big(0, h(t)\big), \qquad (\boldsymbol{x}-\boldsymbol{h})^\perp = (h - x_2, x_1).$$

The unknowns in (2.1) are $\boldsymbol{u}$ and p for the motion of the fluid and h and θ for the position of the body; their knowledge fully describes the evolution of the fluid-structure interaction.

2.2. Dimensionless equations. In order to write (2.1) in dimensionless form, we introduce the scaling quantities

$$\begin{aligned}
&\delta \text{ (length)}, \quad V = \frac{\mu}{\rho\delta} \text{ (velocity)}, \quad T = \frac{\delta}{V} = \frac{\rho\delta^2}{\mu} \text{ (time)}, \quad m \text{ (mass)},\\
&I \text{ (moment of inertia)},
\end{aligned}$$

and we set

$$\mathcal{R} := \frac{\wp L^2 \delta\rho}{2\mu^2}, \qquad \zeta := \frac{\rho\delta^2}{m}, \qquad \varpi := \frac{\rho\delta^4}{I}, \qquad \mathsf{v}_P(x_2) := 1 - \frac{x_2^2}{L^2}, \tag{2.2}$$

where $\mathcal{R}$ is the relevant Reynolds number governing the flow. Of course, the width of the channel and the length of the body changed but, to avoid new notation, we will not use d/δ and L/δ as new lengths and still write $\mathcal{C}_L = \mathbb{R} \times (-L, L)$ and $B = [-d, d] \times [-1, 1]$. After scaling, the admissible (noncollision) configurations of B are given by

$$B_{h,\theta} = \begin{pmatrix} \cos\theta & -\sin\theta \\ \sin\theta & \cos\theta \end{pmatrix} B + h\,\boldsymbol{e}_2 =: Q(\theta)B + h\,\boldsymbol{e}_2 \qquad \forall\,(h,\theta) \in A_d \tag{2.3}$$

with

$$A_d := \left\{ (h,\theta) \in \mathbb{R}^2 : |\theta| < \frac{\pi}{2} \text{ and } |h| + d|\sin\theta| + \cos\theta < L \right\}. \tag{2.4}$$

The configurations $\theta = \pm\frac{\pi}{2}$ are not included in A_d because the deck would be in a straight-up position, which is not physically acceptable. The other constraints defining A_d prevent collisions between the cross-section $B_{h,\theta}$ and the boundary $\partial\mathcal{C}_L = \mathbb{R}\times\{\pm L\}$ of the channel. By fixing $\theta = 0$ or $h = 0$, we recover the decoupled dynamics described in Figure 1. We assume that

$$L > \sqrt{d^2 + 1} \tag{2.5}$$

so that $L - d|\sin\theta| - \cos\theta > 0$ for all $|\theta| < \frac{\pi}{2}$ (the body is not allowed to move vertically on the whole range $|h| < L - 1$ for all θ). In Figure 2 we depict A_d for a couple (L, d) satisfying (2.5).

The scaling quantities in (2.2) enable us to derive the dimensionless form of the fluid motion. Accordingly, we need to introduce the dimensionless restoring forces. We consider a smooth potential $F \in C^2(A_d)$ satisfying the following assumptions:

$$\begin{aligned} &\partial_h F(0,\theta) = 0 = \partial_\theta F(h,0) \quad \forall |\theta| < \frac{\pi}{2},\ \forall |h| < L-1, \quad \kappa_1 = \partial_{hh} F(0,0) > 0, \\ &\kappa_2 = \partial_{\theta\theta} F(0,0) > 0, \end{aligned} \tag{2.6}$$

$$h\partial_h F(h,\theta) > 0 \quad \forall (h,\theta) \in A_d,\ h \neq 0, \quad \text{and} \quad \theta\partial_\theta F(0,\theta) > 0 \quad \forall\, 0 < |\theta| < \frac{\pi}{2}, \tag{2.7}$$

where κ_1 (resp., κ_2) represents the dimensionless linearized vertical (resp., rotational) stiffness around the equilibrium configuration ($h = \theta = 0$). Hence,

$$\kappa_1 = \frac{\rho^2\delta^4}{m\mu^2}\sigma_1, \qquad \kappa_2 = \frac{\rho^2\delta^4}{I\mu^2}\sigma_2,$$

with σ_1 (resp., σ_2) being the original dimensional vertical (resp., rotational) stiffness, and, therefore, $\partial_h F$ and $\partial_\theta F$ are the restoring forces in dimensionless form. Clearly, F is defined up to an additive constant and we can take $F(0,0) = 0$. Since (2.6) yields $\partial_{h\theta} F(0,0) = 0$, we then have

$$F(h,\theta) = \frac{\kappa_1}{2}h^2 + \frac{\kappa_2}{2}\theta^2 + o(h^2 + \theta^2) \quad \text{as } (h,\theta) \to (0,0),$$

which is the uncoupled Hooke's elastic law for h and θ small.

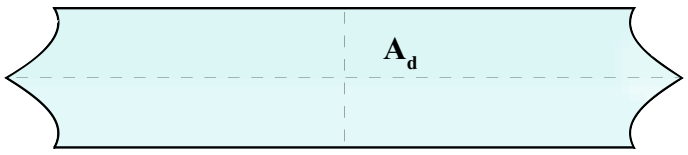

FIG. 2. *The set A_d in* (2.4).

Although our results also hold in more general situations, the above assumptions are justified by the behavior of real bridges. Indeed, at the collapsed Tacoma Bridge the vertical modes of oscillations frequently changed into each other [1, pp. 20, 28], and small torsional oscillations were never observed [31]; see also [1, p. 31]. Assumption (2.6) states that neither vertical nor torsional oscillations can appear if they are not already part of the oscillation. The second condition in (2.7) states that the action of the cables is a restoring force but only in a neighborhood of the central position $h=0$.

When modeling the wind hitting a bridge, the boundary of the channel is virtual and the physical model breaks down in the case of a collision between B and $\partial\mathcal{C}_L$. Hence, without affecting the modeling, we can assume that

$$\liminf_{(|h|+d|\sin\theta|+\cos\theta)\to L^-} |\partial_h F(h,\theta)|(L-|h|-d|\sin\theta|-\cos\theta)^{3/2}>0, \tag{2.8}$$

$$\lim_{|\theta|\to\frac{\pi}{2}} |\partial_\theta F(h,\theta)|=+\infty \quad \text{uniformly w.r.t. } |h|\le L-d, \tag{2.9}$$

namely, there exist a *strong force* $\partial_h F$ preventing the collision between the cross-section B and the boundary $\partial\mathcal{C}_L$ of the virtual channel, and a *weak force* $\partial_\theta F$ preventing the cross-section from reaching a straight-up position. One could also assume that (2.9) holds with $\frac{\pi}{2}$ replaced by a smaller angle, $|\theta|<\theta_{\max}$, where the elastic behavior of the bridge becomes plastic and leads to a fracture of the deck, as in the Tacoma Bridge collapse. The power $3/2$ in (2.8) is related to Proposition 3.1; an improvement on estimate (3.4) would allow us to relax (2.8). The rotational (torsional) displacements depicted in Figure 1 (right) are due to the possible different behaviors of the hangers and cables at the two endpoints of the cross-section. Assumptions (2.8)–(2.9) state that the angular restoring force $\partial_\theta F$ in proximity of straight-up positions may have a weaker behavior than the vertical force $\partial_h F$ in proximity of collisions. Without assumptions (2.8)–(2.9), a weaker (merely local) form of Theorem 4.3 still holds; see Remark 4.5. Our numerical results in section 6 suggest that (2.8) is not needed to prevent collisions. We also refer to section 8 for more comments.

The scaling quantities (2.2) and the dimensionless linearized stiffness defined in (2.6) enable us to rewrite (2.1) as

$$\begin{aligned}
&\boldsymbol{u}_t+\boldsymbol{u}\cdot\nabla\boldsymbol{u}-\ \operatorname{div}\boldsymbol{T}(\boldsymbol{u},p)=0,\ \operatorname{div}\boldsymbol{u}=0 \quad \text{in } \Omega_+,\\
&\boldsymbol{u}|_{S_{h,\theta}}=\dot\theta\,(\boldsymbol{x}-\boldsymbol{h})^\perp+\dot{\boldsymbol{h}},\ \boldsymbol{u}|_{\partial\mathcal{C}_L}=0,\ \lim_{|x_1|\to+\infty}\boldsymbol{u}(t,x_1,x_2)=\mathcal{R}\mathsf{v}_P(x_2)\boldsymbol{e}_1,\\
&\ddot h+\partial_h F(h,\theta)=-\zeta\boldsymbol{e}_2\cdot\int_{S_{h,\theta}}\boldsymbol{T}(\boldsymbol{u},p)\cdot\boldsymbol{n},\quad t>0,\\
&\ddot\theta+\partial_\theta F(h,\theta)=-\varpi\int_{S_{h,\theta}}(\boldsymbol{x}-\boldsymbol{h})^\perp\cdot(\boldsymbol{T}(\boldsymbol{u},p)\cdot\boldsymbol{n}),\quad t>0,
\end{aligned} \tag{2.10}$$

where

$$\boldsymbol{T}(\boldsymbol{u},p)=\nabla\boldsymbol{u}+\nabla\boldsymbol{u}^\top-p\boldsymbol{I}$$

denotes the (dimensionless) stress tensor. We emphasize that the dimensionless stiffness constants are included in the dimensionless forms of $\partial_h F$ and $\partial_\theta F$. Our goal is to provide a qualitative analysis.

Existence, uniqueness, and long-time behavior for (2.10) are studied in [11, 19, 34]. In the present paper we aim to study the equilibrium configurations of B, and therefor, we eliminate all time derivatives from (2.10) and consider the steady-state problems

$$
\begin{aligned}
&-\operatorname{div}\boldsymbol{T}(\boldsymbol{u},p)+\boldsymbol{u}\cdot\nabla\boldsymbol{u}=0,\ \operatorname{div}\boldsymbol{u}=0 \quad \text{in } \Omega_{h,\theta},\\
&\boldsymbol{u}|_{S_{h,\theta}}=\boldsymbol{u}|_{\partial\mathcal{C}_L}=0,\ \lim_{|x_1|\to+\infty}\boldsymbol{u}(x_1,x_2)=\mathcal{R}\mathsf{v}_P(x_2)\boldsymbol{e}_1,
\end{aligned}
\tag{2.11}
$$

$$
\begin{aligned}
\partial_h F(h,\theta)&=-\zeta\boldsymbol{e}_2\cdot\int_{S_{h,\theta}}\boldsymbol{T}(\boldsymbol{u},p)\cdot\boldsymbol{n},\\
\partial_\theta F(h,\theta)&=-\varpi\int_{S_{h,\theta}}(\boldsymbol{x}-\boldsymbol{h})^\perp\cdot(\boldsymbol{T}(\boldsymbol{u},p)\cdot\boldsymbol{n}).
\end{aligned}
\tag{2.12}
$$

Our plan is first to solve (2.11) for any $(h,\theta)\in A_d$ and then to find for which couples $(h,\theta)\in A_d$ is (2.12) satisfied. These couples are called *equilibrium configurations* for B.

2.3. The steady-states of the fluid equations. In order to write the weak formulation of (2.11), we introduce a specific solenoidal extension $\boldsymbol{a}$ of the Poiseuille inflow/outflow to all $\mathcal{C}_L$ which vanishes in $B_{h,\theta}$ but does not depend on h and θ. Let $D\in(\sqrt{d^2+1},L)$ be the radius of an open ball centered at 0 and containing $B_{0,\theta}$ for all $|\theta|<\frac{\pi}{2}$; we may assume that $B_{h,\theta}$ lies entirely above the horizontal line $x_2=-\frac{L+D}{2}$, otherwise $B_{h,\theta}$ lies entirely below the horizontal line $x_2=\frac{L+D}{2}$ and we can argue in a symmetric way. Then, as depicted in Figure 3, we define

$$
\begin{aligned}
\Sigma_D&=\Big\{(-4D,-2D)\times(-L,L)\Big\}\cup\left\{[-2D,2D]\times\left(-L,-\frac{L+D}{2}\right)\right\}\\
&\quad\cup\Big\{(2D,4D)\times(-L,L)\Big\},\\
\Omega_*&=(-2D,2D)\times\left(-\frac{L+D}{2},L\right),\quad \Omega_\infty=\{(x_1,x_2)\in\mathcal{C}_L:\,|x_1|>4D\},\\
\Omega_D&=\Omega_{h,\theta}\setminus\Omega_\infty.
\end{aligned}
$$

Let $\zeta\in C^\infty\big(\mathbb{R}\times[-L,L]\big)$ be a cutoff function separating the obstacle and the Poiseuille flow at infinity such that

$$
\zeta(x_1,x_2)=\zeta(x_1)=\begin{cases}0 & \text{if } |x_1|<3D,\\ 1 & \text{if } |x_1|>4D\end{cases}\qquad\text{and } \zeta \text{ even w.r.t. } x_1.
$$

Let $\boldsymbol{z}\in H^2_0(\Sigma_D)$ be the solution to the problem

$$
\operatorname{div}\boldsymbol{z}=\zeta'(x_1)\mathsf{v}_P(x_2)\quad\text{in }\Sigma_D,\quad \boldsymbol{z}=0\quad\text{on }\partial\Sigma_D.
$$

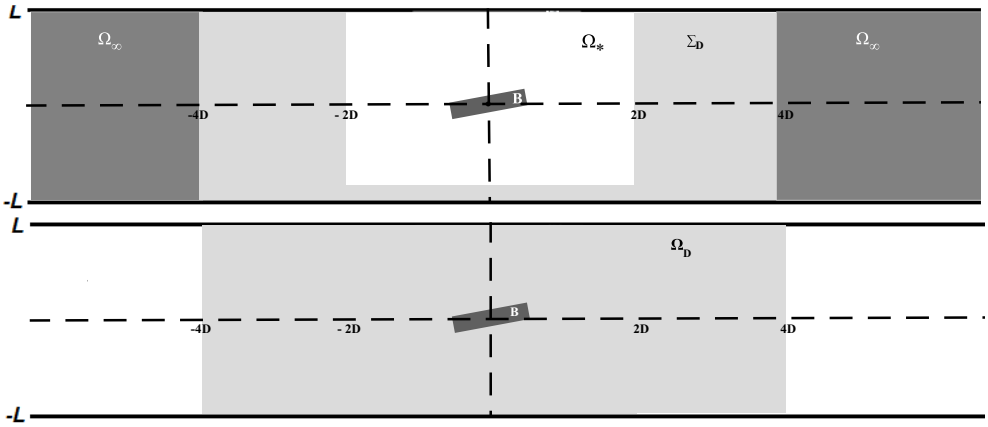

FIG. 3. *The regions Σ_D, Ω_*, and Ω_∞ (above). The region Ω_D (below).*

Since $\zeta'(x_1)\mathsf{v}_P(x_2) \in H^1_0(\Sigma_D)$ and $\int_{\Sigma_D} \zeta'(x_1)\mathsf{v}_P(x_2) = 0$, such $\boldsymbol{z}$ does exist [15, Theorem III.3.3]. Hence, if we extend $\boldsymbol{z}$ by zero outside Σ_D we obtain that $\boldsymbol{z} \in H^2_0(\mathcal{C}_L)$ and we define

$$\boldsymbol{a}(x_1,x_2) := \zeta(x_1)\mathsf{v}_P(x_2)\boldsymbol{e}_1 - \boldsymbol{z}(x_1,x_2), \qquad (x_1,x_2) \in \mathcal{C}_L. \tag{2.13}$$

Then $\mathrm{div}\boldsymbol{a} = 0$ in $\mathcal{C}_L$, $\boldsymbol{a} \in H^2_{loc}(\Omega_{h,\theta})$ and $\boldsymbol{a}(x_1,x_2) = \mathsf{v}_P(x_2)\boldsymbol{e}_1$ in Ω_∞. Therefore,

(2.14)

$$\boldsymbol{a} \equiv 0 \quad \text{in } \Omega_*, \quad \boldsymbol{a}\cdot\nabla\boldsymbol{a} \equiv 0 \quad \text{in } \Omega_\infty, \quad -\Delta\boldsymbol{a} = \nabla\Pi \quad \text{in } \Omega_\infty, \text{ where } \Pi(x_1,x_2) = \frac{2x_1}{L^2}.$$

We can now define weak solutions of (2.11).

DEFINITION 2.1. *Let* $V_{h,\theta} := \{\boldsymbol{v} \in H^1_0(\Omega_{h,\theta}) : \mathrm{div}\boldsymbol{v} = 0$ *a.e. in* $\Omega_{h,\theta}\}$. *We say that* $\boldsymbol{u} \in H^1_{loc}(\Omega_{h,\theta})$ *(solenoidal) is a weak solution to* (2.11) *if* $\boldsymbol{v} := \boldsymbol{u} - \mathcal{R}\boldsymbol{a}$ *satisfies* $\boldsymbol{v} \in V_{h,\theta}$ *and*

$$\begin{aligned}\int_{\Omega_{h,\theta}} \nabla\boldsymbol{v} : \nabla\boldsymbol{\varphi} = \int_{\Omega_{h,\theta}} (\boldsymbol{v}+\mathcal{R}\boldsymbol{a})\cdot\nabla\boldsymbol{\varphi}\cdot\boldsymbol{v} - \mathcal{R}\int_{\Omega_{h,\theta}} (\boldsymbol{v}+\mathcal{R}\boldsymbol{a})\cdot\nabla\boldsymbol{a}\cdot\boldsymbol{\varphi} \\ + \mathcal{R}\int_{\Omega_{h,\theta}} \Delta\boldsymbol{a}\cdot\boldsymbol{\varphi} \quad \forall\boldsymbol{\varphi} \in V_{h,\theta}.\end{aligned} \tag{2.15}$$

One can then associate a pressure $p \in L^2_{loc}(\Omega_{h,\theta})$ to the weak solution $\boldsymbol{u}$; see [15, section XIII.1].

The next result states existence and uniqueness of the weak solution of (2.11) for small $\mathcal{R}$. The fundamental aspect is the a priori bound which is independent of the position of B.

PROPOSITION 2.2. *There exists* $\gamma > 0$ *(independent of* $(h,\theta) \in A_d$*) such that if* $0 \le \mathcal{R} < \gamma$, *then problem* (2.11) *admits a unique weak solution* $(\boldsymbol{u},p) \in H^1_{loc}(\Omega_{h,\theta}) \times L^2_{loc}(\Omega_{h,\theta})/\mathbb{R}$ *with* $(\boldsymbol{u} - \mathcal{R}\mathsf{v}_P\boldsymbol{e}_1) \in V_{h,\theta}$ *(see Definition* 2.1*); moreover,* $(\boldsymbol{u},p) \in C^\infty(\Omega_{h,\theta}) \times C^\infty(\Omega_{h,\theta})$. *Finally, there exists* $C > 0$ *depending on* L *and* d, *but not on* h *and* θ, *such that*

$$\|\nabla(\boldsymbol{u} - \mathcal{R}\mathsf{v}_P\boldsymbol{e}_1)\|_{L^2(\Omega_{h,\theta})} \le C\mathcal{R}(1+\mathcal{R}). \tag{2.16}$$

In particular, if $\mathcal{R} = 0$, *then* $\boldsymbol{u} = \boldsymbol{0}$ *for all* $(h,\theta) \in A_d$.

Proof. The proof is a revision of [5, Lemma 1]; see also [6]. In particular, it is enough to show the validity of the a priori estimate (2.16) since this allows us to prove the stated properties by the same (classical) arguments given in [15, section XIII.3]. Taking $\boldsymbol{\varphi} = \boldsymbol{v}$ as test function in (2.15), by (2.14) we obtain

$$\|\nabla\boldsymbol{v}\|^2_{L^2(\Omega_{h,\theta})} = -\mathcal{R}\int_{\Omega_{h,\theta}} \boldsymbol{v}\cdot\nabla\boldsymbol{a}\cdot\boldsymbol{v} - \mathcal{R}^2\int_{\Omega_D} \boldsymbol{a}\cdot\nabla\boldsymbol{a}\cdot\boldsymbol{v} - \mathcal{R}\int_{\Omega_D} \nabla\boldsymbol{a} : \nabla\boldsymbol{v}.$$

By the Ladyzhenskaya and Poincaré inequalities, we obtain the bounds

$$\left|\int_{\Omega_{h,\theta}} \boldsymbol{v}\cdot\nabla\boldsymbol{a}\cdot\boldsymbol{v}\right| \le \|\nabla\boldsymbol{a}\|_{L^\infty(\Omega_\infty)}\|\boldsymbol{v}\|^2_{L^2(\Omega_\infty)} + \|\nabla\boldsymbol{a}\|_{L^2(\Omega_D)}\|\boldsymbol{v}\|^2_{L^4(\Omega_D)} \le C_1\|\nabla\boldsymbol{v}\|^2_{L^2(\Omega_{h,\theta})},$$

$$\left|\int_{\Omega_D} \boldsymbol{a}\cdot\nabla\boldsymbol{a}\cdot\boldsymbol{v}\right| \le \|\boldsymbol{a}\|_{L^4(\Omega_D)}\|\nabla\boldsymbol{a}\|_{L^2(\Omega_D)}\|\boldsymbol{v}\|_{L^4(\Omega_D)} \le C_2\|\nabla\boldsymbol{v}\|_{L^2(\Omega_{h,\theta})}.$$

Observe that C_1, C_2 do not depend on h, θ. Indeed, $\boldsymbol{a}$ is independent of (h,θ) by construction in (2.13), and $\Omega_{h,\theta} \subset \mathcal{C}_L$ for all $(h,\theta) \in A_d$, implying $H^1_0(\Omega_{h,\theta}) \subset H^1_0(\mathcal{C}_L)$ by trivial extension inside $B_{h,\theta}$. Summarizing, we have the estimate

$$\|\nabla \boldsymbol{v}\|_{L^2(\Omega_{h,\theta})} \le C_1 \mathcal{R} \, \|\nabla \boldsymbol{v}\|_{L^2(\Omega_{h,\theta})} + C_2 \mathcal{R}^2 + \mathcal{R} \|\nabla \boldsymbol{a}\|_{L^2(\Omega_D)}$$

by which (2.16) follows by taking $\mathcal{R}$ small and by noticing that $\|\nabla(\boldsymbol{a} - \mathsf{v}_P)\boldsymbol{e}_1\|_{L^2(\Omega_{h,\theta})}$ is bounded by a constant independent of h and θ. ∎

Remark 2.3. For $(h,\theta) \in A_d$, let $V^i_{h,\theta}$ $(i = 1, \dots, 4)$ be the four corners of the rectangle $B_{h,\theta}$. Then, by elliptic regularity on the smooth parts of the boundary, the solution $(\boldsymbol{u}, p)$ of (2.11) found in Proposition 2.2 satisfies $(\boldsymbol{u}, p) \in C^\infty\big(\overline{\Omega_{h,\theta}} \setminus \{V^1_{h,\theta}, V^2_{h,\theta}, V^3_{h,\theta}, V^4_{h,\theta}\}\big)$.

In what follows it will be useful to decompose $\boldsymbol{v}$ as follows.

LEMMA 2.4. *Let $\gamma > 0$ be as in Proposition* 2.2*, let $\mathcal{R} < \gamma$, let $\boldsymbol{v}$ be as in Definition* 2.1*, and let $\boldsymbol{w} := \boldsymbol{v}/\mathcal{R}$. Then*

$$\begin{aligned} \int_{\Omega_{h,\theta}} \nabla \boldsymbol{w} : \nabla \boldsymbol{\varphi} + \int_{\Omega_{h,\theta}} \nabla \boldsymbol{a} : \nabla \boldsymbol{\varphi} &= \mathcal{R} \int_{\Omega_{h,\theta}} (\boldsymbol{w} + \boldsymbol{a}) \cdot \nabla \boldsymbol{\varphi} \cdot \boldsymbol{w} \\ &\quad - \mathcal{R} \int_{\Omega_{h,\theta}} (\boldsymbol{w} + \boldsymbol{a}) \cdot \nabla \boldsymbol{a} \cdot \boldsymbol{\varphi} \quad \forall \boldsymbol{\varphi} \in V_{h,\theta}. \end{aligned} \tag{2.17}$$

Let $\boldsymbol{w}^{(s)} \in V_{h,\theta}$ be the Stokes flow (independent of $\mathcal{R}$) weakly defined by

$$\int_{\Omega_{h,\theta}} \big(\nabla \boldsymbol{w}^{(s)} + \nabla \boldsymbol{a}\big) : \nabla \boldsymbol{\varphi} = 0 \quad \forall \boldsymbol{\varphi} \in V_{h,\theta} \tag{2.18}$$

and let $\boldsymbol{w}^{(n)}(\mathcal{R}) := \mathcal{R}^{-1}(\boldsymbol{w} - \boldsymbol{w}^{(s)})$, so that $\boldsymbol{w} = \boldsymbol{w}^{(s)} + \mathcal{R}\boldsymbol{w}^{(n)}(\mathcal{R})$ and $\boldsymbol{v} = \mathcal{R}\boldsymbol{w}^{(s)} + \mathcal{R}^2 \boldsymbol{w}^{(n)}(\mathcal{R})$. Then $\|\nabla \boldsymbol{w}^{(s)}\|_{L^2(\Omega_{h,\theta})}$ and $\|\nabla \boldsymbol{w}^{(n)}(\mathcal{R})\|_{L^2(\Omega_{h,\theta})}$ are bounded independently of $(h,\theta) \in A_d$.

Proof. By definition of $\boldsymbol{w}$ we have that $\boldsymbol{u} = \mathcal{R}(\boldsymbol{w} + \boldsymbol{a})$ and (2.15) implies (2.17).

By taking $\boldsymbol{\varphi} = \boldsymbol{w}^{(s)}$ in (2.18), we obtain

$$\|\nabla \boldsymbol{w}^{(s)}\|_{L^2(\Omega_{h,\theta})} \le \|\nabla \boldsymbol{a}\|_{L^2(\Omega_D)} \quad \forall (h,\theta) \in A_d.$$

By (2.17) and by definition of $\boldsymbol{w}^{(s)}$, we infer that $\boldsymbol{w}^{(n)} \in V_{h,\theta}$ is weakly defined by

$$\begin{aligned} &\int_{\Omega_{h,\theta}} \nabla \boldsymbol{w}^{(n)} : \nabla \boldsymbol{\varphi} \\ &\quad = \int_{\Omega_{h,\theta}} \boldsymbol{w}^{(s)} \cdot \nabla \boldsymbol{\varphi} \cdot \boldsymbol{w}^{(s)} + \int_{\Omega_{h,\theta}} \boldsymbol{a} \cdot \nabla \boldsymbol{\varphi} \cdot \boldsymbol{w}^{(s)} - \int_{\Omega_{h,\theta}} \boldsymbol{a} \cdot \nabla \boldsymbol{a} \cdot \boldsymbol{\varphi} \\ &\qquad - \int_{\Omega_{h,\theta}} \boldsymbol{w}^{(s)} \cdot \nabla \boldsymbol{a} \cdot \boldsymbol{\varphi} + \mathcal{R} \int_{\Omega_{h,\theta}} \boldsymbol{w}^{(n)} \cdot \nabla \boldsymbol{\varphi} \cdot \boldsymbol{w}^{(s)} + \mathcal{R} \int_{\Omega_{h,\theta}} \boldsymbol{w}^{(s)} \cdot \nabla \boldsymbol{\varphi} \cdot \boldsymbol{w}^{(n)} \\ &\qquad + \mathcal{R} \int_{\Omega_{h,\theta}} \boldsymbol{a} \cdot \nabla \boldsymbol{\varphi} \cdot \boldsymbol{w}^{(n)} - \mathcal{R} \int_{\Omega_{h,\theta}} \boldsymbol{w}^{(n)} \cdot \nabla \boldsymbol{a} \cdot \boldsymbol{\varphi} + \mathcal{R}^2 \int_{\Omega_{h,\theta}} \boldsymbol{w}^{(n)} \cdot \nabla \boldsymbol{\varphi} \cdot \boldsymbol{w}^{(n)}. \end{aligned}$$

By taking $\varphi = \boldsymbol{w}^{(n)}$ and using the bound for $\boldsymbol{w}^{(s)}$, we have the estimate

$$(1 - c_1 \mathcal{R}) \|\nabla \boldsymbol{w}^{(n)}\|_{L^2(\Omega_{h,\theta})} \le c_2,$$

where c_1 and c_2 only depend on $\boldsymbol{a}$ and $\boldsymbol{w}^{(s)}$; in fact, $\boldsymbol{w}^{(s)}$ depends linearly on $\boldsymbol{a}$ through (2.18). ∎

Observe that, in the previous proof, we obtained the following estimate for $\boldsymbol{w} = \boldsymbol{v}/\mathcal{R}$:

$$\|\nabla \boldsymbol{w}\|_{L^2(\Omega_{h,\theta})} \le \|\nabla \boldsymbol{a}\|_{L^2(\Omega_D)} + \frac{c_2 \mathcal{R}}{1 - c_1 \mathcal{R}},$$

where c_1 and c_2 only depend on $\boldsymbol{a}$. This gives further insight into (2.16).

3. Lift and torque.

3.1. Basic properties.

With a solution $(\boldsymbol{u}, p)$ of (2.11) in hand, it is standard to define the *lift* and *torque* by

$$\mathcal{L}(h,\theta,\mathcal{R}) := -\boldsymbol{e}_2 \cdot \int_{S_{h,\theta}} \boldsymbol{T}(\boldsymbol{u},p)\cdot \boldsymbol{n}, \quad \mathcal{T}(h,\theta,\mathcal{R}) := -\int_{S_{h,\theta}} (\boldsymbol{x}-\boldsymbol{h})^{\perp} \cdot (\boldsymbol{T}(\boldsymbol{u},p)\cdot \boldsymbol{n}). \tag{3.1}$$

However, the formulas in (3.1) are rigorous only if $\boldsymbol{T}(\boldsymbol{u},p)\cdot\boldsymbol{n} \in L^1(S_{h,\theta})$, a condition which is guaranteed, for instance, if $(\boldsymbol{u},p) \in H^2_{loc}(\Omega_{h,\theta}) \times H^1_{loc}(\Omega_{h,\theta})$. In our case $S_{h,\theta}$ is only Lipschitz, and this regularity is not ensured so that the integrals in (3.1) should be read as dualities; see, for instance, [21]. We will not go deeper into this discussion both because we prefer to maintain a simpler notation and because we will compute $\mathcal{L}$ and $\mathcal{T}$ with alternative formulas. To this end, for $j = 1,2,3$, we consider the following Stokes flows, first introduced in [26]:

$$\begin{gathered} \operatorname{div} \boldsymbol{T}(\boldsymbol{w}^j, P^j) = 0,\ \operatorname{div} \boldsymbol{w}^j = 0 \quad \text{in } \Omega_{h,\theta}, \\ \boldsymbol{w}^j|_{S_{h,\theta}} = \boldsymbol{k}_j,\ \boldsymbol{w}^j|_{\partial \mathcal{C}_L} = 0 = \lim_{|x_1|\to+\infty} \boldsymbol{w}^j(x_1,x_2), \end{gathered} \tag{3.2}$$

with

$$\boldsymbol{k}_j = \boldsymbol{e}_j \text{ for } j = 1,2 \quad \text{and} \quad \boldsymbol{k}_3 := \boldsymbol{x}^{\perp} = (-x_2, x_1). \tag{3.3}$$

Then we prove the following.

PROPOSITION 3.1. *Let $(h,\theta) \in A_d$. For $j = 1,2,3$, the problem* (3.2) *admits a unique weak solution $(\boldsymbol{w}^j, P^j) = (\boldsymbol{w}^j_{(h,\theta)}, P^j_{(h,\theta)}) \in H^1(\Omega_{h,\theta}) \times L^2_{loc}(\Omega_{h,\theta})/\mathbb{R}$ and $(\boldsymbol{w}^j, P^j) \in C^\infty\big(\overline{\Omega_{h,\theta}} \setminus \{V^1_{h,\theta}, V^2_{h,\theta}, V^3_{h,\theta}, V^4_{h,\theta}\}\big)$; see Remark* 2.3. *Moreover, after setting*

$$\varepsilon = \begin{cases} \frac{\operatorname{dist}(B_{h,\theta}, \partial \mathcal{C}_L)}{2} & \text{if } \operatorname{dist}(B_{h,\theta}, \partial \mathcal{C}_L) \le 2, \\ 1 & \text{otherwise,} \end{cases}$$

there exist constants $c_j = c_j(L,D) > 0$ (for $j = 1,2,3$ and independent of ε), such that

$$\|\nabla \boldsymbol{w}^j\|_{L^2(\Omega_{h,\theta})} \le c_j \varepsilon^{-\frac{3}{2}}. \tag{3.4}$$

Furthermore, (3.1) *can be equivalently (and rigorously) rewritten as*

$$\begin{aligned} \mathcal{L}(h,\theta,\mathcal{R}) &= -\int_{\Omega_{h,\theta}} \nabla \boldsymbol{u} : \nabla \boldsymbol{w}^2 - \int_{\Omega_{h,\theta}} \boldsymbol{u}\cdot\nabla\boldsymbol{u}\cdot\boldsymbol{w}^2, \\ \mathcal{T}(h,\theta,\mathcal{R}) &= -\int_{\Omega_{h,\theta}} \nabla \boldsymbol{u} : (h\nabla \boldsymbol{w}^1 + \nabla \boldsymbol{w}^3) - \int_{\Omega_{h,\theta}} \boldsymbol{u}\cdot\nabla\boldsymbol{u}\cdot(h\boldsymbol{w}^1 + \boldsymbol{w}^3). \end{aligned}$$

Proof. Existence, uniqueness, and regularity for problems (3.2) are well-known, see e.g. [15, Chapter VI]. To get the a priori bounds (3.4), we take a smooth cut-off function ϕ such that

$$\phi(\boldsymbol{x})=\phi(x_1,x_2)=\begin{cases}1 & \text{in } \left(-D-\frac{\varepsilon}{2},D+\frac{\varepsilon}{2}\right)\times\left(-L+\frac{3\varepsilon}{2},L-\frac{3\varepsilon}{2}\right),\\ 0 & \text{in } \mathbb{R}\times(-L,L)\setminus(-D-\varepsilon,D+\varepsilon)\times(-L+\varepsilon,L-\varepsilon),\end{cases} \tag{3.5}$$

where, as above, $D\in(\sqrt{d^2+1},L)$ is the radius of an open ball centered at 0 and containing $B_{0,\theta}$ for all $|\theta|<\frac{\pi}{2}$ and $0<\varepsilon<\frac{2L}{3}$ is fixed. We set $K=\operatorname{supp}\phi$ and

$$\boldsymbol{\Phi}^1(\boldsymbol{x}):=((x_2\phi)_{x_2},-(x_2\phi)_{x_1}),\quad \boldsymbol{\Phi}^2(\boldsymbol{x}):=(-(x_1\phi)_{x_2},(x_1\phi)_{x_1}). \tag{3.6}$$

Then, for $j=1,2$, we have $\operatorname{supp}\boldsymbol{\Phi}^j\subset(-D-\varepsilon,D+\varepsilon)\times(-L+\varepsilon,L-\varepsilon)$, $\operatorname{div}\boldsymbol{\Phi}^j=0$, and $\boldsymbol{\Phi}^j|_{S_{h,\theta}}=\boldsymbol{e}_j$. Finally, we set

$$\boldsymbol{\Phi}^3(\boldsymbol{x})=\left(-\frac{1}{2}\left(|\boldsymbol{x}|^2\phi\right)_{x_2},\frac{1}{2}\left(|\boldsymbol{x}|^2\phi\right)_{x_1}\right), \tag{3.7}$$

which satisfies $\operatorname{supp}\boldsymbol{\Phi}^3\subset(-D-\varepsilon,D+\varepsilon)\times(-L+\varepsilon,L-\varepsilon)$, $\operatorname{div}\boldsymbol{\Phi}^3=0$, and $\boldsymbol{\Phi}^3|_{S_{h,\theta}}=(-x_2,x_1)$.

The a priori bounds (3.4) for $\boldsymbol{w}^j$ then follow by adapting the proof of [5, Lemma 2] and by exploiting the auxiliary fields $\boldsymbol{\Phi}^j$ defined in (3.6) and in (3.7). Some computations yield

$$\|\boldsymbol{\Phi}^j\|_{L^2(K)}\le c_0\varepsilon^{-1/2},\quad \|\nabla\boldsymbol{\Phi}^j\|_{L^2(K)}\le c_1\varepsilon^{-3/2}$$

with $c_0=c_0(L,D)$ and $c_1=c_1(L,D)$ independent of ε. On the other hand, by multiplying both sides of (3.2) by $\boldsymbol{w}^j-\boldsymbol{\Phi}^j$, integrating over $\Omega_{h,\theta}$, and recalling that $\operatorname{div}\boldsymbol{\Phi}^j=0$ we get

$$\|\nabla\boldsymbol{w}^j\|^2_{L^2(\Omega_{h,\theta})}=\int_{\Omega_{h,\theta}}|\nabla\boldsymbol{w}^j|^2=\int_K\nabla\boldsymbol{w}^j:\nabla\boldsymbol{\Phi}^j\le c_1\varepsilon^{-3/2}\|\nabla\boldsymbol{w}^j\|_{L^2(\Omega_{h,\theta})},$$

which proves the claimed inequalities when $j=1,2$. The proof of the estimate (3.4) for $\boldsymbol{w}^3$ follows with similar arguments by exploiting the auxiliary function $\boldsymbol{\Phi}^3$.

Consider the unique solution $(\boldsymbol{w}^j,P^j)=(\boldsymbol{w}^j_{(h,\theta)},P^j_{(h,\theta)})$ of (3.2), which is smooth in $\Omega_{h,\theta}$; for simplicity, we omit emphasizing h and θ. Moreover, by arguing as in [15, sections VI.1 and VI.2] we know that there exist $C,\nu>0$ and $P^j_\pm\in\mathbb{R}$ such that

$$\begin{aligned}&|D^\alpha\boldsymbol{w}^j(\boldsymbol{x})|+|D^\alpha(P^j(\boldsymbol{x})-P^j_+)|\le Ce^{-\nu x_1} && \forall\boldsymbol{x}\in\Omega_{h,\theta}\text{ such that } x_1\gg d,\\ &|D^\alpha\boldsymbol{w}^j(\boldsymbol{x})|+|D^\alpha(P^j(\boldsymbol{x})-P^j_-)|\le Ce^{\nu x_1} && \forall\boldsymbol{x}\in\Omega_{h,\theta}\text{ such that } x_1\ll -d\end{aligned} \tag{3.8}$$

for every $|\alpha|\ge 0$. In view of the regularity stated in Proposition 2.2, we may multiply (2.11) by $\boldsymbol{w}^j$ and integrate over $\Omega_{h,\theta}$ to formally obtain (recall that the integrals over $S_{h,\theta}$ are, in fact, dualities)

$$\begin{aligned}0&=-\int_{\Omega_{h,\theta}}\boldsymbol{w}^j\cdot\operatorname{div}\boldsymbol{T}(\boldsymbol{u},p)+\int_{\Omega_{h,\theta}}\boldsymbol{u}\cdot\nabla\boldsymbol{u}\cdot\boldsymbol{w}^j\\ &=\int_{\Omega_{h,\theta}}\nabla\boldsymbol{u}:\nabla\boldsymbol{w}^j-\int_{S_{h,\theta}}\boldsymbol{w}^j\cdot(\boldsymbol{T}(\boldsymbol{u},p)\cdot\boldsymbol{n})+\int_{\Omega_{h,\theta}}\boldsymbol{u}\cdot\nabla\boldsymbol{u}\cdot\boldsymbol{w}^j,\end{aligned}$$

which, recalling (3.3), leads to the conclusion that

$$\int_{S_{h,\theta}} \boldsymbol{k}_j \cdot (\boldsymbol{T}(\boldsymbol{u},p)\cdot \boldsymbol{n}) = \int_{\Omega_{h,\theta}} \nabla \boldsymbol{u} : \nabla \boldsymbol{w}^j + \int_{\Omega_{h,\theta}} \boldsymbol{u}\cdot\nabla\boldsymbol{u}\cdot\boldsymbol{w}^j.$$

All the integration by parts are justified by (3.8). ∎

Then we prove some useful symmetry properties of $\mathcal{L}$ and $\mathcal{T}$. In particular, we show that if $h=0$ or $\theta=0$, symmetry arguments simplify the formulas in Proposition 3.1 and reduce them to the formulas used in [5, 6] for models with a unique degree of freedom.

PROPOSITION 3.2. *Let $\gamma>0$ be as in Proposition 2.2 and let $0\le\mathcal{R}<\gamma$. Then*

$$\mathcal{L}(-h,-\theta,\mathcal{R}) = -\mathcal{L}(h,\theta,\mathcal{R}), \quad \mathcal{T}(-h,-\theta,\mathcal{R}) = -\mathcal{T}(h,\theta,\mathcal{R}) \qquad \forall (h,\theta)\in A_d \tag{3.9}$$

and, therefore,

$$\mathcal{L}(0,0,\mathcal{R}) = \mathcal{T}(0,0,\mathcal{R}) = 0 \qquad \forall \mathcal{R}\in[0,\gamma). \tag{3.10}$$

Let $\boldsymbol{w}^j$ be the unique solution to (3.2) for $j=2,3$; see Proposition 3.1. Then

$$\mathcal{L}(h,0,\mathcal{R}) = -\int_{\Omega_{h,0}} \boldsymbol{u}\cdot\nabla\boldsymbol{u}\cdot\boldsymbol{w}^2 \qquad \textit{and} \qquad \mathcal{T}(0,\theta,\mathcal{R}) = -\int_{\Omega_{0,\theta}} \boldsymbol{u}\cdot\nabla\boldsymbol{u}\cdot\boldsymbol{w}^3 \tag{3.11}$$

for all $|h|<L-1$ and all $|\theta|<\frac{\pi}{2}$, respectively.

Proof. Let $(h,\theta)\in A_d$. By Proposition 2.2, problem (2.11) in $\Omega_{h,\theta}$ admits a unique weak solution $(\boldsymbol{u},p)=\big(\boldsymbol{u}_{(h,\theta)},p_{(h,\theta)}\big)$, with $\boldsymbol{u}(x_1,x_2)=\big(u_1^{(h,\theta)}(x_1,x_2),u_2^{(h,\theta)}(x_1,x_2)\big)$.

By symmetry, we know that $(-h,-\theta)\in A_d$ and, using again Proposition 2.2, also the problem (2.11) in $\Omega_{-h,-\theta}$ admits a unique weak solution $\big(\boldsymbol{u}_{(-h,-\theta)},p_{(-h,-\theta)}\big)$. With some computations, one can show that

$$\boldsymbol{v}(x_1,x_2) := \Big(u_1(x_1,-x_2),-u_2(x_1,-x_2)\Big), \quad q(x_1,x_2)=p(x_1,-x_2)$$

weakly solves (2.11) in $\Omega_{-h,-\theta}$. By uniqueness, this proves that $\boldsymbol{u}_{(-h,-\theta)}=\boldsymbol{v}$ and $p_{(-h,-\theta)}=q$, namely,

$$\begin{aligned}
&\boldsymbol{u}_{(-h,-\theta)}(\boldsymbol{x}) = \Big([u_{(h,\theta)}]_1(x_1,-x_2),-[u_{(h,\theta)}]_2(x_1,-x_2)\Big) \quad \text{and}\\
&p_{(-h,-\theta)}(\boldsymbol{x}) = p_{(h,\theta)}(x_1,-x_2).
\end{aligned}$$

By formally using these symmetry properties in (3.1), we obtain (3.9). However, we recall that (3.1) is not rigourous because the integral should be replaced by a duality. In order to make (3.9) rigorous, we can use Proposition 3.1 and notice that similar arguments yield

$$\begin{aligned}
&\boldsymbol{w}^1_{(-h,-\theta)}(\boldsymbol{x}) = \Big([w^1_{(h,\theta)}]_1(x_1,-x_2),-[w^1_{(h,\theta)}]_2(x_1,-x_2)\Big) \quad \text{and}\\
&P^1_{(-h,-\theta)}(\boldsymbol{x}) = P^1_{(h,\theta)}(x_1,-x_2)
\end{aligned}$$

and

$$\begin{aligned}
&\boldsymbol{w}^j_{(-h,-\theta)}(\boldsymbol{x}) = \Big(-[w^j_{(h,\theta)}]_1(x_1,-x_2),[w^j_{(h,\theta)}]_2(x_1,-x_2)\Big) \quad \text{and}\\
&P^j_{(-h,-\theta)}(\boldsymbol{x}) = -P^j_{(h,\theta)}(x_1,-x_2)
\end{aligned}$$

for $j=2,3$. A change of variables, combined with the formulas for $\mathcal{L}$ and $\mathcal{T}$ given in Proposition 3.1, then proves (3.9).

By Proposition 3.1, in order to prove (3.11) it suffices to show that

$$\int_{\Omega_{h,0}} \nabla \boldsymbol{u} : \nabla \boldsymbol{w}^2 = 0 \quad \text{and} \quad \int_{\Omega_{0,\theta}} \nabla \boldsymbol{u} : \nabla \boldsymbol{w}^3 = 0. \tag{3.12}$$

For all $R > \sqrt{d^2+1}$ and $(h,\theta) \in A_d$, we set $\Omega^R_{h,\theta} = \Omega_{h,\theta} \cap \{|x_1| < R\}$. By Proposition 3.1 we may multiply (3.2) by $\boldsymbol{u}$ and, upon integration, get (for $j=2,3$)

$$0 = \int_{S_{h,\theta}} \boldsymbol{u} \cdot \mathbf{T}(\boldsymbol{w}^j, P^j) \cdot \boldsymbol{n} + \int_{|x_1|=R} \boldsymbol{u} \cdot \mathbf{T}(\boldsymbol{w}^j, P^j) \cdot \boldsymbol{n} - \int_{\Omega^R_{h,\theta}} \nabla \boldsymbol{u} : \nabla \boldsymbol{w}^j,$$

recalling that the boundary integrals are, in fact, dualities. Since $\boldsymbol{u} = 0$ on $S_{h,\theta}$, this yields

$$\begin{aligned} \int_{\Omega^R_{h,\theta}} \nabla \boldsymbol{u} : \nabla \boldsymbol{w}^j &= \int_{|x_1|=R} \boldsymbol{u} \cdot \mathbf{T}(\boldsymbol{w}^j, P^j) \cdot \boldsymbol{n} \\ &= \int_{x_1=R} \boldsymbol{u} \cdot (\nabla \boldsymbol{w}^j + \nabla \boldsymbol{w}^{j\top}) \cdot \mathbf{e_1} - \int_{x_1=-R} \boldsymbol{u} \cdot (\nabla \boldsymbol{w}^j + \nabla \boldsymbol{w}^{j\top}) \cdot \mathbf{e_1} \\ &\quad + \int_{x_1=-R} (\boldsymbol{u} \cdot \mathbf{e}_1) P^j - \int_{x_1=R} (\boldsymbol{u} \cdot \mathbf{e}_1) P^j. \end{aligned} \tag{3.13}$$

In view of (3.8), the first two terms in (3.13) disappear as $R \to \infty$ since $\partial_{x_1} w^j \to 0$ exponentially fast and $\boldsymbol{u} \to \mathcal{R}\mathsf{v}_P(x_2)\boldsymbol{e}_1$. Moreover,

$$\boldsymbol{u}(\pm R, x_2) \cdot \boldsymbol{e}_1 \to \mathcal{R}\mathsf{v}_P(x_2) \quad \text{and} \quad P^j(-R,x_2) - P^j(R,x_2) \to P^j_- - P^j_+ \quad \text{as} \quad R \to \infty.$$

Therefore, we deduce that

$$\begin{aligned} \int_{\Omega_{h,\theta}} \nabla \boldsymbol{u} : \nabla \boldsymbol{w}^j = \lim_{R\to\infty} \int_{\Omega^R_{h,\theta}} \nabla \boldsymbol{u} : \nabla \boldsymbol{w}^j &= (P^j_- - P^j_+)\mathcal{R} \int_{-L}^{L} \mathsf{v}_P(x_2)\, dx_2 \\ &= (P^j_- - P^j_+)\mathcal{R}\frac{4L}{3}, \end{aligned}$$

where we used the explicit form of v_P in (2.2). Hence, (3.12) follows if we prove that $P^j_- = P^j_+$ when $\theta = 0$ ($j=2$) or $h=0$ ($j=3$).

Let $\theta = 0$ and let $(\boldsymbol{w}^2, P^2)$ be the unique solution to (3.2) for $j=2$ in $\Omega_{h,0}$. By exploiting the symmetries of $\Omega_{h,0}$, we see that also the couple

$$\boldsymbol{v}^2(x_1,x_2) := \big(-w^2_1(-x_1,x_2), w^2_2(-x_1,x_2)\big), \quad Q^2(x_1,x_2) := P^2(-x_1,x_2)$$

solves (3.2). By uniqueness, this shows that P^2 is even with respect to x_1, so that $P^2_+ = P^2_-$.

Let $h=0$ and let $(\boldsymbol{w}^3, P^3)$ be the unique solution to (3.2) for $j=3$ in $\Omega_{0,\theta}$. By exploiting the symmetries of $\Omega_{0,\theta}$, we see that also the couple

$$\boldsymbol{v}^3(\boldsymbol{x}) := -\boldsymbol{w}^3(-\boldsymbol{x}), \quad Q^3(\boldsymbol{x}) := P^3(-\boldsymbol{x})$$

solves (3.2). By uniqueness, this shows that $P^3(-\boldsymbol{x}) = P^3(\boldsymbol{x})$, so that $P^3_+ = P^3_-$. ∎

Remark 3.3. The quantities $P_+^j - P_-^j$ are pressure drops that determine the forces for a Stokes flow (for which there is no convection), and it is numerically observed in [10] that the configurations where $h = 0$ and $\theta = 0$ are the only ones for which the torque and the lift (respectively) vanish. This leads to the conjecture that $\int_{\Omega_{h,\theta}} \nabla \boldsymbol{u} : \nabla \boldsymbol{w}^j \neq 0$ also for the Navier–Stokes flow (2.11) if $(h,\theta) \in A_d$ with $h\theta \neq 0$.

Remark 3.3 shows the importance of the solutions $\boldsymbol{w}^j$ to (3.2) for $j = 2, 3$: they allow us to compute the pressure drops that characterize the one-degree-of-freedom configurations. But a careful look at the proof of Proposition 3.1 emphasizes that there is no need to introduce Stokes problems such as (3.2). This is why we conclude this subsection by showing that the auxiliary vector fields (3.6)–(3.7) also allow us to prove further alternative forms of (3.1). This flexibility will be used in section 3.2 since (3.6)–(3.7) can be chosen independently of the position of B close to a reference configuration.

PROPOSITION 3.4. *Let $\chi^j \in H_0^1(\mathcal{C}_L)$ be any vector field such that* div $\chi^j = 0$ *in $\mathcal{C}_L$,* supp$\chi^j \subset \Omega_*$ *and $\chi^j = \boldsymbol{k}_j$ in $\overline{B_{h,\theta}}$ for $j = 1, 2, 3$; see* (3.3) *and Figure* 3. *Then* (3.1) *can be written as*

(3.14)
$$\mathcal{L}(h,\theta,\mathcal{R}) = -\int_{\Omega_{h,\theta}} \nabla \boldsymbol{u} : \nabla \chi^2 - \int_{\Omega_{h,\theta}} \boldsymbol{u} \cdot \nabla \boldsymbol{u} \cdot \chi^2 \qquad \forall (h,\theta) \in A_d,$$

(3.15)
$$\mathcal{T}(h,\theta,\mathcal{R}) = -\int_{\Omega_{h,\theta}} \nabla \boldsymbol{u} : (h\nabla \chi^1 + \nabla \chi^3) - \int_{\Omega_{h,\theta}} \boldsymbol{u} \cdot \nabla \boldsymbol{u} \cdot (h\chi^1 + \chi^3) \qquad \forall (h,\theta) \in A_d.$$

Furthermore, if $\boldsymbol{w} = \boldsymbol{w}^{(s)} + \mathcal{R}\boldsymbol{w}^{(n)}$ is as in Lemma 2.4, *then*

$$\mathcal{L}(h,0,\mathcal{R}) = -\mathcal{R}^2 \int_{\Omega_{h,0}} \nabla \boldsymbol{w}^{(n)} : \nabla \chi^2 - \mathcal{R}^2 \int_{\Omega_{h,0}} \boldsymbol{w} \cdot \nabla \boldsymbol{w} \cdot \chi^2 \qquad \forall |h| < L - 1, \tag{3.16}$$

$$\mathcal{T}(0,\theta,\mathcal{R}) = -\mathcal{R}^2 \int_{\Omega_{0,\theta}} \nabla \boldsymbol{w}^{(n)} : \nabla \chi^3 - \mathcal{R}^2 \int_{\Omega_{0,\theta}} \boldsymbol{w} \cdot \nabla \boldsymbol{w} \cdot \chi^3 \qquad \forall |\theta| < \frac{\pi}{2}. \tag{3.17}$$

Proof. Formulas (3.14)–(3.15) are derived by repeating the arguments of the proof of Proposition 3.1 with $\boldsymbol{w}^j$ replaced by χ^j. Note that supp$\chi^j \cap$ supp$\boldsymbol{a} = \emptyset$; see (2.14). We then use the decomposition of Lemma 2.4, with $\boldsymbol{u} = \boldsymbol{w}$ in suppχ^j, to obtain

$$\mathcal{L}(h,0,\mathcal{R}) = -\mathcal{R}\int_{\Omega_{h,\theta}} \nabla \boldsymbol{w}^{(s)} : \nabla \chi^2 - \mathcal{R}^2 \int_{\Omega_{h,\theta}} \nabla \boldsymbol{w}^{(n)} : \nabla \chi^2 - \mathcal{R}^2 \int_{\Omega_{h,\theta}} \boldsymbol{w} \cdot \nabla \boldsymbol{w} \cdot \chi^2,$$
$$\mathcal{T}(0,\theta,\mathcal{R}) = -\mathcal{R}\int_{\Omega_{h,\theta}} \nabla \boldsymbol{w}^{(s)} : \nabla \chi^3 - \mathcal{R}^2 \int_{\Omega_{h,\theta}} \nabla \boldsymbol{w}^{(n)} : \nabla \chi^3 - \mathcal{R}^2 \int_{\Omega_{h,\theta}} \boldsymbol{w} \cdot \nabla \boldsymbol{w} \cdot \chi^3.$$

We voluntarily did not expand the last terms in these expressions. The proof follows if we show that

$$\int_{\Omega_{h,0}} \nabla \boldsymbol{w}^{(s)} : \nabla \chi^2 = \int_{\Omega_{0,\theta}} \nabla \boldsymbol{w}^{(s)} : \nabla \chi^3 = 0. \tag{3.18}$$

Since $\boldsymbol{w}^{(s)}$ solves (2.18), the vector field $\boldsymbol{w}^\infty := \boldsymbol{w}^{(s)} + \boldsymbol{a}$ satisfies

$$-\operatorname{div}\boldsymbol{T}(\boldsymbol{w}^\infty, p^\infty) = 0,\ \operatorname{div}\boldsymbol{w}^\infty = 0 \quad \text{in } \Omega_{h,\theta},$$
$$\boldsymbol{w}^\infty|_{S_{h,\theta}} = \boldsymbol{w}^\infty|_{\partial\mathcal{C}_L} = 0, \quad \lim_{|x_1|\to+\infty} \boldsymbol{w}^\infty(x_1,x_2) = \mathsf{v}_P(x_2)\boldsymbol{e}_1$$

for some $p^\infty \in L^2_{loc}(\Omega_{h,\theta})$. The lift and torque associated to $\boldsymbol{w}^\infty$ can be computed with the arguments of Propositions 3.1 and 3.4. This shows that

$$\int_{S_{h,\theta}} \boldsymbol{k}_j \cdot \boldsymbol{T}(\boldsymbol{w}^\infty, p^\infty) \cdot \boldsymbol{n} = \int_{\Omega_{h,\theta}} \nabla \boldsymbol{w}^\infty : \nabla \chi^j = \int_{\Omega_{h,\theta}} \nabla \boldsymbol{w}^s : \nabla \chi^j,$$

where the latter equality follows by recalling that $\mathrm{supp}\chi^j \cap \mathrm{supp}\boldsymbol{a} = \emptyset$. Arguing as in Proposition 3.2, namely, by exploiting the symmetry properties of $\boldsymbol{w}^\infty$ and $\boldsymbol{w}^j$, we deduce (3.18). ∎

3.2. Differentiability with respect to h and θ. Our next purpose is to study the regularity of $\mathcal{L}$ and $\mathcal{T}$ and their asymptotic behavior for $\mathcal{R} \to 0$. For simplicity, we will prove the continuity and differentiability of $\mathcal{L}$ and $\mathcal{T}$ at $(h,\theta) = (0,0)$ only. While the very same argument works for any $(h,\theta) \in A_d$, the asymptotics are specific to the configuration $(h,\theta) = (0,0)$.

THEOREM 3.5. *Let $\gamma > 0$ be as in Proposition 2.2. There exist $\gamma_0 \in (0,\gamma]$ and $(h_0,\theta_0) \in A_d$ (with $h_0,\theta_0 > 0$) such that $\mathcal{L},\mathcal{T} \in C^1\big((-h_0,h_0)\times(-\theta_0,\theta_0)\times[0,\gamma_0)\big)$ and*

$$\begin{aligned} &\partial_h \mathcal{L}(h,\theta,0) = \partial_\theta \mathcal{L}(h,\theta,0) = \partial_h \mathcal{T}(h,\theta,0) = \partial_\theta \mathcal{T}(h,\theta,0) = 0 \\ &\qquad \forall (h,\theta) \in (-h_0,h_0)\times(-\theta_0,\theta_0). \end{aligned} \tag{3.19}$$

Even more, there exist $\ell_0, \tau_0 \in \mathbb{R}$ such that

$$\begin{aligned} &\partial_h \mathcal{L}(0,0,\mathcal{R}) = O(\mathcal{R}^2), \quad \partial_\theta \mathcal{L}(0,0,\mathcal{R}) = \ell_0 \mathcal{R} + O(\mathcal{R}^2) \quad \text{as } \mathcal{R} \to 0, \\ &\partial_h \mathcal{T}(0,0,\mathcal{R}) = \tau_0 \mathcal{R} + O(\mathcal{R}^2), \quad \partial_\theta \mathcal{T}(0,0,\mathcal{R}) = O(\mathcal{R}^2) \quad \text{as } \mathcal{R} \to 0. \end{aligned} \tag{3.20}$$

The proof of Theorem 3.5 relies on two lemmas and is given at the end of the subsection. Let $\mathscr{O} \subset \mathscr{A} \subset \Omega_*$ be two open neighborhoods of $B_{0,0}$ so that, for $\boldsymbol{a}$ as in (2.13), we have $\mathrm{supp}\boldsymbol{a} \subset \mathcal{C}_L \setminus \mathscr{A}$ (see (2.14)); compare Figure 4 with Figure 3.

By arguing as in [36, section 4.1] (see also [11, 27]), the following result can be proved.

LEMMA 3.6. *Consider $h(t) = \eta t$ and $\theta(t) = \tau t$ with $\eta, \tau \in \{-1,0,1\}$. For small $T > 0$ there exists a volume-preserving diffeomorphism*

$$\xi(t,\cdot) : \Omega_{0,0} \longrightarrow \Omega_{\eta t, \tau t} \tag{3.21}$$

satisfying, for all $t \in [0,T]$, the following properties:

$$\xi(t,\boldsymbol{y}) = \begin{cases} Q(\tau t)\boldsymbol{y} + (0,\eta t) & \text{if } \boldsymbol{y} \in \mathscr{O}, \\ \boldsymbol{y} & \text{if } \boldsymbol{y} \in \mathcal{C}_L \setminus \mathscr{A}, \end{cases}$$

$$\xi^{-1}(t,\boldsymbol{x}) = \begin{cases} Q(\tau t)^\top \big(\boldsymbol{x} - (0,\eta t)\big) & \text{if } \boldsymbol{x} \in \mathscr{O}, \\ \boldsymbol{x} & \text{if } \boldsymbol{x} \in \mathcal{C}_L \setminus \mathscr{A}, \end{cases}$$

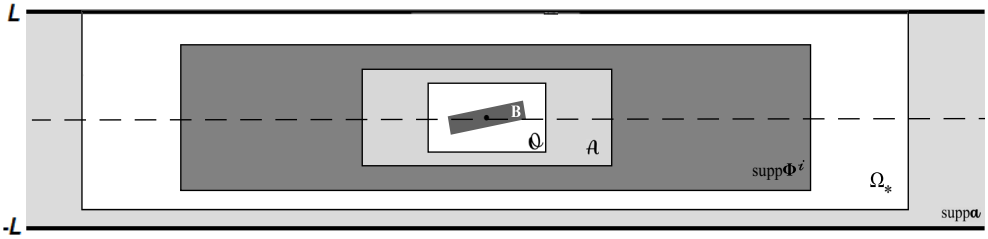

FIG. 4. *The regions $\mathscr{O}$ and $\mathscr{A}$ in the definition of the diffeomorphism ξ.*

with the matrix Q defined as in (2.3). *Furthermore, we have that $\xi, \dot{\xi} \in \mathcal{C}^\infty(\Omega_{0,0})$ for all $t \in [0,T]$ (here $\dot{\xi} = \partial\xi/\partial t$) and*

$$\|\xi(t,\boldsymbol{y}) - \boldsymbol{y}\|_{\mathcal{C}^1(0,T;W^{2,\infty}(\mathcal{C}_L;\mathcal{C}_L))} \le Ct \tag{3.22}$$

for some constant $C > 0$ independent of $t \in [0,T]$.

Using Lemma 3.6 we can rewrite the weak formulation (2.15) in the reference configuration $\Omega_{0,0}$. To this end, for any vector field $\boldsymbol{z}$ defined as in $\Omega_{\eta t,\tau t}$ we put

$$\widehat{\boldsymbol{z}}(\boldsymbol{y}) = \boldsymbol{z}(\xi(t,\boldsymbol{y})) \qquad \forall \boldsymbol{y} \in \Omega_{0,0}, \quad \forall t \in [0,T].$$

From now on, we omit the t-dependence to save space and simplify notation. By changing variables in (2.15), we obtain

$$\begin{aligned}\int_{\Omega_{0,0}} \nabla \boldsymbol{v}(\xi(\boldsymbol{y})) : \nabla \boldsymbol{\varphi}(\xi(\boldsymbol{y})) = &\int_{\Omega_{0,0}} (\boldsymbol{v}(\xi(\boldsymbol{y})) + \mathcal{R}\boldsymbol{a}(\xi(\boldsymbol{y}))) \cdot \nabla \boldsymbol{\varphi}(\xi(\boldsymbol{y})) \cdot \boldsymbol{v}(\xi(\boldsymbol{y})) \\ &- \mathcal{R} \int_{\Omega_{0,0}} (\boldsymbol{v}(\xi(\boldsymbol{y})) + \mathcal{R}\boldsymbol{a}(\xi(\boldsymbol{y}))) \cdot \nabla \boldsymbol{a}(\xi(\boldsymbol{y})) \cdot \boldsymbol{\varphi}(\xi(\boldsymbol{y})) \\ &- \mathcal{R} \int_{\Omega_{0,0}} \nabla \boldsymbol{a}(\xi(\boldsymbol{y})) : \nabla \boldsymbol{\varphi}(\xi(\boldsymbol{y})) \quad \forall \boldsymbol{\varphi} \in V_{h,\theta}.\end{aligned} \tag{3.23}$$

Recall that ξ is volume-preserving so that the determinant of the Jacobian $\boldsymbol{J}$ is 1. Then we have $\nabla \boldsymbol{z}(\xi(\boldsymbol{y})) = \nabla \widehat{\boldsymbol{z}}(\boldsymbol{y}) \boldsymbol{J}^{-1}$. Let $\boldsymbol{A}$ be the symmetric matrix $\boldsymbol{J}^{-1} \left(\boldsymbol{J}^{-1}\right)^\top$ so that, for small t, both $\boldsymbol{A}$ and $\boldsymbol{J}$ are close to the identity in view of (3.22). Then, since $\xi = \boldsymbol{I}$ where $\boldsymbol{a} \neq \boldsymbol{0}$, we have $\widehat{\boldsymbol{a}} = \boldsymbol{a}$ and (3.23) becomes (summation over repeated indexes is intended)

$$\begin{aligned}\int_{\Omega_{0,0}} \boldsymbol{A}_{ij} \partial_i \widehat{\boldsymbol{v}}_k \partial_j \widehat{\boldsymbol{\varphi}}_k = &\int_{\Omega_{0,0}} \left(\widehat{\boldsymbol{v}} \cdot \nabla \widehat{\boldsymbol{\varphi}} \boldsymbol{J}^{-1}\right) \cdot \widehat{\boldsymbol{v}} + \mathcal{R} \int_{\Omega_{0,0}} (\boldsymbol{a} \cdot \nabla \widehat{\boldsymbol{\varphi}}) \cdot \widehat{\boldsymbol{v}} \\ &- \mathcal{R} \int_{\Omega_{0,0}} (\widehat{\boldsymbol{v}} + \mathcal{R}\boldsymbol{a}) \cdot \nabla \boldsymbol{a} \cdot \widehat{\boldsymbol{\varphi}} - \mathcal{R} \int_{\Omega_{0,0}} \nabla \boldsymbol{a} : \nabla \widehat{\boldsymbol{\varphi}}.\end{aligned}$$

Observe that if $\operatorname{div} \boldsymbol{\varphi} = 0$ in $\Omega_{h,\theta}$, then $\operatorname{div} \widehat{\boldsymbol{\varphi}} \neq 0$ in $\Omega_{0,0}$ but $\operatorname{div} \overline{\boldsymbol{\varphi}} = 0$ in $\Omega_{0,0}$, where $\overline{\boldsymbol{\varphi}} = \boldsymbol{J}^{-1} \widehat{\boldsymbol{\varphi}}$ (we use the same notation for all the other functions). We then rewrite the last formula as

$$\begin{aligned}\int_{\Omega_{0,0}} \boldsymbol{A}_{ij} \partial_i \left(\boldsymbol{J}\overline{\boldsymbol{v}}\right)_k \partial_j \left(\boldsymbol{J}\overline{\boldsymbol{\varphi}}\right)_k = &\int_{\Omega_{0,0}} \boldsymbol{J}\overline{\boldsymbol{v}} \cdot \nabla \left(\boldsymbol{J}\overline{\boldsymbol{\varphi}}\right) \cdot \overline{\boldsymbol{v}} + \mathcal{R} \int_{\Omega_{0,0}} \boldsymbol{a} \cdot \nabla \overline{\boldsymbol{\varphi}} \cdot \overline{\boldsymbol{v}} \\ &- \mathcal{R} \int_{\Omega_{0,0}} (\overline{\boldsymbol{v}} + \mathcal{R}\boldsymbol{a}) \cdot \nabla \boldsymbol{a} \cdot \overline{\boldsymbol{\varphi}} - \mathcal{R} \int_{\Omega_{0,0}} \nabla \boldsymbol{a} : \nabla \overline{\boldsymbol{\varphi}}\end{aligned} \tag{3.24}$$

for every $\overline{\boldsymbol{\varphi}} \in V_{0,0}$ (recall that $\widehat{\boldsymbol{v}} = \overline{\boldsymbol{v}} = \boldsymbol{v}$ and $\widehat{\boldsymbol{\varphi}} = \overline{\boldsymbol{\varphi}} = \boldsymbol{\varphi}$ on $\operatorname{supp} \boldsymbol{a}$). Formula (3.24) is the weak formulation (2.15) in the reference configuration $\Omega_{0,0}$.

As in subsection 2.3, we write $\overline{\boldsymbol{v}} = \mathcal{R}\overline{\boldsymbol{w}}$, where $\overline{\boldsymbol{w}}$ satisfies

$$\begin{aligned}\int_{\Omega_{0,0}} \boldsymbol{A}_{ij} \partial_i \left(\boldsymbol{J}\overline{\boldsymbol{w}}\right)_k \partial_j \left(\boldsymbol{J}\overline{\boldsymbol{\varphi}}\right)_k = &\mathcal{R} \int_{\Omega_{0,0}} \boldsymbol{J}\overline{\boldsymbol{w}} \cdot \nabla \left(\boldsymbol{J}\overline{\boldsymbol{\varphi}}\right) \cdot \overline{\boldsymbol{w}} + \mathcal{R} \int_{\Omega_{0,0}} \boldsymbol{a} \cdot \nabla \overline{\boldsymbol{\varphi}} \cdot \overline{\boldsymbol{w}} \\ &- \mathcal{R} \int_{\Omega_{0,0}} (\overline{\boldsymbol{w}} + \boldsymbol{a}) \cdot \nabla \boldsymbol{a} \cdot \overline{\boldsymbol{\varphi}} - \int_{\Omega_{0,0}} \nabla \boldsymbol{a} : \nabla \overline{\boldsymbol{\varphi}} \quad \forall \overline{\boldsymbol{\varphi}} \in V_{0,0},\end{aligned} \tag{3.25}$$

which is an equivalent formulation of (2.17). Next we prove the following.

LEMMA 3.7. *Let $\gamma>0$ be as in Proposition* 2.2. *There exist $\gamma_0\in(0,\gamma]$, $(h_0,\theta_0)\in A_d$ (with $h_0,\theta_0>0$), $0<T_0\le T$, and $0\le\gamma_0\le\gamma$ such that the solution maps $S:(-h_0,h_0)\times(-\theta_0,\theta_0)\times[0,\gamma_0)\to V_{h,\theta}$ and $\overline{S}:[0,\gamma_0)\times[0,T_0]\to V_{0,0}$ defined by*

$$S(h,\theta,\mathcal{R})=\boldsymbol{w}_{\mathcal{R}}\quad\text{and}\quad\overline{S}(\mathcal{R},t)=\overline{\boldsymbol{w}}_{\mathcal{R}}$$

are C^1; in particular, $\dot{\overline{\boldsymbol{w}}}_0=0$. Here $\boldsymbol{w}_{\mathcal{R}}$ (resp., $\overline{\boldsymbol{w}}_{\mathcal{R}}$) is the unique solution of (2.17) *(resp.,* (3.25)*).*

Proof. Let $V_{0,0}^*$ be the dual space of $V_{0,0}$ and G be the map

$$G:([0,\gamma)\times[0,T]\times V_{0,0})\to V_{0,0}^*$$

defined by

(3.26)
$$\begin{aligned}\langle G(\mathcal{R},t,\overline{\boldsymbol{w}}),\overline{\boldsymbol{\varphi}}\rangle=&\int_{\Omega_{0,0}}\boldsymbol{A}_{ij}\partial_i\left(\boldsymbol{J}\overline{\boldsymbol{w}}\right)_k\partial_j\left(\boldsymbol{J}\overline{\boldsymbol{\varphi}}\right)_k-\mathcal{R}\int_{\Omega_{0,0}}\boldsymbol{J}\overline{\boldsymbol{w}}\cdot\nabla\left(\boldsymbol{J}\overline{\boldsymbol{\varphi}}\right)\cdot\overline{\boldsymbol{w}}\\&-\mathcal{R}\int_{\Omega_{0,0}}\boldsymbol{a}\cdot\nabla\overline{\boldsymbol{\varphi}}\cdot\overline{\boldsymbol{w}}+\mathcal{R}\int_{\Omega_{0,0}}(\overline{\boldsymbol{w}}+\boldsymbol{a})\cdot\nabla\boldsymbol{a}\cdot\overline{\boldsymbol{\varphi}}+\int_{\Omega_{0,0}}\nabla\boldsymbol{a}:\nabla\overline{\boldsymbol{\varphi}},\end{aligned}$$

where $\overline{\boldsymbol{\varphi}}\in V_{0,0}$. By definition, $\overline{\boldsymbol{w}}_{\mathcal{R}}\in V_{0,0}$ is the unique weak solution of (3.25) if and only if

$$G(\mathcal{R},t,\overline{\boldsymbol{w}}_{\mathcal{R}})=0.$$

For a given $\overline{\boldsymbol{w}}\in V_{0,0}$, $(\mathcal{R},t)\mapsto G(\mathcal{R},t,\overline{\boldsymbol{w}})$ is C^1 since $\boldsymbol{A}$ and $\boldsymbol{J}$ depend smoothly on t. Let us compute the Gâteaux derivative of $G(\mathcal{R},t,\cdot)$ at a given $\overline{\boldsymbol{w}}\in V_{0,0}$ in the direction $\overline{\boldsymbol{u}}\in V_{0,0}$:

$$\begin{aligned}\langle D_{\overline{\boldsymbol{w}}}G(\mathcal{R},t,\overline{\boldsymbol{w}})(\overline{\boldsymbol{u}}),\overline{\boldsymbol{\varphi}}\rangle=&\int_{\Omega_{0,0}}\boldsymbol{A}_{ij}\partial_i\left(\boldsymbol{J}\overline{\boldsymbol{u}}\right)_k\partial_j\left(\boldsymbol{J}\overline{\boldsymbol{\varphi}}\right)_k-\mathcal{R}\int_{\Omega_{0,0}}\boldsymbol{J}\overline{\boldsymbol{u}}\cdot\nabla\left(\boldsymbol{J}\overline{\boldsymbol{\varphi}}\right)\cdot\overline{\boldsymbol{w}}\\&-\mathcal{R}\int_{\Omega_{0,0}}\boldsymbol{J}\overline{\boldsymbol{w}}\cdot\nabla\left(\boldsymbol{J}\overline{\boldsymbol{\varphi}}\right)\cdot\overline{\boldsymbol{u}}-\mathcal{R}\int_{\Omega_{0,0}}\boldsymbol{a}\cdot\nabla\overline{\boldsymbol{\varphi}}\cdot\overline{\boldsymbol{u}}\\&+\mathcal{R}\int_{\Omega_{0,0}}\overline{\boldsymbol{u}}\cdot\nabla\boldsymbol{a}\cdot\overline{\boldsymbol{\varphi}}.\end{aligned}\tag{3.27}$$

To show that G is Fréchet differentiable, it is enough to estimate the quadratic term

$$\left|\int_{\Omega_{0,0}}\boldsymbol{J}\overline{\boldsymbol{u}}\cdot\nabla\left(\boldsymbol{J}\overline{\boldsymbol{\varphi}}\right)\cdot\overline{\boldsymbol{u}}\right|\le\|\boldsymbol{J}\overline{\boldsymbol{u}}\|_{L^4(\Omega_{0,0})}\|\overline{\boldsymbol{u}}\|_{L^4(\Omega_{0,0})}\|\nabla(\boldsymbol{J}\overline{\varphi})\|_{L^2(\Omega_{0,0})}.$$

By (3.22) and using the Ladyzhenskaya and Poincaré inequalities, we infer that for $t\in[0,T]$

$$\left|\int_{\Omega_{0,0}}\boldsymbol{J}\overline{\boldsymbol{u}}\cdot\nabla\left(\boldsymbol{J}\overline{\boldsymbol{\varphi}}\right)\cdot\overline{\boldsymbol{u}}\right|\le C\|\nabla\overline{\boldsymbol{u}}\|_{L^2(\Omega_{0,0})}^2\|\nabla\overline{\boldsymbol{\varphi}}\|_{L^2(\Omega_{0,0})}.$$

By similar arguments one obtains that $G\in C^1([0,\gamma)\times[0,T]\times V_{0,0};V_{0,0}^*)$. Observe that

$$D_{\overline{\boldsymbol{w}}}G(0,0,\overline{\boldsymbol{w}})(\overline{\boldsymbol{u}})(\overline{\boldsymbol{\varphi}})=\int_{\Omega_{0,0}}\nabla\overline{\boldsymbol{u}}:\nabla\overline{\boldsymbol{\varphi}}$$

and, since for every $\boldsymbol{f} \in V_{0,0}^*$, there exists a unique weak solution of the Stokes equation

$$\int_{\Omega_{0,0}} \nabla \overline{\boldsymbol{u}} : \nabla \overline{\boldsymbol{\varphi}} = \langle \boldsymbol{f}, \overline{\boldsymbol{\varphi}} \rangle \quad \forall \overline{\boldsymbol{\varphi}} \in V_{0,0},$$

the map $D_{\overline{\boldsymbol{w}}} G(0,0,\boldsymbol{w}_0)$ is an isomorphism. Then the Implicit Function Theorem implies that the unique solution $\overline{\boldsymbol{w}}_{\mathcal{R}}$ of (3.25) is C^1 in a neighborhood $[0,\gamma_0) \times [0,T_0)$ of $(0,0)$. Since the mappings involved are smooth, the same conclusion follows for $\boldsymbol{w}_{\mathcal{R}} = \boldsymbol{J}\overline{\boldsymbol{w}}_{\mathcal{R}}(\xi^{-1}(\boldsymbol{y}))$.

The Implicit Function Theorem also implies that

$$\dot{G}(\mathcal{R}, t, \overline{\boldsymbol{w}}_{\mathcal{R}}) + D_{\overline{\boldsymbol{w}}_{\mathcal{R}}} G(\mathcal{R}, t, \overline{\boldsymbol{w}}_{\mathcal{R}})(\dot{\overline{\boldsymbol{w}}}_{\mathcal{R}}) = 0, \tag{3.28}$$

that is,

$$\begin{aligned}
&\int_{\Omega_{0,0}} \boldsymbol{A}_{ij} \partial_i \left(\boldsymbol{J} \dot{\overline{\boldsymbol{w}}}_{\mathcal{R}} \right)_k \partial_j \left(\boldsymbol{J} \overline{\boldsymbol{\varphi}} \right)_k \\
&\quad = \mathcal{R} \int_{\Omega_{0,0}} \Big[\boldsymbol{J} \dot{\overline{\boldsymbol{w}}}_{\mathcal{R}} \cdot \nabla (\boldsymbol{J} \overline{\boldsymbol{\varphi}}) \cdot \overline{\boldsymbol{w}}_{\mathcal{R}} + (\boldsymbol{J} \overline{\boldsymbol{w}}_{\mathcal{R}} + \boldsymbol{a}) \cdot \nabla (\boldsymbol{J} \overline{\boldsymbol{\varphi}}) \cdot \dot{\overline{\boldsymbol{w}}}_{\mathcal{R}} - \dot{\overline{\boldsymbol{w}}}_{\mathcal{R}} \cdot \nabla \boldsymbol{a} \cdot \overline{\boldsymbol{\varphi}} \Big] \\
&\qquad - \int_{\Omega_{0,0}} \dot{\boldsymbol{A}}_{ij} \partial_i \left(\boldsymbol{J} \overline{\boldsymbol{w}}_{\mathcal{R}} \right)_k \partial_j \left(\boldsymbol{J} \overline{\boldsymbol{\varphi}} \right)_k - \int_{\Omega_{0,0}} \boldsymbol{A}_{ij} \partial_i (\dot{\boldsymbol{J}} \overline{\boldsymbol{w}}_{\mathcal{R}})_k \partial_j \left(\boldsymbol{J} \overline{\boldsymbol{\varphi}} \right)_k \\
&\qquad - \int_{\Omega_{0,0}} \boldsymbol{A}_{ij} \partial_i (\boldsymbol{J} \overline{\boldsymbol{w}}_{\mathcal{R}})_k \partial_j (\dot{\boldsymbol{J}} \overline{\boldsymbol{\varphi}})_k \\
&\qquad - \mathcal{R} \int_{\Omega_{0,0}} \dot{\boldsymbol{J}} \overline{\boldsymbol{w}}_{\mathcal{R}} \cdot \nabla (\boldsymbol{J} \overline{\boldsymbol{\varphi}}) \cdot \overline{\boldsymbol{w}}_{\mathcal{R}} - \mathcal{R} \int_{\Omega_{0,0}} \boldsymbol{J} \overline{\boldsymbol{w}}_{\mathcal{R}} \cdot \nabla (\dot{\boldsymbol{J}} \overline{\boldsymbol{\varphi}}) \cdot \overline{\boldsymbol{w}}_{\mathcal{R}}.
\end{aligned}$$

Since $\dot{G}(0,0,\overline{\boldsymbol{w}}_0) = 0$ and $D_{\overline{\boldsymbol{w}}} G(0,0,\boldsymbol{w}_0)$ is an isomorphism, we conclude that $\dot{\overline{\boldsymbol{w}}}_0 = 0$. ∎

By definition, $\overline{\boldsymbol{v}}_{\mathcal{R}} = \mathcal{R}\overline{\boldsymbol{w}}_{\mathcal{R}}$, so that $\dot{\overline{\boldsymbol{v}}}_0 = 0$. Since $\dot{\overline{\boldsymbol{v}}}_{\mathcal{R}}$ is C^1 with respect to $\mathcal{R}$ and t, we also infer that there exists $C > 0$ such that

$$\| \nabla \dot{\overline{\boldsymbol{v}}}_{\mathcal{R}} \|_{L^2(\Omega_{0,0})} \leq C\mathcal{R} \tag{3.29}$$

for $(\mathcal{R}, t) \in [0,\gamma_0) \times [0,T_0]$. We are now in a position to prove Theorem 3.5.

Proof of Theorem 3.5. We use the formulation of Proposition 3.4 (see (3.14)–(3.15)) with vector fields χ^i $(i = 1,2,3)$ defined as in (3.6)–(3.7) and such that $K := \mathrm{supp}\chi^j \subset \Omega_*$. As in the proof of Lemma 2.4, the solution of (2.11) can be written as $\boldsymbol{u} = \mathcal{R}(\boldsymbol{w} + \boldsymbol{a})$ and, since $K \cap \mathrm{supp}\boldsymbol{a} = \emptyset$, we deduce that

$$\begin{aligned}
&\int_K \boldsymbol{u} \cdot \nabla \boldsymbol{u} \cdot \chi^i = \mathcal{R}^2 \int_K (\boldsymbol{w} + \boldsymbol{a}) \cdot \nabla (\boldsymbol{w} + \boldsymbol{a}) \cdot \chi^i = \mathcal{R}^2 \int_K \boldsymbol{w} \cdot \nabla \boldsymbol{w} \cdot \chi^i \quad \text{and} \\
&\int_K \nabla \boldsymbol{u} : \nabla \chi^i = \mathcal{R} \int_K \nabla \boldsymbol{w} : \nabla \chi^i.
\end{aligned}$$

To compute the derivatives of the forces, we take $h(t) = \eta t$ and $\theta(t) = \tau t$ with $\eta, \tau \in \{-1, 0, 1\}$. Then $\mathcal{L}$ and $\mathcal{T}$ are functions of t and $\mathcal{R}$ through the formulas

$$\begin{aligned}
\mathcal{L}(h(t), \theta(t), \mathcal{R}) &= -\mathcal{R}^2 \int_K \boldsymbol{w} \cdot \nabla \boldsymbol{w} \cdot \chi^2 - \mathcal{R} \int_K \nabla \boldsymbol{w} : \nabla \chi^2, \\
\mathcal{T}(h(t), \theta(t), \mathcal{R}) &= -\mathcal{R}^2 \int_K \boldsymbol{w} \cdot \nabla \boldsymbol{w} \cdot (\eta t \chi^1 + \chi^3) - \mathcal{R} \int_K \nabla \boldsymbol{w} : (\eta t \nabla \chi^1 + \nabla \chi^3),
\end{aligned}$$

where $\boldsymbol{w}$ is defined by (2.17) with $h(t) = \eta t$ and $\theta(t) = \tau t$. The derivatives (3.19) follow if we prove that the above functions are differentiable with respect to t. To this end, consider the integrals

$$\int_K \boldsymbol{w} \cdot \nabla \boldsymbol{w} \cdot \chi + \int_K \nabla \boldsymbol{w} : \nabla \chi, \tag{3.30}$$

where $\chi = \chi^i$ for some $i = 1, 2, 4$ (with $\chi^4 := \eta t \chi^1 + \chi^3$). To compute the derivative with respect to t, we first write the integrals in the reference configuration $\Omega_{0,0}$ and obtain

$$\int_{\Omega_{0,0} \cap K} \boldsymbol{w}(\xi(\boldsymbol{y})) \cdot \nabla \boldsymbol{w}(\xi(\boldsymbol{y})) \cdot \chi(\xi(\boldsymbol{y})) + \int_{\Omega_{0,0} \cap K} \nabla \boldsymbol{w}(\xi(\boldsymbol{y})) : \nabla \chi(\xi(\boldsymbol{y})).$$

Observe that χ^1 and χ^2 are constant in the set where ξ is not the identity, but not χ^3. We then get

$$\int_{\Omega_{0,0} \cap K} \boldsymbol{J}\overline{\boldsymbol{w}} \cdot \nabla \left(\boldsymbol{J}\overline{\boldsymbol{w}}\right) \cdot \overline{\chi} + \int_{\Omega_{0,0} \cap K} \boldsymbol{A}_{ij} \partial_i \left(\boldsymbol{J}\overline{\boldsymbol{w}}\right)_k \partial_j \left(\boldsymbol{J}\overline{\chi}\right)_k. \tag{3.31}$$

Lemma 3.7 implies that every term in (3.31) is C^1 with respect to t, and we obtain an a priori bound for $\dot{\overline{\boldsymbol{w}}}$ from (3.29). We can therefore use the Lebesgue Theorem and differentiate with respect to t inside the integrals:

$$\begin{aligned}
(3.\dot{3}1) = &\int_{\Omega_{0,0} \cap K} \boldsymbol{J}\dot{\overline{\boldsymbol{w}}} \cdot \nabla(\boldsymbol{J}\overline{\boldsymbol{w}}) \cdot \overline{\chi} + \int_{\Omega_{0,0} \cap K} \overline{\boldsymbol{w}} \cdot \nabla(\boldsymbol{J}\dot{\overline{\boldsymbol{w}}}) \cdot \overline{\chi} + \int_{\Omega_{0,0} \cap K} \boldsymbol{J}\overline{\boldsymbol{w}} \cdot \nabla(\boldsymbol{J}\overline{\boldsymbol{w}}) \cdot \dot{\overline{\chi}} \\
&+ \int_{\Omega_{0,0} \cap K} \dot{\boldsymbol{J}}\overline{\boldsymbol{w}} \cdot \nabla \left(\boldsymbol{J}\overline{\boldsymbol{w}}\right) \cdot \overline{\chi} + \int_{\Omega_{0,0} \cap K} \boldsymbol{J}\overline{\boldsymbol{w}} \cdot \nabla \left(\dot{\boldsymbol{J}}\overline{\boldsymbol{w}}\right) \cdot \overline{\chi} \\
&+ \int_{\Omega_{0,0} \cap K} \dot{\boldsymbol{A}}_{ij} \partial_i \left(\boldsymbol{J}\overline{\boldsymbol{w}}\right)_k \partial_j \left(\boldsymbol{J}\overline{\chi}\right)_k \\
&+ \int_{\Omega_{0,0} \cap K} \boldsymbol{A}_{ij} \partial_i \left(\dot{\boldsymbol{J}}\overline{\boldsymbol{w}}\right)_k \partial_j \left(\boldsymbol{J}\overline{\chi}\right)_k + \int_{\Omega_{0,0} \cap K} \boldsymbol{A}_{ij} \partial_i \left(\boldsymbol{J}\overline{\boldsymbol{w}}\right)_k \partial_j \left(\dot{\boldsymbol{J}}\overline{\chi}\right)_k \\
&+ \int_{\Omega_{0,0} \cap K} \boldsymbol{A}_{ij} \partial_i \left(\boldsymbol{J}\dot{\overline{\boldsymbol{w}}}\right)_k \partial_j \left(\boldsymbol{J}\overline{\chi}\right)_k + \int_{\Omega_{0,0} \cap K} \boldsymbol{A}_{ij} \partial_i \left(\boldsymbol{J}\overline{\boldsymbol{w}}\right)_k \partial_j \left(\boldsymbol{J}\dot{\overline{\chi}}\right)_k.
\end{aligned}$$

All the terms inside the integrals are continuous with respect to t, showing that the integrals defined by (3.30) are C^1 with respect to t.

We therefore deduce the asymptotics (3.20) for $\partial_\theta \mathcal{L}$ and $\partial_h \mathcal{T}$ for some $\ell_0, \tau_0 \in \mathbb{R}$ because $\boldsymbol{w}^{(s)}$ is independent of $\mathcal{R}$; see (2.18). Furthermore, (3.16)–(3.17) prove the remaining asymptotics in (3.20). ∎

Remark 3.8. Since the change of variable (3.21) is C^∞, further smoothness for $\mathcal{L}$ and $\mathcal{T}$ can be proved. Also notice that, by (3.10), any order derivative of $\mathcal{L}$ and $\mathcal{T}$ with respect to $\mathcal{R}$ vanishes at $(h, \theta, \mathcal{R}) = (0, 0, 0)$:

$$\mathcal{L}(0,0,0) = \mathcal{T}(0,0,0) = \mathcal{L}_{\mathcal{R}}(0,0,0) = \mathcal{T}_{\mathcal{R}}(0,0,0) = \mathcal{L}_{\mathcal{R}\mathcal{R}}(0,0,0) = \mathcal{T}_{\mathcal{R}\mathcal{R}}(0,0,0) = \cdots = 0.$$

By exploiting the oddness of $h \mapsto \mathcal{L}(h, 0, \mathcal{R})$ and of $\theta \mapsto \mathcal{T}(0, \theta, \mathcal{R})$ (see (3.9)), one can also obtain the following expression through a formal Taylor expansion of $\mathcal{L}$ as $(h, \mathcal{R}) \to (0, 0)$ and of $\mathcal{T}$ as $(\theta, \mathcal{R}) \to (0, 0)$:

$$\begin{aligned}
\mathcal{L}(h, 0, \mathcal{R}) &= \frac{\partial_{h\mathcal{R}\mathcal{R}} \mathcal{L}(0,0,0)}{2} h\mathcal{R}^2 + o(|h^2 + \mathcal{R}^2|^{3/2}), \\
\mathcal{T}(0, \theta, \mathcal{R}) &= \frac{\partial_{\theta\mathcal{R}\mathcal{R}} \mathcal{T}(0,0,0)}{2} \theta\mathcal{R}^2 + o(|h^2 + \mathcal{R}^2|^{3/2}).
\end{aligned}$$

4. Existence, uniqueness, and stability of the equilibrium configuration for small $\mathcal{R}$. In view of (2.12) and (3.1) we define the following.

DEFINITION 4.1. *Let $\mathcal{R}>0$. Given a solution (u,p) to (2.11), a couple $(h,\theta)\in A_d$ defines an* equilibrium configuration *$B_{h,\theta}$ of the body B if the restoring forces balance the fluid forces, i.e., if*

$$\partial_h F(h,\theta)=\zeta\,\mathcal{L}(h,\theta,\mathcal{R}),\qquad \partial_\theta F(h,\theta)=\varpi\,\mathcal{T}(h,\theta,\mathcal{R}). \tag{4.1}$$

Moreover, the configuration $B_{\overline{h},\overline{\theta}}$ is called stable if there exists $\varrho>0$ such that

$$\begin{aligned}0<|h-\overline{h}|+|\theta-\overline{\theta}|<\varrho \implies (h-\overline{h})\big(\zeta\mathcal{L}(h,\theta,\mathcal{R})-\partial_h F(h,\theta)\big)\\ +(\theta-\overline{\theta})\big(\varpi\mathcal{T}(h,\theta,\mathcal{R})-\partial_\theta F(h,\theta)\big)<0.\end{aligned}$$

It is called unstable otherwise.

In what follows, we are also interested in dealing with a unique degree of freedom by keeping $\theta=0$ (horizontal position of the body), in which case the above definition specializes to the following one.

DEFINITION 4.2. *Let $\mathcal{R}>0$. A couple $(h,0)\in A_d$ defines a* horizontal equilibrium configuration *$B_{h,0}$ of the body B if the vertical restoring force $\partial_h F(h,0)$ balances the lift, i.e., if*

$$\partial_h F(h,0)=\zeta\,\mathcal{L}(h,0,\mathcal{R}). \tag{4.2}$$

Moreover, the horizontal configuration $B_{\overline{h},0}$ is called stable if there exists $\varrho>0$ such that

$$0<|h-\overline{h}|<\varrho \implies (h-\overline{h})\big(\zeta\mathcal{L}(h,0,\mathcal{R})-\partial_h F(h,0)\big)<0.$$

It is unstable otherwise.

We prove the following result.

THEOREM 4.3. *Let $F\in C^2(A_d)$ satisfy (2.6)–(2.9) and let $\gamma>0$ be as in Proposition 2.2. There exists $\mathcal{R}_0(\zeta,\varpi)\in(0,\gamma]$ such that problem (2.11)+(4.1) admits the unique solution $(\boldsymbol{u}_{(h,\theta)},h,\theta)\equiv(\boldsymbol{u}_{(0,0)},0,0)$ for all $\mathcal{R}\in(0,\mathcal{R}_0)$. Moreover, this configuration is stable.*

Proof. By Proposition 2.2 we know that if $\mathcal{R}<\gamma$, then problem (2.11) admits a unique weak solution $(\boldsymbol{u},p)=(\boldsymbol{u}_{(h,\theta)},p_{(h,\theta)})$, which also depends on $\mathcal{R}$, although this will not be emphasized. Using this solution $(\boldsymbol{u},p)$ we build the map $\boldsymbol{\Psi}:A_d\times[0,\gamma)\subset\mathbb{R}^3\to\mathbb{R}^2$ defined by

$$\begin{cases}\Psi_1(h,\theta,\mathcal{R})=\partial_h F(h,\theta)-\zeta\mathcal{L}(h,\theta,\mathcal{R}),\\ \Psi_2(h,\theta,\mathcal{R})=\partial_\theta F(h,\theta)-\varpi\mathcal{T}(h,\theta,\mathcal{R}),\end{cases}$$

where $\mathcal{L}$ and $\mathcal{T}$ are computed through the alternative forms obtained in Proposition 3.1. By continuous dependence (on $\mathcal{R}$) and by exploiting the uniform bound given in Proposition 2.2 (for h and θ), we infer that $\boldsymbol{\Psi}\in C^0(A_d\times[0,\gamma))$. Moreover, the equilibrium conditions (4.1) can be rewritten as

$$\Psi_1(h,\theta,\mathcal{R})=0\quad\text{and}\quad\Psi_2(h,\theta,\mathcal{R})=0. \tag{4.3}$$

Obviously, $\big(\boldsymbol{u}_{(h,\theta)}, p_{(h,\theta)}, h, \theta\big)$ solves (2.11)–(4.1) if and only if $\boldsymbol{\Psi}(h,\theta,\mathcal{R}) = \mathbf{0}$. By (2.6) and (3.10), we know that

$$\boldsymbol{\Psi}(0,0,\mathcal{R}) = \mathbf{0} \quad \forall 0 \le \mathcal{R} < \gamma. \tag{4.4}$$

This proves the existence of at least one equilibrium configuration. Its stability follows if we prove that there exist $\varrho > 0$ and $\mathcal{R}_1(\zeta,\varpi) \in (0,\gamma]$ such that

$$0 < |h| + |\theta| < \varrho,\ \mathcal{R} < \mathcal{R}_1 \implies h\Psi_1(h,\theta,\mathcal{R}) + \theta\Psi_2(h,\theta,\mathcal{R}) > 0.$$

This is a direct consequence of (2.7), (3.10), and Theorem 3.5.

Concerning uniqueness, we have to show that

$$\exists \mathcal{R}_0 > 0 :\ 0 < \mathcal{R} < \mathcal{R}_0 \text{ and } \boldsymbol{\Psi}(h,\theta,\mathcal{R}) = \mathbf{0} \quad \implies \quad (h,\theta) = (0,0). \tag{4.5}$$

We prove (4.5) by studying the behavior of $\boldsymbol{\Psi}$ for all $(h,\theta) \in A_d$. In order to do this, we divide A_d into four subregions A_d^i, $i = 1,\dots,4$; see the sketch in Figure 5.

★ $A_d^1 = \{(h,\theta) \in A_d : 0 \le |h|, |\theta| \le \gamma_1\}$ for some $\gamma_1 > 0$.

From Theorem 3.5 we know that $\Psi \in C^1((-h_0,h_0)\times(-\theta_0,\theta_0)\times[0,\gamma_0))$. On the other hand, Proposition 2.2 yields $\Psi_1(h,\theta,0) = \partial_h F(h,\theta)$ and $\Psi_2(h,\theta,0) = \partial_\theta F(h,\theta)$ for all $(h,\theta) \in (-h_0,h_0)\times(-\theta_0,\theta_0)$. It follows from (4.4), (2.6), and Theorem 3.5 that

$$\boldsymbol{\Psi}(0,0,0) = (0,0) \quad \text{and} \quad \det \frac{\partial \boldsymbol{\Psi}(0,0,0)}{\partial(h,\theta)} = \partial_{hh}F(0,0)\partial_{\theta\theta}F(0,0) = \kappa_1\kappa_2 > 0. \tag{4.6}$$

Therefore, by the Implicit Function Theorem combined with (4.4), we infer that there exists $0 < \gamma_1 < \min\{h_0,\theta_0,\gamma_0\}$ such that $\boldsymbol{\Psi}(h,\theta,\mathcal{R}) \neq \mathbf{0}$ if $0 < |h|, |\theta|, \mathcal{R} < \gamma_1$. This proves (4.5) in A_d^1.

★ $A_d^2 = \{(h,\theta) \in A_d : |h| \ge L - d|\sin\theta| - \cos\theta - \gamma_2\}$ for some $\gamma_2 > 0$.

Let $a > 0$ be the liminf in (2.8). Then there exists $\gamma_2 > 0$ such that if $|h| > L - d|\sin\theta| - \cos\theta - \gamma_2$, there holds

$$|\partial_h F(h,\theta)| > \frac{a}{2(L - \cos\theta - |h| - d|\sin\theta|)^{3/2}}.$$

We set $\boldsymbol{U} = \boldsymbol{u} - \mathcal{R}\mathsf{v}_P\boldsymbol{e}_1$. Then we have

$$\mathcal{L}(h,\theta,\mathcal{R}) = -\int_{\Omega_{h,\theta}} \nabla\boldsymbol{U} : \nabla\boldsymbol{w}^2 - \int_{\Omega_{h,\theta}} \Big(\boldsymbol{U}\cdot\nabla\boldsymbol{U} + \mathcal{R}\boldsymbol{U}\cdot\nabla(\mathsf{v}_P\boldsymbol{e}_1) + \mathcal{R}\mathsf{v}_P\boldsymbol{e}_1\cdot\nabla\boldsymbol{U}\Big)\cdot\boldsymbol{w}^2,$$

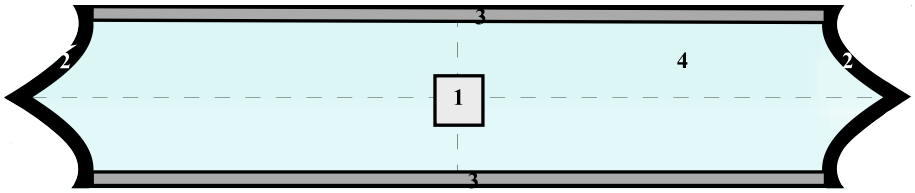

FIG. 5. *Subsets of* $A_d \setminus (0,0)$ *where* $\Psi_1 \neq 0$ *or* $\Psi_2 \neq 0$.

because $\mathsf{v}_P \boldsymbol{e}_1$ is a Stokes solution in $\mathcal{C}_L$ (thus including inside $B_{h,\theta}$). From Proposition 2.2 and (3.4) we infer that

$$\|\nabla \boldsymbol{U}\|_{L^2(\Omega_{h,\theta})} \le C\mathcal{R}(1+\mathcal{R}) \quad \text{and} \quad \|\nabla \boldsymbol{w}^2\|_{L^2(\Omega_{h,\theta})} \le \frac{\overline{C}}{(L-\cos\theta-|h|-d|\sin\theta|)^{3/2}}$$

for some $\overline{C} = \overline{C}(L,d)$ and $C = C(L,d) > 0$. By combining these facts with the Poincaré and Ladyzhenskaya inequalities, we obtain

$$\begin{aligned}\left| \int_{\Omega_{h,\theta}} \Big(\boldsymbol{U}\cdot\nabla\boldsymbol{U} + \mathcal{R}\boldsymbol{U}\cdot\nabla(\mathsf{v}_P\boldsymbol{e}_1) + \mathcal{R}\mathsf{v}_P\boldsymbol{e}_1\cdot\nabla\boldsymbol{U}\Big)\cdot \boldsymbol{w}^2 \right| \\ \le C\mathcal{R}(1+\mathcal{R})\,\|\nabla \boldsymbol{w}^2\|_{L^2(\Omega_{h,\theta})} \\ \le \frac{a}{8\zeta(L-\cos\theta-|h|-d|\sin\theta|)^{3/2}}\end{aligned}$$

for some $C>0$. In turn, we infer that

$$|\Psi_1(h,\theta,\mathcal{R})| > \frac{a}{4(L-\cos\theta-|h|-d|\sin\theta|)^{3/2}} \qquad \forall (h,\theta)\in A_d^2,$$

and, in turn, that $\boldsymbol{\Psi}(h,\theta,\mathcal{R}) \neq \boldsymbol{0}$ for $(h,\theta)\in A_d^2$, provided that $0<\mathcal{R}<\gamma_2$.

★ $$A_d^3 = \left\{ (h,\theta)\in A_d : |h| < L - d|\sin\theta| - \cos\theta - \gamma_2,\ |\theta| \ge \frac{\pi}{2} - \gamma_3 \right\} \text{ for some } \gamma_3>0.$$

By arguing as for the region A_d^2, we obtain

$$\begin{aligned}\Big|\mathcal{T}(h,\theta,\mathcal{R})\Big| = \Bigg| \int_{\Omega_{h,\theta}} \big(\nabla\boldsymbol{U} : \nabla(h\boldsymbol{w}^1 + \boldsymbol{w}^3) \\ + \Big(\boldsymbol{U}\cdot\nabla\boldsymbol{U} + \mathcal{R}\boldsymbol{U}\cdot\nabla(\mathsf{v}_P\boldsymbol{e}_1) + \mathcal{R}\mathsf{v}_P\boldsymbol{e}_1\cdot\nabla\boldsymbol{U}\Big)\cdot(h\boldsymbol{w}^1+\boldsymbol{w}^3)\Big) \Bigg| \\ \le \frac{\overline{K}}{\gamma_2^{3/2}}\end{aligned}$$

for $\overline{K}>0$ independent of h,θ and $\mathcal{R}<\gamma$. Then, by exploiting (2.9), we deduce that there exists $\gamma_3 = \gamma_3(\overline{K},\gamma_2) > 0$ such that for all $|\theta| \ge \frac{\pi}{2} - \gamma_3$ there holds

$$|\partial_\theta F(h,\theta)| > \frac{2\varpi\overline{K}}{\gamma_2^{3/2}} \implies |\Psi_2(h,\theta,\mathcal{R})| \ge \frac{\varpi\overline{K}}{\gamma_2^{3/2}}.$$

Therefore, $\boldsymbol{\Psi}(h,\theta,\mathcal{R}) \neq \boldsymbol{0}$ for $(h,\theta)\in A_d^3$.

★ $$A_d^4 = \overline{A_d \setminus \{A_d^1 \cup A_d^2 \cup A_d^3\}}.$$

By (2.7), we know that $|\nabla F(h,\theta)| > 0$ in A_d^4. Hence, by compactness, there exists $M>0$ such that

$$|\nabla F(h,\theta)|^2 \ge M \qquad \forall (h,\theta)\in A_d^4. \tag{4.7}$$

On the other hand, arguing as in the previous cases, we infer that $\mathcal{L}(h,\theta,\mathcal{R}) \to 0$ and $\mathcal{T}(h,\theta,\mathcal{R}) \to 0$ as $\mathcal{R}\to 0$ uniformly with respect to $(h,\theta)\in A_d^4$; therefore there exists $\mathcal{R}_0 \in (0,\gamma]$ such that

$$\zeta^2\mathcal{L}(h,\theta,\mathcal{R})^2 + \varpi^2\mathcal{T}(h,\theta,\mathcal{R})^2 \le \frac{M}{2} \qquad \forall (h,\theta)\in A_d^4,\ \mathcal{R}<\mathcal{R}_0.$$

Combined with (4.7), this shows that (4.3) does not hold if $(h,\theta) \in A_d^4$ and $\mathcal{R} < \mathcal{R}_0$.

Since $A_d = \cup_{i=1}^4 A_d^i$ (see again Figure 5), (4.5) holds and the proof of Theorem 4.3 is complete. ∎

Remark 4.4. Theorem 4.3 states that for small $\mathcal{R}$, the lift and the torque (3.1) are small so that the restoring forces are the dominant contributions to the overall forces acting on the body. This result should be complemented with some information on the number of equilibrium configurations for larger flow rates. Theoretically, this appears a hard open question. In section 6 we tackle this issue numerically; see Numerical Results 6.2, 6.4, 6.3, and 6.9 for multiple equilibria in some simple situations.

Remark 4.5. In a model intended to study the behavior of particles in a fluid, the study of the behavior of the particle close to collision with a wall is certainly much more relevant, and the assumptions (2.8)–(2.9) would not be realistic. We do not intend to address this issue here (see, however, section 8 for a short discussion), but we just observe that if conditions (2.8)–(2.9) are not imposed, then the arguments used in the proof of Theorem 4.3 still lead to a local conclusion. Namely, for any $\varepsilon > 0$, there exists $\mathcal{R}_0(\zeta, \varpi, \varepsilon) \in (0, \gamma]$ such that for all $\mathcal{R} \in (0, \mathcal{R}_0)$, the position $(0,0)$ yields the unique stable equilibrium configuration among the positions $(h,\theta) \in A_d(\varepsilon)$, where

$$A_d(\varepsilon) := \Big\{ (h,\theta) \in \mathbb{R}^2 : |\theta| < \frac{\pi}{2} - \varepsilon \text{ and } |h| + d|\sin\theta| + \cos\theta < L - \varepsilon \Big\}.$$

As a straightforward consequence of Theorem 4.3 we have the following result.

COROLLARY 4.6. *Let $F(\cdot,0) \in C^2(-L+1, L-1)$ satisfy* (2.6)–(2.8) *and let $\gamma > 0$ be as in Proposition* 2.2. *There exists $\mathcal{R}_0(\zeta) \in (0,\gamma]$ such that problem* (2.11)+(4.2) *admits the unique solution $(\boldsymbol{u}_{(h,0)}, h, 0) \equiv (\boldsymbol{u}_{(0,0)}, 0, 0)$ (with $\boldsymbol{u}$ as in Proposition* 2.2*) for all $\mathcal{R} \in (0, \mathcal{R}_0)$. Moreover, this solution is stable.*

Up to the stability statement, this was already proved in [5, 6] where a similar result was also obtained when dealing with the unique degree of freedom θ, by keeping $h = 0$ (the center of mass of the body is fixed).

5. A discrete model of coupled 2D sections to describe a 3D plate. Let $B = [-d, d] \times [-\delta, \delta] \subset \mathbb{R}^2$ be the cross-section of a 3D plate (for instance, the deck of a bridge) as in section 2.2. From Ventsel and Krauthammer [38, section 1.1] we learn that plates may be classified according to the ratio between the width $2d$ and the thickness 2δ:

- if $d \le 8\delta$, we have a thick plate and the analysis of these plates includes all the components of stresses, strains, and displacements as for solid 3D bodies;
- if $8\delta \le d \le 80\delta$, we have a thin plate which may behave in both linear and nonlinear regimes according to how large the ratio is between its deflection and its thickness $2d$;
- if $d \ge 80\delta$, the plate behaves like a membrane and lacks flexural rigidity.

Let us now turn to a suspension bridge. We view the roadway of the bridge as a long narrow rectangular plate, hinged on its short edges where the bridge is supported by the ground, and free on its long edges. If Λ denotes its length and $2d$ denotes its width, a realistic assumption is that $2d \cong \frac{\Lambda}{100}$. For instance, the main span of the Tacoma Narrows Bridge had the measurements

$$\Lambda = 2800\,\text{ft.} \approx 853.44\,m, \quad 2d = 39\,\text{ft.} \approx 11.89\,m, \quad 2\delta = 4\,\text{ft.}4\frac{1}{2}'' \approx 1.33\,m;$$

see p.11 and Drawings 2 and 3 in [1]. Therefore, $d/\delta \approx 8.94$ and the Tacoma Bridge may be considered as a thin plate. This is even more evident in present and future bridges that can all be classified as thin plates.

But a full thin plate model is inappropriate since the ratio between the length and the width of the deck is very large. In [2], the main span of the bridge was modeled by $2n+1$ parallel rods labeled by $i = 1, ..., 2n+1$. Each rod interacts with the two nearest ones by means of linear attractive elastic forces and is free to move vertically and to rotate around its barycenter; see Figure 6.

Here, we enrich the purely structural model of [2] by introducing the effect of a flow (i.e., the wind) and replace the 1D rods with 2D cross-sections. The main novelty is that each cross-section is immersed in a fluid as in section 2.1, and this yields $2n+1$ 2D Navier–Stokes equations with fluid-structure constraints, as sketched in Figure 7.

Following section 2.1, we still denote by $B = [-d, d] \times [-1, 1] \subset \mathbb{R}^2$ the cross-sections at the central position and by $\mathcal{C}_L = \mathbb{R} \times (-L, L)$ the atmosphere layer on which each cross-section is free to move vertically and rotate around its barycenter under the action of both a Poiseuille fluid flow and restoring forces. The position of each cross-section is identified by a couple of parameters $(h_i, \theta_i) \in A_d$ and is denoted by B_{h_i,θ_i}. After setting $(H, \Theta) = (h_1, \dots, h_{2n+1}, \theta_1, \dots, \theta_{2n+1}) \in \mathbb{R}^{4n+2}$, the potential energy of the overall multiple cross-sections system reads

$$U(H,\Theta) = \sum_{i=1}^{2n+1} \frac{F(h_i,\theta_i)}{\alpha_i} + \frac{K_v}{2} \sum_{i=0}^{2n+1} (h_{i+1} - h_i)^2 + \frac{K_t}{2} \sum_{i=0}^{2n+1} (\theta_{i+1} - \theta_i)^2, \tag{5.1}$$

where $h_0 = h_{2n+2} = \theta_0 = \theta_{2n+2} = 0$ (fixed extremal cross-sections), while $K_v, K_t > 0$ represent the vertical and torsional stiffness of the bridge and

$$\alpha_i := (2n+1-i)(i-1) + 1$$

FIG. 6. *Discrete suspension bridges.*

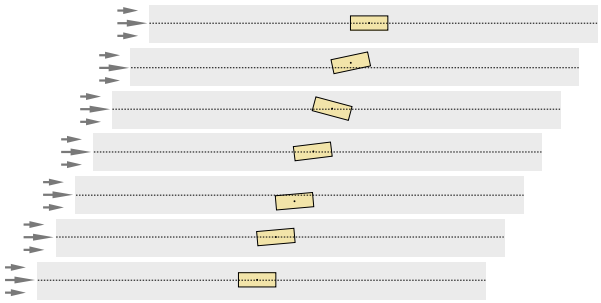

FIG. 7. *Air flow interacting with cross-sections of a suspension bridge.*

are weights that measure the action of the main cables on the ith cross-section. As expected, α_i takes its minimum at the penultimate cross-sections of the span (for $i=1$ and $i=2n+1$) and its maximum in the middle (for $i=n+1$). Finally, $F\in C^2(A_d)$ (with A_d as in (2.4)) satisfies assumptions (2.6)–(2.9). Each cross-section ($i=1,\dots,2n+1$) is subject to the two restoring forces

$$\begin{aligned}\partial_{h_i}U(H,\Theta)&=\frac{1}{\alpha_i}\,\partial_{h_i}F(h_i,\theta_i)+K_v(2h_i-h_{i+1}-h_{i-1}),\\ \partial_{\theta_i}U(H,\Theta)&=\frac{1}{\alpha_i}\,\partial_{\theta_i}F(h_i,\theta_i)+K_t(2\theta_i-\theta_{i+1}-\theta_{i-1}).\end{aligned}\tag{5.2}$$

Let $\boldsymbol{u}^i$ and p^i be the velocity and pressure of the fluid in the plane containing the cross-section B_{h_i,θ_i}. Let $S_{h_i,\theta_i}=\partial B_{h_i,\theta_i}$ and let $\Omega_{h_i,\theta_i}=\mathcal{C}_L\setminus B_{h_i,\theta_i}$ be the domain occupied by the fluid in each plane; as in section 2.2, we have the dimensionless system ($i=1,\dots,2n+1$) of steady-state Navier–Stokes equations:

$$\begin{aligned}&\operatorname{div}\boldsymbol{T}(\boldsymbol{u}^i,p^i)=\boldsymbol{u}^i\cdot\nabla\boldsymbol{u}^i,\ \operatorname{div}\boldsymbol{u}^i=0\quad\text{in }\Omega_{h_i,\theta_i},\\ &\boldsymbol{u}^i|_{S_{h_i,\theta_i}}=\boldsymbol{u}^i|_{\partial\mathcal{C}_L}=0,\ \lim_{|x_1|\to+\infty}\boldsymbol{u}^i(x_1,x_2)=\mathcal{R}\vee_P(x_2)\boldsymbol{e}_1.\end{aligned}\tag{5.3}$$

For a given $(H,\Theta)\in[A_d]^{2n+1}$ (the cartesian product of $2n+1$ times A_d, not to be confused with the A_d^i defined in the proof of Theorem 4.3), we say that

$$\Big(\boldsymbol{u}^1_{(h_1,\theta_1)},p^1_{(h_1,\theta_1)},\dots,\boldsymbol{u}^{2n+1}_{(h_{2n+1},\theta_{2n+1})},p^{2n+1}_{(h_{2n+1},\theta_{2n+1})}\Big)$$

is a weak solution of the coupled system made of (5.3) for $i=1,\dots,2n+1$ if $\boldsymbol{u}^i\in H^1_{loc}(\Omega_{h_i,\theta_i},\,\boldsymbol{u}^i-\mathcal{R}\vee_P\boldsymbol{e}_1)\in V_{h_i,\theta_i})$ for all $i=1,\dots,2n+1$ and $\boldsymbol{u}^i$ is a weak solution of (5.3) in the sense of Definition 2.1.

For a weak solution of (5.3), we compute all the lifts and torques through Proposition 3.1 and, so far, there is *no interaction* between the $2n+1$ equations in (5.3). The interaction is provided by the linear terms within the restoring forces (5.2) that lead to the full fluid-structure interaction problem. A position $(H,\Theta)\in[A_d]^{2n+1}$ is an *equilibrium position of the bodies* B_{h_i,θ_i} if *each restoring force balances the fluid forces,* i.e., if

$$\partial_{h_i}U(H,\Theta)=\zeta\,\mathcal{L}(h_i,\theta_i,\mathcal{R}),\qquad\partial_{\theta_i}U(H,\Theta)=\varpi\,\mathcal{T}(h_i,\theta_i,\mathcal{R})\quad(i=1,\dots,2n+1).\tag{5.4}$$

We now state the counterpart of Proposition 2.2 and Theorem 4.3 for problem (5.3)–(5.4). For the sake of simplicity, we give the proof only in the case of 3 cross-sections; the extension to more cross-sections requires lots of technical computations.

THEOREM 5.1. *Let $F\in C^2(A_d)$ satisfy assumptions* (2.6)–(2.9) *and take $n=1$ in problem* (5.3)–(5.4). *There exists $\mathcal{R}_0\in(0,\gamma]$ such that Proposition* 2.2 *applies to* (5.3) *for $i=1,2,3$ and problem* (5.3)–(5.4) *admits the unique solution*

$$\Big(\boldsymbol{u}^1_{(h_1,\theta_1)},\boldsymbol{u}^2_{(h_2,\theta_2)},\boldsymbol{u}^3_{(h_3,\theta_3)},H,\Theta\Big)=\Big(\boldsymbol{u}^1_{(0,0)},\boldsymbol{u}^2_{(0,0)},\boldsymbol{u}^3_{(0,0)},\boldsymbol{0},\boldsymbol{0}\Big).$$

Proof. The only delicate part is to prove the uniqueness issue for problem (5.3)–(5.4). To this aim, we properly modify the proof of Theorem 4.3. Assume that $0<\mathcal{R}<\gamma$ and fix $(H,\Theta)\in[A_d]^3$. To the unique weak solution

$$\Big(\boldsymbol{u}^1_{(h_1,\theta_1)},p^1_{(h_1,\theta_1)},\boldsymbol{u}^2_{(h_2,\theta_2)},p^2_{(h_2,\theta_2)},\boldsymbol{u}^3_{(h_3,\theta_3)},p^3_{(h_3,\theta_3)}\Big)$$

of (5.3) (for $i=1,2,3$) we associate the map $\mathbf{\Psi}:[A_d]^3\times[0,\gamma)\to\mathbb{R}^6$ defined by

$$\begin{cases} \Psi_\ell(H,\Theta,\mathcal{R})=\partial_{h_\ell}U(H,\Theta)-\zeta\,\mathcal{L}(h_\ell,\theta_\ell,\mathcal{R}) & \text{if } \ell=1,2,3,\\ \Psi_\ell(H,\Theta,\mathcal{R})=\partial_{\theta_{\ell-3}}U(H,\Theta)-\varpi\,\mathcal{T}(h_{\ell-3},\theta_{\ell-3},\mathcal{R}) & \text{if } \ell=4,5,6. \end{cases} \tag{5.5}$$

Note that $[A_d]^3\times[0,\gamma)\subset\mathbb{R}^7$ and recall that $h_0=h_4=\theta_0=\theta_4=0$. Therefore, the equilibrium conditions (5.4) can be rewritten as

$$\Psi_\ell(H,\Theta,\mathcal{R})=0 \qquad \forall \ell=1,\dots,6 \tag{5.6}$$

and the proof of Theorem 5.1 follows if we show that

$$\exists \mathcal{R}_0\in(0,\gamma]: \quad 0<\mathcal{R}<\mathcal{R}_0 \text{ and } \mathbf{\Psi}(H,\Theta,\mathcal{R})=\mathbf{0} \quad\Longrightarrow\quad (H,\Theta)=(\mathbf{0},\mathbf{0}). \tag{5.7}$$

We prove (5.7) by studying the behavior of $\mathbf{\Psi}$ for all $(H,\Theta)\in[A_d]^3$. We divide again A_d in the four subregions A_d^k, $k=1,\dots,4$, introduced in the proof of Theorem 4.3 (see Figure 5), and we obtain $4^3=64$ subregions of $[A_d]^3$, namely,

$$[A_d]^3=\bigcup_{k_1,k_2,k_3=1}^{4} A_d^{k_1}\times A_d^{k_2}\times A_d^{k_3}. \tag{5.8}$$

We start by showing (5.7) when

$$(H,\Theta)\in[A_d^1]^3.$$

From Theorem 3.5 we know that $\Psi\in C^1((-h_0,h_0)^3\times(-\theta_0,\theta_0)^3\times[0,\gamma))$. Then, since by (4.4) $\mathbf{\Psi}(\mathbf{0},\mathbf{0},\mathcal{R})=\mathbf{0}$ for all $0\le\mathcal{R}\le\gamma$, the validity of (5.7) for some $\mathcal{R}_0>0$ sufficiently small follows from the Implicit Function Theorem, provided we prove that

$$\left(\frac{\partial\mathbf{\Psi}(\mathbf{0},\mathbf{0},\mathbf{0})}{\partial(H,\Theta)}\right) \text{ is invertible.} \tag{5.9}$$

This is a 6×6 tridiagonal matrix of components:

$$\begin{cases} a_{ii}=\dfrac{1}{\alpha_i}\partial_{hh}F(0,0)+2K_v & \text{if } 1\le i\le3,\\ a_{ii}=\dfrac{1}{\alpha_{i-3}}\partial_{\theta\theta}F(0,0)+2K_t & \text{if } 4\le i\le6,\\ a_{12}=a_{21}=a_{23}=a_{32}=-K_v,\\ a_{45}=a_{54}=a_{56}=a_{65}=-K_t,\\ a_{ij}=0 & \text{in all the remaining cases.} \end{cases}$$

By row reduction, the matrix $(\frac{\partial\mathbf{\Psi}(\mathbf{0},\mathbf{0},\mathbf{0})}{\partial(H,\Theta)})$ can be reduced to an upper triangular matrix of diagonal components d_i given by

$$
\begin{aligned}
d_1 =& \frac{1}{\alpha_1}\partial_{hh}F(0,0) + 2K_v > 0,\\
d_2 =& \left(\frac{1}{\alpha_1}\partial_{hh}F(0,0) + 2K_v\right)\left(\frac{1}{\alpha_2}\partial_{hh}F(0,0) + 2K_v\right) - K_v^2 > 0,\\
d_3 =& \left(\frac{1}{\alpha_1}\partial_{hh}F(0,0) + 2K_v\right)\left(\frac{1}{\alpha_2}\partial_{hh}F(0,0) + 2K_v\right)\left(\frac{1}{\alpha_3}\partial_{hh}F(0,0) + 2K_v\right)\\
&- K_v^2\left(\frac{1}{\alpha_1}\partial_{hh}F(0,0) + \frac{1}{\alpha_3}\partial_{hh}F(0,0) + 4K_v\right)\\
&> 3K_v^2\left(\frac{1}{\alpha_1}\partial_{hh}F(0,0) + \frac{1}{\alpha_3}\partial_{hh}F(0,0)\right) + 4K_v^3 > 0,\\
d_4 =& \frac{1}{\alpha_1}\partial_{\theta\theta}F(0,0) + 2K_t > 0,\\
d_5 =& \left(\frac{1}{\alpha_1}\partial_{\theta\theta}F(0,0) + 2K_t\right)\left(\frac{1}{\alpha_2}\partial_{\theta\theta}F(0,0) + 2K_t\right) - K_t^2 > 0,\\
d_6 =& \left(\frac{1}{\alpha_1}\partial_{\theta\theta}F(0,0) + 2K_t\right)\left(\frac{1}{\alpha_2}\partial_{\theta\theta}F(0,0) + 2K_t\right)\left(\frac{1}{\alpha_3}\partial_{\theta\theta}F(0,0) + 2K_t\right)\\
&- K_t^2\left(\frac{1}{\alpha_1}\partial_{\theta\theta}F(0,0) + \frac{1}{\alpha_3}\partial_{\theta\theta}F(0,0) + 4K_t\right)\\
&> 3K_t^2\left(\frac{1}{\alpha_1}\partial_{\theta\theta}F(0,0) + \frac{1}{\alpha_3}\partial_{\theta\theta}F(0,0)\right) + 4K_t^3 > 0,
\end{aligned}
$$

where the above inequalities come from assumption (2.6) and recalling that K_v, $K_t > 0$. Therefore, $|(\frac{\partial \mathbf{\Psi}(\mathbf{0},\mathbf{0},\mathbf{0})}{\partial(H,\Theta)})| = \prod_{i=1}^{6} d_i \neq 0$; this concludes the proof of (5.9).

We conclude the proof of (5.7) by showing that $\mathbf{\Psi} \neq \mathbf{0}$ in the remaining 63 regions of $[A_d]^3$. The same kind of estimates and arguments exploited in the proof of Theorem 4.3 for the regions A_d^2, A_d^3, and A_d^4 allow us to prove that for $0 < \mathcal{R} < \mathcal{R}_0$,

- if $(h_\ell, \theta_\ell) \in A_d^2$ for some $\ell \in \{1,2,3\}$, then $\Psi_\ell(H,\Theta,\mathcal{R}) \neq 0$ and $\mathbf{\Psi}(H,\Theta,\mathcal{R}) \neq \mathbf{0}$;
- if $(h_\ell, \theta_\ell) \in A_d^3$ for some $\ell \in \{1,2,3\}$, then $\Psi_{\ell+3}(H,\Theta,\mathcal{R}) \neq 0$ and $\mathbf{\Psi}(H,\Theta,\mathcal{R}) \neq \mathbf{0}$;
- if $(h_\ell, \theta_\ell) \in A_d^4$ for some $\ell \in \{1,2,3\}$, then $|\nabla U(H,\Theta)| > 0$, in view of (2.7), and $\mathbf{\Psi}(H,\Theta,\mathcal{R}) \neq \mathbf{0}$. This completes the proof of Theorem 5.1. ∎

6. Numerical analysis of equilibrium configurations. In this section we perform a numerical analysis that complements and enriches the analytical results obtained in the previous one. More precisely, Theorem 4.3 is silent about the critical value $\mathcal{R}_c$ of the Reynolds number $\mathcal{R}$, below which the uniqueness of the equilibrium configuration (and its stability) is guaranteed. This leads us, on the one hand, to give a quantitative estimate of $\mathcal{R}_c$ and, on the other hand, to investigate existence and stability of other equilibrium configurations for $\mathcal{R} > \mathcal{R}_c$. For simplicity, we normalize the coefficients of the lift and torque, and the stiffness constants, namely, we set

$$\zeta = \varpi = 1. \tag{6.1}$$

In all the experiments we take $\mathcal{R} \leq 50$, a restricted range of Reynolds numbers. There are two reasons for this choice. First, large values of $\mathcal{R}$ yield numerical instability. Second, as we shall see, already in the range $\mathcal{R} \in (0, 50]$ several significant differences already appear between the cases $\mathcal{R} \lessapprox 1$ and $\mathcal{R} \gtrapprox 1$. In fact, in the latter, numerical tests show completely new features not predicted yet by the mathematical analysis, such as multiple stable equilibrium configurations. We will qualitatively refer to these two regimes as *small* and *large* Reynolds numbers.

6.1. Numerical assessment. We discretize both the Stokes problem (3.2) and the Navier–Stokes equations (2.11) by resorting to piecewise quadratic and linear finite elements to approximate the velocity and the pressure, respectively. The discretization is performed on an unstructured mesh, consisting of 65878 triangles, with a local refinement around the obstacle. The nonlinearity of the Navier–Stokes equations is tackled by employing the Newton scheme. In particular, to stop the iterative procedure, we assign a maximum number of iterations set to 15, and we control the relative increment with respect to the $H^1(\Omega)$-norm of the velocity and the $L^2(\Omega)$-norm of the pressure, by setting a tolerance equal to 10^{-3}. Moreover, to ensure the convergence of the Newton method we replace the boundary condition at the outflow in (2.11) with a homogeneous Neumann data.

Concerning the geometry of the computational setting, we replace the infinite channel $\mathcal{C}_L$ in (1.1) with the finite domain $(0, 500) \times (-50, 50)$, while identifying the obstacle B with the rectangle $[244, 256] \times [-0.7, 0.7]$ (so that $L = 50$, $d = 6$, $\delta = 0.7$). We numerically verified that the dimensions selected for the channel provide a reliable approximation of the infinite domain configuration.

From a practical viewpoint, we have adopted a dimensionless formulation by rescaling all the lengths with respect to the obstacle thickness, $2\,\delta = 1.4$, so that $\mathcal{C}_L = [0, 357.1429] \times [-35.71, 35.71]$ and $B = [174.2857, 182.8571] \times [-0.5, 0.5]$. In view of the characterization of A_d in (2.4), we know that B may collide with $\partial\mathcal{C}_L$, which gives numerical instability. For this reason,

(6.2)
the graphs of functions depending on h are plotted on the interval $h \in (-30, 30)$.

The numerical results merely concern the behavior of $\mathcal{L}$ and $\mathcal{T}$, and we explain how they can be applied to find multiple solutions to the fluid-structure interaction problem (2.11)+(4.1). In most cases (but not all!) we assume that $F = 0$ (no restoring force). Therefore the bridge model is no longer suitable to describe the applications. The case $F = 0$ well describes the behavior of the Leonardo da Vinci ferry; see section 7. In view of this application, it appears more convenient to argue in terms of the *attack angle* φ defined by $\varphi = -\theta$ for $|\theta| < \frac{\pi}{2}$. Therefore, $\mathcal{L}(h, \varphi, \mathcal{R}) = \mathcal{L}(h, -\theta, \mathcal{R})$ and $\mathcal{T}(h, \varphi, \mathcal{R}) = \mathcal{T}(h, -\theta, \mathcal{R})$.

6.2. Equilibrium and stability of horizontal configurations. We consider the horizontal configurations of the body, that is, we take

$$\varphi = 0.$$

For all h we numerically compute the solution $\boldsymbol{u}_{(h,0)}$ of (2.11) (when $B = B_{h,0}$). With the solution $\boldsymbol{u}_{(h,0)}$ of (2.11) in hand, we first seek the values of h that satisfy

$$\mathcal{L}(h, 0, \mathcal{R}) = 0. \tag{6.3}$$

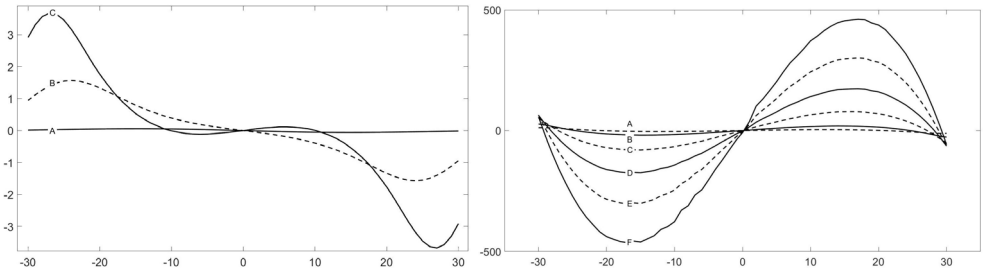

FIG. 8. *Left: plot of* $h \mapsto \mathcal{L}(h,0,\mathcal{R})$ *for* $\mathcal{R}=0.1$ (A), $\mathcal{R}=1$ (B), $\mathcal{R}=2$ (C). *Right: plot of* $h \mapsto \mathcal{L}(h,0,\mathcal{R})$ *for* $\mathcal{R}=5$ (A), $\mathcal{R}=10$ (B), $\mathcal{R}=20$ (C), $\mathcal{R}=30$ (D), $\mathcal{R}=40$ (E), $\mathcal{R}=50$ (F).

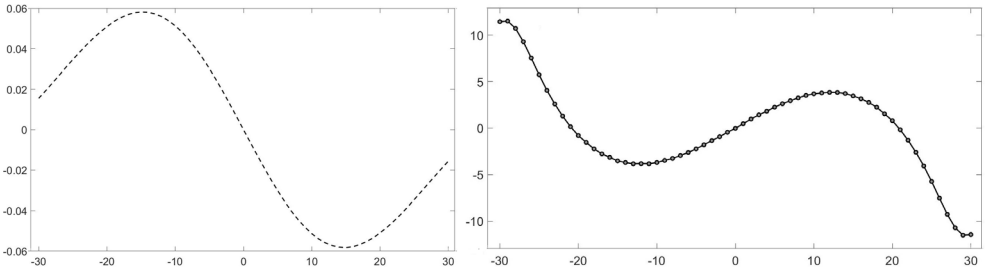

FIG. 9. *Left: plot of* $h \mapsto \mathcal{L}(h,0,0.1)$. *Right: plot of* $h \mapsto \mathcal{L}(h,0,5)$.

According to Definition 4.2, an equilibrium configuration $B_{h,0}$ (with h solving (6.3)) is called stable if there exists $\varrho > 0$ such that

$$0 < |h-\overline{h}| < \varrho \implies (h-\overline{h})\mathcal{L}(h,0,\mathcal{R}) < 0,$$

and is called unstable otherwise. Roughly speaking, stable equilibria tend to be restored by the lift force, while unstable equilibria do not. In view of (3.9), for any fixed $\mathcal{R}>0$ the map $h \mapsto \mathcal{L}(h,0,\mathcal{R})$ is an odd function of h. This is clearly visible in the plots in Figure 8 (recall (6.2)) for several values of $\mathcal{R}$.

Since the behavior is less evident for the smallest values of $\mathcal{R}$ in both pictures, we focus on these specific graphs with ad hoc scales in Figure 9.

Figures 8 and 9 can then be used to solve (6.3) numerically, namely, the *horizontal equilibrium configurations* of the body B within the fluid for which there is no lift. We infer that if $\mathcal{R}>0$ is small, then (6.3) admits the unique solution $h_0=0$ and the corresponding configuration $\boldsymbol{h}_0=(0,0)$ is stable, whereas if $\mathcal{R}>0$ is large, then (6.3) admits three solutions ($h_0=0$, $h_+>0$, $h_-=-h_+$), and the configuration $\boldsymbol{h}_0=(0,0)$ is unstable, while the configurations $\boldsymbol{h}_\pm=(h_\pm,0)$ are stable. From Figure 9 (right) we also infer that

NUMERICAL RESULT 6.1. *The map* $h \mapsto \mathcal{L}(h,0,5)$ *is positive for* $h \in (-L+1, h_-) \cup (0,h_+)$ *and negative for* $h \in (h_-,0) \cup (h_+, L-1)$.

All these results are sketched in Figure 10.

At least for horizontal positions of the body and in the absence of restoring forces, these numerical results give a first hint that Theorem 4.3 should be sharp. Indeed, they suggest the next statement.

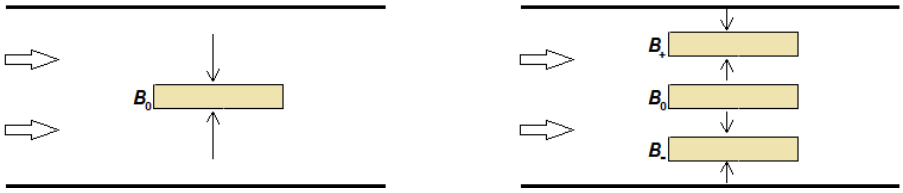

FIG. 10. *Stability of the horizontal equilibria for $\mathcal{R}$ small (left) and $\mathcal{R}$ large (right).*

NUMERICAL RESULT 6.2. *The problem*

$$-\mathrm{div}\boldsymbol{T}(\boldsymbol{u},p)+\boldsymbol{u}\cdot\nabla\boldsymbol{u}=0,\ \mathrm{div}\boldsymbol{u}=0 \quad \text{in } \Omega_{h,0},$$
$$\boldsymbol{u}|_{S_{h,0}}=\boldsymbol{u}|_{\partial\mathcal{C}_L}=0, \quad \lim_{|x_1|\to+\infty}\boldsymbol{u}(x_1,x_2)=\mathcal{R}\mathsf{v}_P(x_2)\boldsymbol{e}_1, \quad \mathcal{L}(h,0,\mathcal{R})=0$$

- *admits the unique (stable) solution $(\boldsymbol{u}_{(h,0)},h,0)\equiv(\boldsymbol{u}_{(0,0)},0,0)$ if $\mathcal{R}>0$ is small;*
- *admits at least three solutions $(\boldsymbol{u}_{(h,0)},h,0)\in\{(\boldsymbol{u}_{(0,0)},0,0);(\boldsymbol{u}_{(h_+,0)},h_+,0);(\boldsymbol{u}_{(h_-,0)},h_-,0)\}$, for some $-h_-=h_+\in(0,L-1)$, if $\mathcal{R}>0$ is large; moreover, the configuration $\boldsymbol{h}_0=(0,0)$ is unstable, whereas the configurations $\boldsymbol{h}_\pm=(h_\pm,0)$ are stable.*

Numerical Result 6.2 is reliable and quite precise; this is due to the fact that $\mathcal{R}$ is large but not huge. For very large values of $\mathcal{R}$, we expect turbulent flows and a less regular behavior of $h\mapsto\mathcal{L}(h,0,\mathcal{R})$. In such a case, the number and stability of the equilibria appear unpredictable.

We then seek horizontal positions annihilating the torque, that is, solutions to $\mathcal{T}(h,0,\mathcal{R})=0$. We obtain somewhat similar behaviors. For small $\mathcal{R}$ the map $h\mapsto\mathcal{T}(h,0,\mathcal{R})$ has a graph as in the left picture of Figure 9. In Figure 11 we plot the map $h\mapsto\mathcal{T}(h,0,5)$, which, as stated in (3.9), is odd. It turns out that, besides $h_0=0$, there exist two additional configurations $h_-<h_0<h_+$ (with $h_-=-h_+$) where $\mathcal{T}$ vanishes.

By comparing the right picture in Figure 9 with Figure 11 one may wonder if they coincide. In section 6.4 we numerically show that this is not the case.

For horizontal positions ($\varphi=0$), the stability analysis for the fluid-structure interaction problem with torque leads to conclusions similar to those of Numerical Result 6.2. Indeed, we can translate Figure 11 into the following.

NUMERICAL RESULT 6.3. *The problem*

$$-\mathrm{div}\boldsymbol{T}(\boldsymbol{u},p)+\boldsymbol{u}\cdot\nabla\boldsymbol{u}=0,\ \mathrm{div}\boldsymbol{u}=0 \quad \text{in } \Omega_{h,0},$$
$$\boldsymbol{u}|_{S_{h,0}}=\boldsymbol{u}|_{\partial\mathcal{C}_L}=0, \quad \lim_{|x_1|\to+\infty}\boldsymbol{u}(x_1,x_2)=5\mathsf{v}_P(x_2)\boldsymbol{e}_1, \quad \mathcal{T}(h,0,5)=0$$

admits three solutions $(\boldsymbol{u}_{(h,0)},h,0)\in\big\{(\boldsymbol{u}_{(0,0)},0,0);(\boldsymbol{u}_{(h_+,0)},h_+,0);(\boldsymbol{u}_{(h_-,0)},h_-,0)\big\}$ for some $-h_-=h_+\in(0,L-1)$. If $h\notin\{h_-,h_0,h_+\}$, the body is subject to a torque which generates a rotation of B.

In order to analyze horizontal equilibria with purely vertical restoring forces ($\partial_hF\neq0=\partial_\varphi F$), take $\zeta=1$ in (4.2); see (6.1). Then the horizontal equilibrium configurations $B_{h,0}$ are found by solving

$$\partial_hF(h,0)=\mathcal{L}(h,0,\mathcal{R}). \tag{6.4}$$

When $\mathcal{R}$ is small, Corollary 4.6 shows that (2.11)+(6.4) admits the unique solution $h=0$ that is also stable. Here we numerically study the existence and stability of

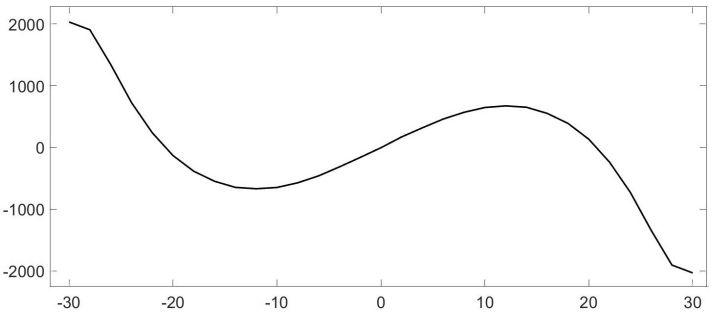

FIG. 11. *Plot of* $h \mapsto \mathcal{T}(h,0,5)$ *for* $|h| < 30$*; see* (6.2).

FIG. 12. *Graphs of* $h \mapsto \partial_h F(h,0)$ (A) *and* $h \mapsto \mathcal{L}(h,0,\mathcal{R})$ (B) *for small (left) and large (right)* $\mathcal{R}$.

other equilibrium configurations for large $\mathcal{R}$. According to Definition 4.2, a sufficient condition for an equilibrium $\overline{h}$ to be stable (at a fixed $\mathcal{R} > 0$) is that the slope of $h \mapsto \partial_h F(h,0)$ at $\overline{h}$ is larger than the slope of $h \mapsto \mathcal{L}(h,0,\mathcal{R})$ at $\overline{h}$. On the one hand, we know by (2.6) that $\partial_h F(h,0) \sim \kappa_1 h$ as $h \to 0$. On the other hand, in Theorem 3.5 it is proved that $\partial_h \mathcal{L}(0,0,\mathcal{R}) = O(\mathcal{R}^2)$ as $\mathcal{R} \to 0$. Figures 8 and 9 show that $\partial_h \mathcal{L}(0,0,\mathcal{R}) < 0$ for small $\mathcal{R}$ and $\partial_h \mathcal{L}(0,0,\mathcal{R}) > 0$ for large $\mathcal{R}$.

Henceforth, two different situations can happen. They are qualitatively described in Figure 12.

The overall conclusion is then similar to that of Numerical Result 6.2.

NUMERICAL RESULT 6.4. *Assume that* F *satisfies* (2.6)–(2.7)*. Then the problem*

$$-\mathrm{div}\boldsymbol{T}(\boldsymbol{u},p) + \boldsymbol{u}\cdot\nabla\boldsymbol{u} = 0,\ \mathrm{div}\boldsymbol{u} = 0 \quad \text{in } \Omega_{h,0},$$
$$\boldsymbol{u}|_{S_{h,0}} = \boldsymbol{u}|_{\partial\mathcal{C}_L} = 0, \quad \lim_{|x_1|\to+\infty} \boldsymbol{u}(x_1,x_2) = \mathcal{R}\mathsf{v}_P(x_2)\boldsymbol{e}_1, \quad \partial_h F(h,0) = \mathcal{L}(h,0,\mathcal{R})$$

- *admits the unique (stable) solution* $(\boldsymbol{u}_{(h,0)},h,0) \equiv (\boldsymbol{u}_{(0,0)},0,0)$ *if* $\mathcal{R} > 0$ *is small;*
- *admits at least three solutions* $(\boldsymbol{u}_{(h,0)},h,0) \in \{(\boldsymbol{u}_{(0,0)},0,0);(\boldsymbol{u}_{(h_+,0)},h_+,0);(\boldsymbol{u}_{(h_-,0)},h_-,0)\}$ *for some* $1-L < h_- < 0 < h_+ < L-1$*, if* $\mathcal{R} > 0$ *is large; moreover, the configuration* $\boldsymbol{h}_0 = (0,0)$ *is unstable, whereas the configurations* $\boldsymbol{h}_\pm = (h_\pm,0)$ *are stable.*

We conclude this section by emphasizing that the stability analysis for two degrees of freedom (both h and φ free) is more complex and will be investigated in subsection 6.5, showing again the appearance of multiple equilibrium configurations for large values of $\mathcal{R}$.

6.3. Vanishing of lift and torque for generic configurations. The goal is to collect sign properties of $\mathcal{L}$ and $\mathcal{T}$ together with information about the location of the maximum point of $\mathcal{L}$; this will be used in section 7.

We first maintain the angle of attack φ fixed, $\varphi \in [0, \frac{\pi}{2})$. Recalling (6.2), in Figure 13 (left) we show the plots of $h \mapsto \mathcal{L}(h, \varphi, \mathcal{R})$ for $\varphi \in \{0, \frac{\pi}{192}, \frac{\pi}{96}, \frac{\pi}{36}, \frac{\pi}{12}, \frac{\pi}{6}, \frac{\pi}{4}, \frac{\pi}{3}\}$.

From Figure 13 (left) we infer the following.

NUMERICAL RESULT 6.5. *There exist* $0 < \varphi_0 < \varphi^0 < \frac{\pi}{2}$ *such that* $\mathcal{L}(h, \varphi, 5) > 0$ *whenever* $\varphi_0 < \varphi < \varphi^0$ *and for all* h *such that* $(h, \varphi) \in A_d$.

From Figure 13 (right) we also notice that, as φ varies, we have the following result.

NUMERICAL RESULT 6.6. *There exist* $\varphi_* \approx \frac{\pi}{96}$ *and* $\varphi^* \approx \frac{15\pi}{32}$ *such that the maximum (lift) of the map* $h \mapsto \mathcal{L}(h, \varphi, 5)$ *is achieved at* $h \approx -29$ *if* $\varphi \in (-\frac{\pi}{2}, \varphi_*) \cup (\varphi^*, \frac{\pi}{2})$ *and at* $h \approx 4$ *if* $\varphi \in (\varphi_*, \varphi^*)$. *Moreover,* $\varphi \mapsto \max_h \mathcal{L}(h, \varphi, 5)$ *is increasing over* $(0, \varphi_0)$ *and decreasing over* $(\varphi_0, \frac{\pi}{2})$ *with* $\varphi_0 \approx \frac{\pi}{6}$.

This result shows that the vertical position h where the lift attains its maximum value (pushing upwards) is a discontinuous function of φ; see the right picture in Figure 13. The choice (6.2) was made in order to avoid the analysis for $|h| > 30$ since B approaches the collision against $\partial\mathcal{C}_L$ (especially for some φ) and the numerical results appear less reliable. But since they seem to be robust enough for $|h| < 30$, we may slightly improve Numerical Result 6.6 as follows.

NUMERICAL RESULT 6.7. *For* $\varphi \in (-\frac{\pi}{2}, \varphi_*) \cup (\varphi^*, \frac{\pi}{2})$ *the maximum (lift) of the map* $h \mapsto \mathcal{L}(h, \varphi, 5)$ *is achieved at some constant* $h \approx -29$ *far away from* $\partial\mathcal{C}_L$.

Next, we maintain h fixed. Since we also aim to study the dependence on $\mathcal{R}$, in Figure 14 we show the plots of $\varphi \mapsto \mathcal{L}(h, \varphi, \mathcal{R})$ for several couples $(h, \mathcal{R})$. It turns out that the angle $\varphi = \varphi(\mathcal{R})$ maximizing the lift $\mathcal{L}$ is decreasing with respect to $\mathcal{R}$. In aerodynamics, it is known [32] that to maximize the lift of an airplane, the flap on the wings has to be inclined at an angle φ satisfying $|\varphi| = \pi/12 \approx 0.26$; obviously, the sign depends on whether the aircraft is taking off or landing. Therefore, it is natural to conjecture that $\varphi(\mathcal{R}) \downarrow \pi/12$ as $\mathcal{R} \to \infty$.

In Figure 15 (left) we display the maximum value of the lift at a given h, uniformly with respect to the angle of attack φ. As a counterpart of Figure 13 (right), in Figure 15 (right) we display the plot of the angle $\varphi = \varphi(h)$ maximizing the lift for any $h \in (-30, 30)$. Also this map is discontinuous and, as expected, the optimal $\varphi(h)$ does not change sign.

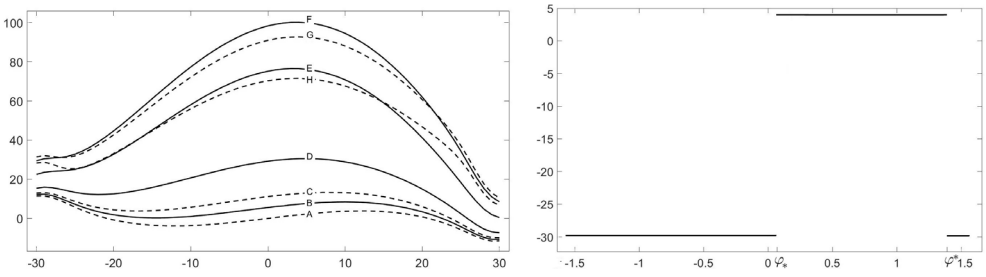

FIG. 13. *Left: plots of* $h \mapsto \mathcal{L}(h, \varphi, 5)$ *for* $\varphi = 0$ (A), $\varphi = \frac{\pi}{192}$ (B), $\varphi = \frac{\pi}{96}$ (C), $\varphi = \frac{\pi}{36}$ (D), $\varphi = \frac{\pi}{12}$ (E), $\varphi = \frac{\pi}{6}$ (F), $\varphi = \frac{\pi}{4}$ (G), $\varphi = \frac{\pi}{3}$ (H). *Right: plot of* $h = h(\varphi)$ *maximizing* $\mathcal{L}(h, \varphi, 5)$ *for* $|\varphi| < \frac{\pi}{2}$.

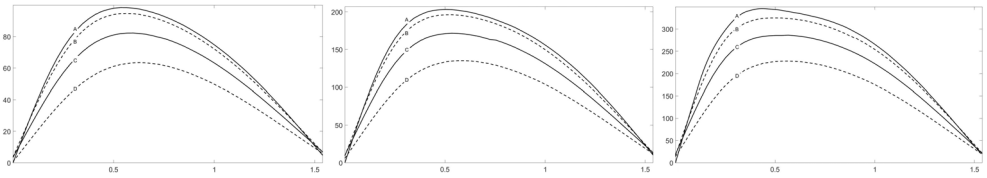

FIG. 14. *Plots of* $\varphi \mapsto \mathcal{L}(h,\varphi,\mathcal{R})$ *with* $h=0$ (A), $h=10$ (B), $h=15$ (C), $h=20$ (D), *and with* $\mathcal{R}=5$ *(left),* $\mathcal{R}=7.5$ *(middle),* $\mathcal{R}=10$ *(right).*

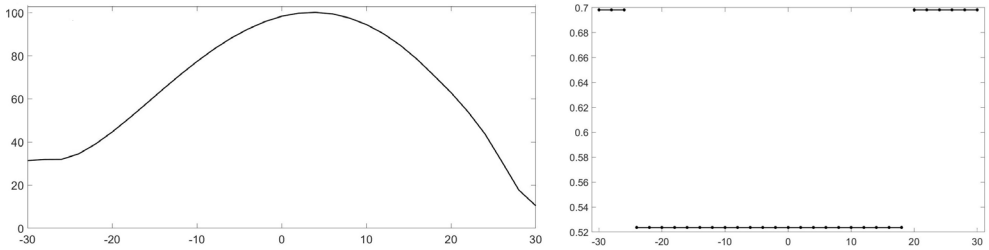

FIG. 15. *Left: plot of the map* $h \mapsto \max_\varphi \mathcal{L}(h,\varphi,5)$. *Right: plot of the angle* $\varphi=\varphi(h)$ *maximizing* $h \mapsto \mathcal{L}(h,\varphi,5)$ *for* $|h|<30$*; see* (6.2).

6.4. Simultaneous annihilation of lift and torque. In Figure 16 we plot the lift and torque as functions of h and φ. The white region represents a positive lift/torque, the black region corresponds to a negative lift/torque, and the gray region is associated with a small lift/torque (in absolute value). The dotted lines indicate the zero level curves.

The corresponding views from above of the surfaces in Figure 16 in the (φ,h)-plane are provided in Figure 17. As observed in Figures 8 and 11, both the maps $h \mapsto \mathcal{L}(h,0,5)$ and $h \mapsto \mathcal{T}(h,0,5)$ vanish at three different values of h: Figure 17 suggests that they vanish for the same couple of values of $h \neq 0$ or, at least, for very close h. A more precise analysis shows that the latter occurs.

As expected, the positions of the zeros of $(\varphi,h) \mapsto \mathcal{L}(h,\varphi,\mathcal{R})$ and $(\varphi,h) \mapsto \mathcal{T}(h,\varphi,\mathcal{R})$ are quite sensitive to the variations of $\mathcal{R}$. We performed numerical tests with $\mathcal{R} \in \{0.01, 0.1, 1, 10\}$ and with two different lengths $d \in \{6, 30\}$ to analyze also the sensitivity to the aspect ratio of B. The zeros of $(\varphi,h) \mapsto \mathcal{L}(h,\varphi,\mathcal{R})$ and $(\varphi,h) \mapsto \mathcal{T}(h,\varphi,\mathcal{R})$ in Figures 18–21 are displayed for integer values of $h \in [-30,0]$ on the vertical axis. The positions of the zeros in the (φ,h)-plane, with $\varphi \in (-\frac{\pi}{2},0)$, are indicated by triangles $\triangledown$ (lift) and $\blacktriangle$ (torque) for a simpler visualization. The dots on the bottom of Figures 19–21 show the difference between the φ-values of the zeros at a common value of h. By continuity, a switch between the order of the zeros indicates that

$$\exists(-\overline{h},-\overline{\varphi}) \in A_d \text{ with } \overline{h},\overline{\varphi}>0 \quad \text{s.t.} \quad \mathcal{L}(-\overline{h},-\overline{\varphi},\mathcal{R}) = \mathcal{T}(-\overline{h},-\overline{\varphi},\mathcal{R}) = 0.$$

By (3.9), we then infer that also $\mathcal{L}(\overline{h},\overline{\varphi},\mathcal{R}) = \mathcal{T}(\overline{h},\overline{\varphi},\mathcal{R}) = 0$ so that, besides $(\varphi,h) = (0,0)$, we obtain two more configurations where $\mathcal{L} = \mathcal{T} = 0$. The guess is that when such equilibria appear, the configuration $(\varphi,h) = (0,0)$ becomes unstable, but we leave this interesting issue for a future investigation.

Before reaching some conclusions, let us display the plots of the zero level curves of $\mathcal{L}$ and $\mathcal{T}$, namely,

$$\mathbb{L}_0^{\mathcal{R}} := \{(h,\varphi) \in A_d : \mathcal{L}(h,\varphi,\mathcal{R}) = 0\}, \qquad \mathbb{T}_0^{\mathcal{R}} := \{(h,\varphi) \in A_d : \mathcal{T}(h,\varphi,\mathcal{R}) = 0\},$$

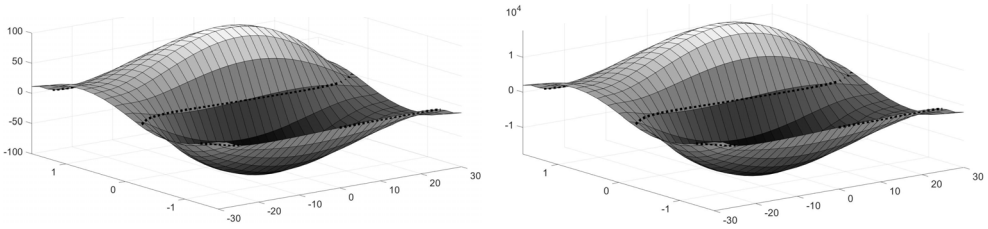

FIG. 16. *Left: plot of* $(h,\varphi)\mapsto\mathcal{L}(h,\varphi,5)$. *Right: plot of* $(h,\varphi)\mapsto\mathcal{T}(h,\varphi,5)$.

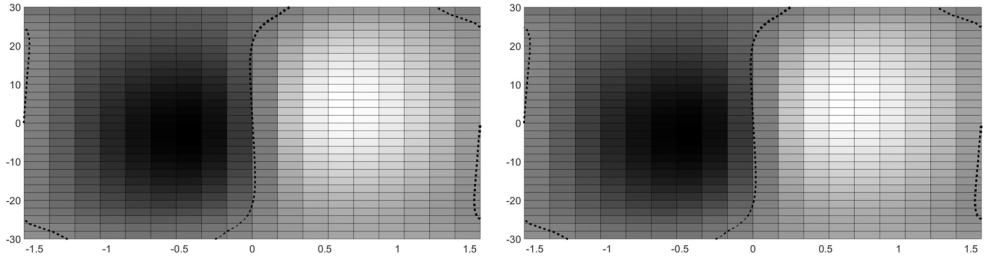

FIG. 17. *View from above of the graphs of* $(\varphi,h)\mapsto\mathcal{L}(h,\varphi,5)$ *(left) and of* $(\varphi,h)\mapsto\mathcal{T}(h,\varphi,5)$ *(right). The dotted lines represent the zero level curves.*

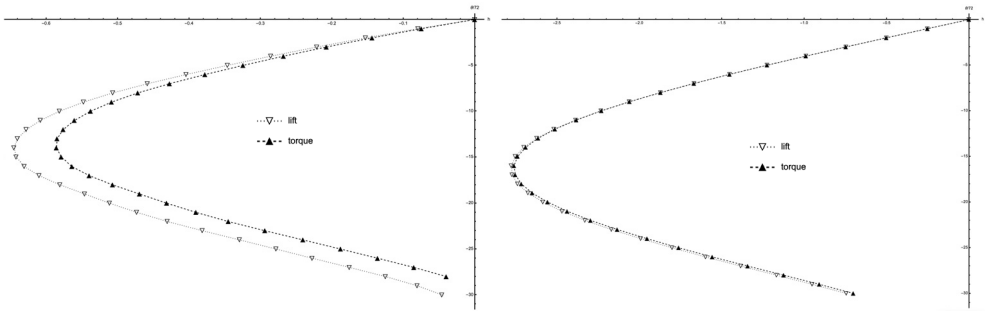

FIG. 18. *The curves* $\mathbb{L}_0^{\mathcal{R}}$ *and* $\mathbb{T}_0^{\mathcal{R}}$ *for* $d=6$, $\mathcal{R}=0.01$ *(left) and* $\mathcal{R}=0.1$ *(right).*

and let us comment on them. In Figures 18–19 we display the plots for $d=6$. In Figure 18 (resp., Figure 19) the φ-axis is stretched by $72/\pi$ (resp., by $36/\pi$) and scaled differently in the two plots.

Hence, for $d=6$, the level curves $\mathbb{L}_0^{\mathcal{R}}$ and $\mathbb{T}_0^{\mathcal{R}}$ do not coincide for small $\mathcal{R}$, even if they are close (see Figure 18): for $\mathcal{R}=0.01$ they are separated with $\mathbb{L}_0^{0.01}\cap\mathbb{T}_0^{0.01}=\{(0,0)\}$, and for $\mathcal{R}=0.1$ they get closer but still intersect only at the origin, i.e. still $\mathbb{L}_0^{0.1}\cap\mathbb{T}_0^{0.1}=\{(0,0)\}$. They continue to approach when $\mathcal{R}$ increases (see Figure 19). For $\mathcal{R}=1$, we see that close to the boundary $\partial\mathcal{C}_L$ of the channel ($h\lessapprox -25$) $\mathcal{T}$ vanishes for a smaller value of $|\varphi|$ than $\mathcal{L}$. The opposite happens after the turning point when the position is closer to the center of the channel ($-25\lessapprox h<0$). Therefore, for $\mathcal{R}=1$ the curves cross and $\{(0,0)\}\subsetneqq\mathbb{L}_0^1\cap\mathbb{T}_0^1$. For $\mathcal{R}=10$, the curves have a different shape and there is no evidence of an intersection on the plotted portion, but a crossing point probably exists closer to $\partial\mathcal{C}_L$ (for some $h\lessapprox -30$), where numerics is not reliable. We have this feeling because, for $\mathcal{R}=10$, we are in the regime where $\mathcal{L}$ has three zeros of the type $(h,0)$; see Numerical Result 6.4.

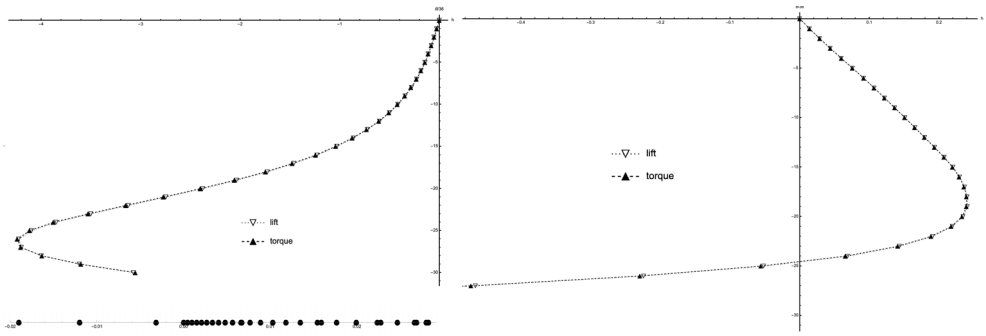

FIG. 19. *The curves* $\mathbb{L}_0^{\mathcal{R}}$ *and* $\mathbb{T}_0^{\mathcal{R}}$ *for* $d=6$, $\mathcal{R}=1$ *(left) and* $\mathcal{R}=10$ *(right).*

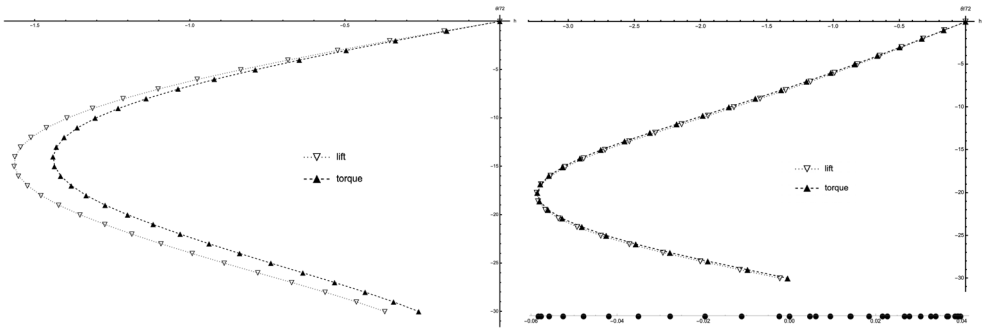

FIG. 20. *The curves* $\mathbb{L}_0^{\mathcal{R}}$ *and* $\mathbb{T}_0^{\mathcal{R}}$ *for* $d=30$, $\mathcal{R}=0.1$ *(left) and* $\mathcal{R}=1$ *(right).*

In Figures 20–21 we display the plots of $\mathbb{L}_0^{\mathcal{R}}$ and $\mathbb{T}_0^{\mathcal{R}}$ for $d=30$, with the φ-axis stretched by $72/\pi$ and scaled differently in the three plots.

For $d=30$ and $\mathcal{R}=0.1$, the curves $\mathbb{L}_0^{0.1}$ and $\mathbb{T}_0^{0.1}$ are well separated; see Figure 20 (left). They approach for $\mathcal{R}=1$ and cross around $h\approx -20$; see Figure 20 (right). Observe that $\mathcal{L}$ and $\mathcal{T}$ vanish for much smaller $|\varphi|$ than for $d=6$; see Figures 18 and 19. For $\mathcal{R}=10$, the curves have a different shape than for $d=6$ at the same value of $\mathcal{R}$ (see Figure 19 (right)), and now the crossing point is visible at $h\approx -28$.

Summarizing, the above discussion and Figures 18–21 lead us to state the following

NUMERICAL RESULT 6.8. *For any* $d>1$ *and any* $\mathcal{R}>0$ *we have* $\mathbb{L}_0^{\mathcal{R}} \neq \mathbb{T}_0^{\mathcal{R}}$. *Moreover,*

- *if* $\mathcal{R}>0$ *is small, then* $\mathbb{L}_0^{\mathcal{R}} \cap \mathbb{T}_0^{\mathcal{R}} = \{(0,0)\}$*;*
- *if* $\mathcal{R}>0$ *is large, then there exist* $\overline{h}, \overline{\varphi}>0$ *such that* $\{(0,0);(\overline{h},\overline{\varphi});(-\overline{h},-\overline{\varphi})\} \subseteq \mathbb{L}_0^{\mathcal{R}} \cap \mathbb{T}_0^{\mathcal{R}}$.

6.5. Stability comparison between one and two degrees of freedom. In this final part, we combine the rigorously proved asymptotics (3.20) from Theorem 3.5 with the qualitative numerical behavior so far obtained. As a first step, we rephrase Numerical Result 6.8 as follows.

NUMERICAL RESULT 6.9. *The problem*

$$-\mathrm{div}\boldsymbol{T}(\boldsymbol{u},p)+\boldsymbol{u}\cdot\nabla\boldsymbol{u}=0,\ \mathrm{div}\boldsymbol{u}=0 \quad \textit{in } \Omega_{h,\varphi},$$
$$\boldsymbol{u}|_{S_{h,\varphi}}=\boldsymbol{u}|_{\partial\mathcal{C}_L}=0,\quad \lim_{|x_1|\to+\infty}\boldsymbol{u}(x_1,x_2)=\mathcal{R}\mathsf{v}_P(x_2)\boldsymbol{e}_1,\quad \mathcal{L}(h,\varphi,\mathcal{R})=\mathcal{T}(h,\varphi,\mathcal{R})=0$$

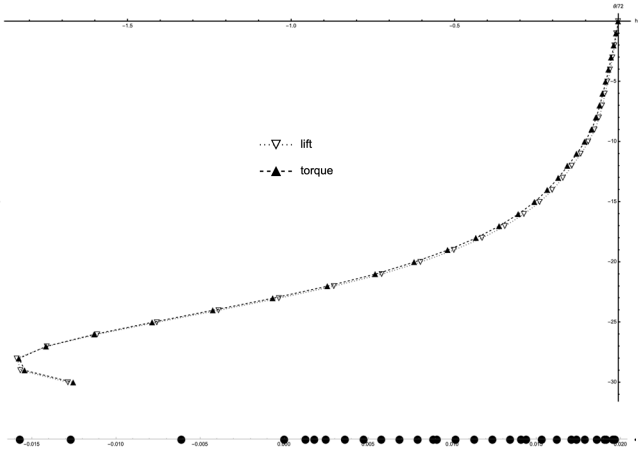

FIG. 21. *The curves* $\mathbb{L}_0^{\mathcal{R}}$ *and* $\mathbb{T}_0^{\mathcal{R}}$ *for* $d=30$ *and* $\mathcal{R}=10$.

- *admits the unique (stable) solution* $(\boldsymbol{u}_{(h,\varphi)},h,\varphi)\equiv(\boldsymbol{u}_{(0,0)},0,0)$ *if* $\mathcal{R}>0$ *is small;*
- *admits at least three solutions* $(\boldsymbol{u}_{(h,\varphi)},h,\varphi)\in\{(\boldsymbol{u}_{(0,0)},0,0);(\boldsymbol{u}_{(\overline{h},\overline{\varphi})},\overline{h},\overline{\varphi});(\boldsymbol{u}_{(-\overline{h},-\overline{\varphi})},-\overline{h},-\overline{\varphi})\}$*, for some* $(\overline{h},\overline{\varphi})\in A_d\setminus\{(0,0)\}$*, if* $\mathcal{R}>0$ *is large.*

This result appears similar to Numerical Results 6.2 and 6.3, where only one degree of freedom is considered but, as we now show, the meaning of small/large $\mathcal{R}$ can be quite different.

The crucial step in the proof of Theorem 4.3 consists in showing the local uniqueness and stability of the configuration $(\boldsymbol{u}_{(0,0)},0,0)$. This follows from (4.6), which, by continuity, leads to the same conclusion for $\mathcal{R}$ small. Recalling (6.1) and that $\theta=-\varphi$, a loss of stability may then occur only at a critical value $\mathcal{R}_c>0$ (if it exists) such that

$$\det\frac{\partial\boldsymbol{\Psi}(0,0,\mathcal{R}_c)}{\partial(h,\theta)}=\det\left[\begin{pmatrix}\kappa_1&0\\0&\kappa_2\end{pmatrix}-\begin{pmatrix}\partial_h\mathcal{L}(0,0,\mathcal{R}_c)&\partial_\theta\mathcal{L}(0,0,\mathcal{R}_c)\\\partial_h\mathcal{T}(0,0,\mathcal{R}_c)&\partial_\theta\mathcal{T}(0,0,\mathcal{R}_c)\end{pmatrix}\right]=0. \tag{6.5}$$

For a single degree of freedom (when $\partial_h\mathcal{T}\partial_\theta\mathcal{L}=0$), the threshold $\mathcal{R}_c>0$ is reached when

$$\big(\kappa_1-\partial_h\mathcal{L}(0,0,\mathcal{R}_c)\big)\big(\kappa_2-\partial_\theta\mathcal{T}(0,0,\mathcal{R}_c)\big)=0. \tag{6.6}$$

In fact,

- ▶ if the unique degree of freedom is h, then $\partial_\theta\mathcal{T}=0$ and (6.6) yields $\kappa_1=\partial_h\mathcal{L}(0,0,\mathcal{R}_c)$;
- ▶ if the unique degree of freedom is θ, then $\partial_h\mathcal{L}=0$ and (6.6) yields $\kappa_2=\partial_\theta\mathcal{T}(0,0,\mathcal{R}_c)$.

This implies, in particular, that the equilibrium configuration remains stable (and locally unique) as long as $\partial_h\mathcal{L}(0,0,\mathcal{R})\le 0$ (first case) and $\partial_\theta\mathcal{T}(0,0,\mathcal{R})\le 0$ (second case). Figures 8, 9, and 16 show that this indeed happens for $\mathcal{R}$ small, while for $\mathcal{R}=5$ these derivatives are both positive. When they are sufficiently large, critical values $\mathcal{R}_c^{vert}>0$ and $\mathcal{R}_c^{rot}>0$ such that

$$\kappa_1=\partial_h\mathcal{L}(0,0,\mathcal{R}_c^{vert})\quad\text{or}\quad\kappa_2=\partial_\theta\mathcal{T}(0,0,\mathcal{R}_c^{rot}) \tag{6.7}$$

may exist. If this happens, by (3.20), one can derive some quantitative bounds.

For the complete two-degrees-of-freedom system (when $\partial_h \mathcal{T} \partial_\theta \mathcal{L} \neq 0$), a new source of possible instability appears because (6.5) yields

$$\kappa_1\kappa_2 - \partial_\theta \mathcal{T}(0,0,\mathcal{R}_c)\kappa_1 - \partial_h \mathcal{L}(0,0,\mathcal{R}_c)\kappa_2 = \partial_\theta \mathcal{L}(0,0,\mathcal{R}_c)\partial_h \mathcal{T}(0,0,\mathcal{R}_c) - \partial_h \mathcal{L}(0,0,\mathcal{R}_c)\partial_\theta \mathcal{T}(0,0,\mathcal{R}_c).$$

In view of (3.20), this may yield different conclusions compared to (6.7), and it may happen that, if any, an instability arises for some $\mathcal{R}_c < \min\{\mathcal{R}_c^{vert}, \mathcal{R}_c^{rot}\}$. This purely qualitative discussion is not at all rigorous. However, it shows that the system with two degrees of freedom may be less stable than the system with a single degree of freedom.

We have no statement similar to Theorem 4.3 when we consider the problem without restoring force ($F = 0$) since the stiffness constants $\kappa_1, \kappa_2 > 0$ give the nondegeneracy when $\mathcal{R} \to 0$; see (4.6). Nevertheless, the numerical plots suggest an earlier loss of uniqueness of the equilibrium configuration with two degrees of freedom (namely, $\mathcal{R}_c < \min\{\mathcal{R}_c^{vert}, \mathcal{R}_c^{rot}\}$) with respect to the single degree of freedom case; see the left plot in Figure 19 and the plot of Figure 21. In those situations, respectively, $(d, \mathcal{R}) = (6, 1)$ and $(d, \mathcal{R}) = (30, 10)$, there is numerical evidence of the existence of two new equilibria, namely,

$$\mathbb{L}_0^{\mathcal{R}} \cap \mathbb{T}_0^{\mathcal{R}} = \{(0,0); (\overline{h}, \overline{\varphi}); (-\overline{h}, -\overline{\varphi})\} \qquad \text{for some } \overline{h}, \overline{\varphi} > 0,$$

while there are no zeros of $h \mapsto \mathcal{L}(h, 0, \mathcal{R})$ and $h \mapsto \mathcal{T}(h, 0, \mathcal{R})$. This means that for the model with a single degree of freedom, we still have a single equilibrium in 0, while the equilibrium $(0, 0)$ already lost its stability in the model with two degrees of freedom. This suggests that $\mathcal{R}_c < \min(\mathcal{R}_c^{vert}, \mathcal{R}_c^{rot})$, at least in absence of restoring forces.

7. The Leonardo da Vinci ferry.

7.1. The model. The Leonardo ferry is a special type of hand ferry which takes its name from its inventor, Leonardo da Vinci (1452–1519). The unique, still-functioning ferry crosses the Adda River and joins the towns of Imbersago and Villa d'Adda (northern Italy); the ferry has a surface of 60 m^2 and can carry up to 100 people and 5 cars. The idea was to exploit the lift of the river current with no use of motorized power. Between the two banks of the river a steel cable is positioned orthogonally to the flow, and the ferry is hooked up to the cable. The ferry is handled by a unique operator who acts on the helm in order to orient it while, with the use of an iron stick, he also initiates the transverse movement. As soon as the ferry is oriented and it is moved away from the bank, the lift starts its action and the ferry moves across the river; see Figure 22.[1] Pictures of the Leonardo ferry are shown in Figure 23.

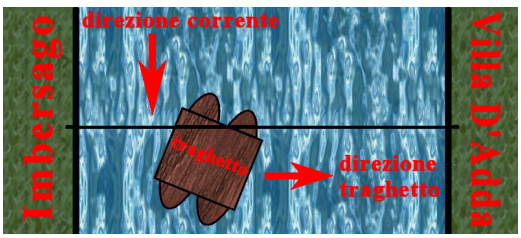

FIG. 22. *Design of the Leonardo ferry.*

[1]Taken from Jalo di Wikipedia (in Italian), public domain, through Wikimedia Commons.

FIG. 23. *The Leonardo da Vinci ferry.*

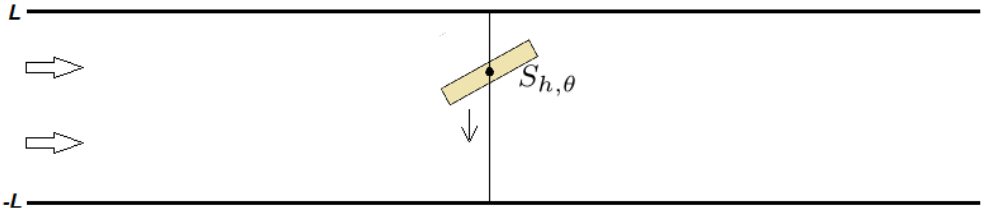

FIG. 24. *Approximation of the Leonardo ferry.*

The purpose of the present section is to use the model equation (2.11) in order to study the behavior of the Leonardo ferry. Although the hull (exposed part of the ferry) has the shape visible in Figure 23, the keel (submerged part of the ferry subject to the action of the flow) has a rectangular shape. This is why the Adda River and the Leonardo ferry can be represented as in the picture in Figure 24, which should be compared with Figure 1.

The main differences are that the fluid is now the water, there is no restoring force tending to bring the ferry towards the center of the channel, and the ferry is not free to rotate since the orientation is kept fixed by the helm. Therefore, we put $F = 0$ in (2.10) and consider the stationary problem (2.11) for some *given* $(h, \theta) \in A_d$, so that also $\Omega_{h,\theta}$ and $S_{h,\theta}$ are assigned. From Proposition 2.2 we know that if $\mathcal{R} > 0$ is sufficiently small, then (2.11) admits a unique solution $\boldsymbol{u}_{(h,\theta)}$ that we determine numerically. In fact, for any reasonable $\mathcal{R} > 0$ (for which the Newton method converges) we numerically find a solution, since the channel is bounded. Then we compute both the lift and the torque as functions of $(h, \theta) \in A_d$.

As already mentioned, for the operator of the Leonardo ferry it is more convenient to argue in terms of the attack angle φ defined by $\varphi = -\theta$ for $|\theta| < \frac{\pi}{2}$. From subsection 6.2, we infer that

- if the operator maintains the horizontal position $\varphi = 0$, then the ferry cannot cross the river (see Numerical Result 6.2 and Figure 10 (and Numerical Result 7.1 below);
- the operator does not need to push the ferry away from the bank because, in the horizontal position $\varphi = 0$, the lift is a repulsive force when the ferry is close to the bank (see Figures 8, 9, and 10).

Therefore, the operator must orient the helm in a suitable way. In subsection 6.3 we analyzed numerically the function $(h, \varphi) \mapsto \mathcal{L}(h, \varphi, \mathcal{R})$ in order to find the *optimal way to maneuver the ferry,* namely, which attack angle φ minimizes the crossing time of the ferry. To increase the upwards velocity of the Leonardo ferry, one should find the angle maximizing $\mathcal{L}$ for any position $h \in (-L + d, L - d)$ of the ferry.

As a further application to the Adda river, one may also be interested in evaluating the torque, for instance, for a canoe race in the river, as there might be configurations that keep a straight trajectory. For both the ferry and the canoe in the next subsection we give hints to the operators, by exploiting the numerical results obtained in section 6.

7.2. How to drive the ferry. As a consequence of Numerical Results 6.2 and 6.5, we obtain the following result.

NUMERICAL RESULT 7.1. *If the angle of attack is zero ($\varphi = 0$), then the ferry cannot cross the river:*

- *if $\mathcal{R} > 0$ is small, then it moves towards the unique (stable) equilibrium position $B_{0,0}$;*
- *if $\mathcal{R} > 0$ is large, then either it is still in the unstable position $B_{0,0}$ or it tends to move towards $B_{h_-,0}$ if $h \in [1-L, 0)$, whereas it tends to move towards $B_{h_+,0}$ if $h \in (0, L-1]$.*

Moreover, if $\mathcal{R} = 5$, then it moves following increasing h whenever $0 < \varphi_0 < \varphi < \varphi^0 < \frac{\pi}{2}$.

Hence, in order to allow the Leonardo ferry to cross the Adda River, the operator needs to modify the attack angle φ; see Figure 23. For $\mathcal{R} = 5$, the last statement shows that if the helm is oriented in such a way that $\varphi_0 < \varphi < \varphi^0$, then, at any position h between the two banks, the ferry is pushed towards the upper bank ($x_2 = L$). But if one seeks the optimal way to reach the upper bank, the operator must follow more precise instructions. Figure 15 (right) shows that in order to reach the maximum speed, the helm should be kept at an angle $\varphi \approx \frac{\pi}{4.5}$ when starting from the lower bank; this is confirmed by Figure 13 (left), in which the graph (G), corresponding to $\varphi = \frac{\pi}{4}$, lies above the other graphs in a right neighborhood of $h = -30$. A few meters far away from the bank (at $h \approx -24$), the helm should be kept at $\varphi \approx \frac{\pi}{6}$. Note that both the angles $\varphi \approx \frac{\pi}{4.5}$ and $\varphi \approx \frac{\pi}{6}$ belong to the interval (φ_*, φ^*) so that the maximal lift is achieved for $h \approx 4$ (see Numerical Result 6.6), namely, slightly after the middle of the Adda River. Finally, a few meters before reaching the upper bank the helm should be kept again at $\varphi \approx \frac{\pi}{4.5}$. Of course, in the latter part, the target of the operator is no longer to reach the maximum speed since, otherwise, the ferry will crash against the upper bank. In view of (3.9), the angle should be $\varphi \approx -\frac{\pi}{4.5}$ in such a way to slow down the ferry.

From Numerical Result 6.8, we infer that for small $\mathcal{R} > 0$ the only "parking position" is $(h, \varphi) = (0, 0)$, while for large $\mathcal{R}$ there are at least three parking positions $\{(0,0); (\overline{h}, \overline{\varphi}); (-\overline{h}, -\overline{\varphi})\}$. If the Leonardo ferry reaches one of these positions, it remains at rest, with no lift or torque being exerted on it. Therefore, in order to leave these parking positions, where the ferry would remain still forever, the operator should either move the helm or pull by hand the ferry with the hook. In other words, these configurations are stationary solutions of (2.10) (with $F = 0$), and to leave them some forcing term is needed.

The numerical results in section 6 also allow us to give hints for a canoe rower on the river. From Numerical Result 6.3 we infer that the canoe can be kept parallel to the flow with no effort, provided that the canoe is placed at $h \in \{h_-, h_0, h_+\}$, while some rowing is needed in order to maintain the canoe parallel to the flow when the canoe is not in these configurations.

Let us emphasize that the above suggestions for the operator of the ferry and for the canoe rower are merely qualitative and do not pretend to be exact. In particular,

by inserting the real physical quantities we find that the Reynolds number (2.2) of the Adda flow can be much larger than $\mathcal{R} = 5$, especially when the dam in Olginate (governing the amount of water from the Lake of Como into the Adda river) is open. Nevertheless, we were also able to show that for some $\mathcal{R}$ larger than 5, the qualitative behavior of the lift does not change.

8. Remarks and open problems in proximity of collisions. An example of potential satisfying assumptions (2.6)–(2.7)–(2.8)–(2.9) is ($\kappa_1, \kappa_2 > 0$)

$$F(h,\theta) = \frac{\kappa_1}{2}h^2 + \frac{\kappa_2}{2}\theta^2 + \frac{h^2\theta^2}{(L - |h| - d|\sin\theta| - \cos\theta)^2} + \tan^4\theta \quad \forall (h,\theta) \in A_d.$$

The assumptions are mostly based on physical motivations, but some of them can be relaxed without altering our proofs. In particular, (2.8) is somewhat technical and is used to prevent collisions of B with $\partial\mathcal{C}_L$ but, most probably, it can be relaxed. When B is close to $\partial\mathcal{C}_L$ the drag force acting on B may vary and, more importantly, B may be subject to an additional lift force known as *wall-induced lift* [41], which is usually caused by two different mechanisms [37, 40]. First, the presence of a wall, such as $\partial\mathcal{C}_L$, breaks the symmetry of the vortex shedding behind B and generates an effective lift force directed away from the wall; see the arrows in Figure 10. Second, according to the inviscid theory, the pressure in the gap between B and $\partial\mathcal{C}_L$ decreases and generates a lift force directed towards $\partial\mathcal{C}_L$. Both these effects decay rapidly as the distance between B and $\partial\mathcal{C}_L$ increases, and for "large" distances they can be reasonably neglected [23]. Figures 8 and 9 show that when B is horizontal, not only does the lift remain bounded in the proximity of the collision but it also behaves repulsively; see also Numerical Result 6.2, Figure 10, and the comments on the Leonardo ferry in subsection 7.1. Given this, most probably, the assumption (2.8) is not needed to prevent collisions.

As far as we are aware, the study of the motion of a solid sphere through a viscous fluid near a plane wall goes back to Goldman, Cox, and Brenner [23], who developed a lubrication theory, following the earlier work by O'Neill [33] and Dean and O'Neill [13]. Other shapes have been considered later on, for instance, by Cox [12]. We also refer the reader to Hillairet and Kelaï [25] for the justification of the lubrication approximation, at least in 3D. Assuming B is an ellipse, Bonheure, Grandmont, and Hillairet [10] considered a *Stokes flow* and show that the lift and the torque are uniformly bounded independently of the configuration. The argument can be adapted to a Navier–Stokes flow, but not to the case of a body B with flat boundary parts. We also mention that some numerical studies—see, for instance, [17, 30, 39]—investigate the effect of wall proximity on the lift and torque for nonspherical shapes.

For the rectangle B, collisions with $\partial\mathcal{C}_L$ can occur only along a full edge or in a corner, two quite different situations. For possible collisions with an edge of B (i.e., when $\theta = \varphi = 0$), we refer the reader to subsection 6.2, where the numerical tests suggest that the lift remains bounded. For possible collisions with a corner of B, we refer the reader to subsection 6.3; it turns out that also in this case the lift appears to remain bounded (see Figure 13), while it is not clear if the lift remains repulsive in proximity of collisions. To this end, one should determine the *sign* of the lift in proximity of collisions, in dependence of the angle $\theta = -\varphi$. More precisely, for any $\theta \in (-\frac{\pi}{2}, \frac{\pi}{2})$ there exists a unique $h_\theta > 0$ such that $(h_\theta, \theta) \in \partial A_d$; recall (2.4) and Figure 2. Explicitly, it is given by

$$h_\theta := \Big| d|\sin\theta| + \cos\theta \Big|.$$

From Figures 16 and 17 we see that the map

$$\theta \mapsto \lim_{h \to h_\theta} \mathcal{L}(h, \theta, \mathcal{R})$$

is not constant, and precise information on its sign would be extremely helpful. In fact, it appears quite interesting to understand in full generality the behavior of $\mathcal{L}$ and $\mathcal{T}$ (boundedness and sign) in proximity of collisions for a wide class of shapes of the colliding body B. We leave this for further investigations.

By comparing the two plots in Figure 16 we infer that lift and torque display a similar qualitative behavior, although with a different order of magnitude (of about 10^2). Therefore, the above comments about the boundedness of the lift apply to the torque as well.

We also mention that some theoretical results have been obtained for unsteady problems; see, for instance [22, 24, 35], still mainly inspired by the lubrication approximation [23, 29]. In those studies, the dynamics is not driven by a Poiseuille flow. The fact that v_P vanishes on $\partial\mathcal{C}_L$ makes the analysis of the lift and the torque quite different; see [11], where (2.1) is considered in the case where B is an ellipse. The arguments of [11] should also allow us to show that for the solutions of (2.1), when the body B is smoothed at the corners, collisions cannot occur, in either finite or infinite time, and without assuming (2.8)–(2.9).

We conclude by mentioning that our results may possibly be obtained also in a 3D unbounded cylinder (not necessarily circular) at the price of much more technical assumptions and computations. In particular, aiming to model the whole deck of the bridge, one should argue in a non-simply-connected unbounded domain; see [20] for the model problem set in a *bounded* domain. Again, we expect existence and uniqueness of an equilibrium configuration for small Reynolds numbers.

Data availability statement. Data sharing is not applicable to this article as no datasets were generated or analyzed during the current study. There are no conflicts of interest.

REFERENCES

[1] O. H. Ammann, T. von Kármán, and G. B. Woodruff, *The Failure of the Tacoma Narrows Bridge*, Federal Works Agency, Washington, DC, 1941.

[2] G. Arioli and F. Gazzola, *A new mathematical explanation of what triggered the catastrophic torsional mode of the Tacoma Narrows Bridge collapse*, Appl. Math. Model., 39 (2015), pp. 901–912.

[3] J. A. Bello, E. Fernández-Cara, J. Lemoine, and J. Simon, *The differentiability of the drag with respect to the variations of a Lipschitz domain in a Navier–Stokes flow*, SIAM J. Control Optim., 35 (1997), pp. 626–640, https://doi.org/10.1137/S0363012994278213.

[4] E. Berchio and F. Gazzola, *A qualitative explanation of the origin of torsional instability in suspension bridges*, Nonlinear Anal., 121 (2015), pp. 54–72.

[5] D. Bonheure, G. P. Galdi, and F. Gazzola, *Equilibrium configuration of a rectangular obstacle immersed in a channel flow*, C. R. Acad. Sci. Paris, 358 (2020), pp. 887–896.

[6] D. Bonheure, G. P. Galdi, and F. Gazzola, *Equilibrium Configuration of a Rectangular Obstacle Immersed in a Channel Flow*, https://arxiv.org/abs/2004.10062v2, 2021.

[7] D. Bonheure, F. Gazzola, I. Lasiecka, and J. Webster, *Long-time dynamics of a hinged-free plate driven by a non-conservative force*, Ann. Inst. H. Poincaré Anal. Non Linéaire, 39 (2022), pp. 457–500.

[8] D. Bonheure, F. Gazzola, and E. Moreira dos Santos, *Periodic solutions and torsional instability in a nonlinear nonlocal plate equation*, SIAM J. Math. Anal., 51 (2019), pp. 3052–3091, https://doi.org/10.1137/18M1221242.

[9] D. Bonheure, F. Gazzola, and G. Sperone, *Eight(y) mathematical questions on fluids and structures*, Atti Accad. Naz. Lincei Rend. Lincei Mat. Appl., 30 (2019), pp. 759–815.

[10] D. Bonheure, C. Grandmont, and M. Hillairet, *Quasistatic approximation of the movement of a solid in a 2D Poiseuille flow*, in preparation.
[11] D. Bonheure, M. Hillairet, C. Patriarca, and G. Sperone, *Long-time behavior of an anisotropic rigid body interacting with a Poiseuille flow in an unbounded 2D channel*, submitted.
[12] R. G. Cox, *The motion of suspended particles almost in contact*, Int. J. Multiphase Flow, 1 (1974), pp. 343–371.
[13] W. R. Dean and M. E. O'Neill, *A slow motion of viscous liquid caused by the rotation of a solid sphere*, Mathematika, 10 (1963), pp. 13–24.
[14] A. L. Dontchev and R. T. Rockafellar, *Implicit Functions and Solution Mappings: A View from Variational Analysis*, Springer, New York, 2014.
[15] G. P. Galdi, *An Introduction to the Mathematical Theory of the Navier-Stokes Equations: Steady-State Problems*, Springer Science & Business Media, 2011.
[16] G. P. Galdi and V. Heuveline, *Lift and sedimentation of particles in the flow of a viscoelastic liquid in a channel*, in Free and Moving Boundaries, Lect. Notes Pure Appl. Math. 252, Chapman & Hall/CRC, Boca Raton, FL, 2007, pp. 75–110.
[17] E. Gavze and M. Shapiro, *Particles in a shear flow near a solid wall: Effect of nonsphericity on forces and velocities*, Int. J. Multiphase Flow, 23 (1997), pp. 155–182.
[18] F. Gazzola, *Mathematical Models for Suspension Bridges*, Model. Simul. Appl. 15, Springer, 2015.
[19] F. Gazzola, V. Pata, and C. Patriarca, *Attractors for a fluid-structure interaction problem in a time-dependent phase space*, J. Funct. Anal., 286 (2024), 110199.
[20] F. Gazzola and C. Patriarca, *An explicit threshold for the appearance of lift on the deck of a bridge*, J. Math. Fluid Mech., 24 (2022), Paper No. 9, 2022, 23 pp.
[21] F. Gazzola and G. Sperone, *Steady Navier-Stokes equations in planar domains with obstacle and explicit bounds for unique solvability*, Arch. Ration. Mech. Anal., 238 (2020), pp. 1283–1347.
[22] D. Gérard-Varet and M. Hillairet, *Regularity issues in the problem of fluid structure interaction*, Arch. Ration. Mech. Anal., 195 (2010), pp. 375–407.
[23] A. J. Goldman, R. G. Cox, and H. Brenner, *Slow viscous motion of a sphere parallel to a plane wall.* I. *Motion through a quiescent fluid*, Chem. Eng. Sci., 22 (1967), pp. 637–651.
[24] M. Hillairet, *Topics in the mathematical theory of interactions of incompressible viscous fluid with rigid bodies*, in Fluid-Structure Interaction and Biomedical Applications, Adv. Math. Fluid Mech., Birkhäuser/Springer, Basel, 2014, pp. 257–320.
[25] M. Hillairet and T. Kelaï, *Justification of lubrication approximation: An application to fluid/solid interactions*, Asymptot. Anal., 95 (2015), pp. 187–241.
[26] B. P. Ho and L. G. Leal, *Inertial migration of rigid spheres in two-dimensional unidirectional flows*, J. Fluid. Mech., 65 (1974), pp. 365–400.
[27] A. Inoue and M. Wakimoto, *On existence of solutions of the Navier-Stokes equation in a time dependent domain*, J. Faculty Sci. Univ. Tokyo. Sect. IA. Math., 24 (1977), pp. 303–319.
[28] International Association for Wind Engineering (IAWE), *A Benchmark on the Aerodynamics of a Rectangular* 5:1 *Cylinder*, https://www.aniv-iawe.org/barc/.
[29] L. G. Leal, *Advanced Transport Phenomena. Fluid Mechanics and Convective Transport Processes*, Camb. Ser. Chem. Eng., Cambridge University Press, Cambridge, UK, 2007.
[30] S. Y. Lee and J. Y. Hyun, *Analysis of force acting on the non-spherical particle near a wall*, Biomed. Eng. Lett., 5 (2015), pp. 289–295.
[31] P. J. McKenna, *Oscillations in suspension bridges, vertical and torsional*, Discrete Contin. Dyn. Syst. S, 7 (2014), pp. 785–791.
[32] L. M. Milne-Thomson, *Theoretical Aerodynamics*, 4th ed., Dover, New York, 1966.
[33] M. E. O'Neill, *A slow motion of viscous liquid caused by a slowly moving solid sphere*, Mathematika, 11 (1964), pp. 67–74.
[34] C. Patriarca, *Existence and uniqueness result for a fluid-structure-interaction evolution problem in an unbounded 2D channel*, NoDEA Nonlinear Differential Equations Appl., 29 (2022), 39.
[35] L. Sabbagh, *On the motion of several disks in an unbounded viscous incompressible fluid*, Nonlinearity, 32 (2019), pp. 2157–2181.
[36] T. Takahashi, *Analysis of strong solutions for the equations modeling the motion of a rigid-fluid system in a bounded domain*, Adv. Differential Equations, 8 (2003), pp. 1499–1532.
[37] F. Takemura and J. Magnaudet, *The transverse force on clean and contaminated bubbles rising near a vertical wall at moderate Reynolds number*, J. Fluid Mech., 495 (2003), pp. 235–253.

[38] E. Ventsel and T. Krauthammer, *Thin Plates and Shells: Theory, Analysis, and Applications*, Marcel Dekker, New York, 2001.
[39] A. Zarghami and J. T. Padding, *Drag, lift and torque acting on a two-dimensional non-spherical particle near a wall*, Adv. Powder Technol., 29 (2018), pp. 1507–1517.
[40] L. Zeng, S. Balachandar, and P. Fischer, *Wall-induced forces on a rigid sphere at finite Reynolds number*, J. Fluid Mech., 536 (2005), pp. 1–25.
[41] L. Zeng, F. Najjar, S. Balachandar, and P. Fischer, *Forces on a finite-sized particle located close to a wall in a linear shear flow*, Phys. Fluids, 21 (2009), 033302.